Studies of Affinity Maturation of Anti-Flavivirus Antibodies during Vaccination

January 2024

Isamu TSUJI

Studies of Affinity Maturation of Anti-Flavivirus Antibodies during Vaccination

A Dissertation Submitted to

the Graduate School of Science and Technology,

University of Tsukuba

in Partial Fulfillment of the Requirements

for the Degree of Doctor of Philosophy in Science

Doctoral Program in Biology

Degree Programs in Life and Earth Sciences

Isamu TSUJI

Table of Contents

Figures

Tables

General Abstract

Antibody affinity maturation is a process of mutating the variable region of antibody amino acid sequences to enhance antibody affinity. The process occurs in the lymph node germinal center, and the mutations are initiated by activation-induced cytidine deaminase to deaminate deoxy-cytidines to deoxy-uracils in antibody variable region. Two main approaches are to assess antibody affinity maturation. Genomic approach is to confirm antibody DNA sequence mutations from germline sequences using B cell isolation technology. Serological approach assesses the strength of polyclonal antibodies in serum. Enzyme immunosorbent assay disrupted with chaotropic reagents is widely used. However, antibody kinetics parameters for evaluating antibody affinity maturation cannot be assessed. Dengue virus (DENV) and Zika virus (ZIKV) were classified as flavivirus and infected humans through mosquitoes. DENV has been one of the most significant pandemic flaviviridae viruses. An estimated 390 million infections occur annually, of which approximately 96 million are symptomatic, and 40,000 deaths occur globally. When ZIKV infects pregnant women, microcephaly or other developmental abnormalities have been shown to occur in fetuses and newborn babies. Antibody affinity maturation enhances antiviral functions, such as virus neutralization, antibody-mediated complement, and effector-dependent cytotoxicity. However, few reports on antibody affinity maturation by flavivirus vaccine have been reported. Here, I reported elucidating antibody affinity maturations of flavivirus vaccines using genomic and serological approaches.

Chapter 1:

Eight novel rabbit monoclonal antibodies (mAbs) that bind to distinct ZIKV envelope protein epitopes were discovered. The majority of the mAbs were ZIKV-specific and targeted the lateral

ridge of the Envelope protein domain III, while mAb with the highest neutralizing activity, recognized a putative quaternary epitope spanning E protein domains I and III. One non-neutralizing mAbs specifically recognized ZIKV precursor membrane protein (prM). Immunoglobulin variable region plays critical roles in binding to antigen surfaces and consists of two regions: complementarity-determining regions (CDR) that recognize antigen epitopes and canonical framework regions (FWR) scaffolded CDR structure. The variable region amino acid mutations, so-called somatic hypermutation (SHM), were analyzed by the international ImMunoGeneTics information system®. SHM were confirmed in antibody heavy and light chains. For five neutralizing anti-ZIKV mAbs, negative correlations were observed between heavy chain SHM, CDR, and FWR mutation rate and antibody binding parameters such as equilibrium dissociation constant (K_D) and dissociation constant (k_{dis}) of mAb binding to ZIKV virus-like particle (VLP). Reversion of FWR amino acids to the rabbit germline sequence decreased anti-ZIKV mAb binding activity of some mAbs. Thus, antibody affinity maturation, SHM, CDR, and FWR mutations contributed to the binding and function of these anti-ZIKV mAbs.

Chapter 2:

Antibody affinity maturation is a critical step in developing functional antiviral immunity. However, accurate measurement of affinity maturation of polyclonal serum antibody responses to particulate antigens such as virions is challenging. I developed a novel avidity assay employing BLI. DENV-VLP was verified using anti-DENV mAbs, antibody purification from human serum and avidity assay conditions were optimized. The optimized assay was used to assess avidity of antibody responses to a tetravalent dengue vaccine candidate (TAK-003) in children, adolescents, and adults during two phase 2 clinical trials conducted in dengue-endemic

regions. For baseline seronegative volunteers without DENV infection history, k_{dis} decreased after one month of vaccinations and remained for one year post-vaccination. Thus, I concluded that DENV vaccinations stimulated antibody affinity maturation. Response, showing anti-DENV antibody concentration, and avidity index calculated by response/k_{dis}, reflecting the strength of antibody, increased one month after vaccination and remained high through one-year post-vaccination. For baseline seropositive volunteers with DENV infection history, k_{dis} had decreased before vaccination due to prior infections and did not decrease further. However, response and avidity index increased after one month of vaccination and remained through one year. Neutralizing antibody titers and avidity index did not correlate overall. However, the correlation was observed in those subjects with lower k_{dis}, the highest degree of antibody affinity maturation. Neutralizing antibodies might be selected during the affinity-maturation process; therefore, low k_{dis} subjects showed a higher correlation. In conclusion, vaccination with TAK-003 stimulates antibody affinity maturation and functional antibody responses, including neutralizing antibodies.

To summarize the thesis, antibody affinity maturation process by flavivirus vaccinations was elucidated from DNA mutations to serum antibody affinity. High CDR mutations were observed for anti-ZIKV mAbs and correlated with antibody affinity parameters, K_D, and k_{dis}. A novel avidity assay to assess k_{dis} values from human serum was developed, and a significant decrease in k_{dis} was observed from DENV vaccination volunteers. The correlation of avidity index and neutralizing titer was found in high affinity matured subjects. Finally, I conclude that antibody affinity maturation is essential for protection from virus infection.

Abbreviations

AA: amino acid

AID: activation-induced cytidine deaminase

AR2G: Amine Reactive Second-Generation biosensor

ASTM: American Society for Testing and Materials

BSA: bovine serum albumin

BLI: bio-layer interferometry

CDC: Centers for Disease Control and Prevention

CDR: complementarity-determining region

CDRH: complementarity-determining region heavy chain

CDRL: complementarity-determining region light chain

COVID19: coronavirus disease 2019

CR: cross-reactive

CV: coefficient of variation

D: diversity region

DC: dendritic cells

DENV: dengue virus

DHF: dengue hemorrhagic fever

DNA: deoxyribonucleic acid

D-PBS: Dulbecco's phosphate-buffered saline

D-PBS++: D-PBS plus calcium and magnesium

DSS: dengue shock syndrome

EC_{50}: half maximal effective concentration

ECD: 1-ethyl-3-[3-dimethylaminopropyl] carbodiimide hydrochloride

ELISA: enzyme immunosorbent assay

E protein: envelope protein

FWR: framework region

FL: fusion loop

GC: germinal center

HAT: hypoxanthine-aminopterin-thymidine

HGPRT: hypoxanthine-guanine phosphoribosyl transferase

HIV: human immunodeficiency virus

IACUC: International Animal Care & Use Committee

IC_{50}: half maximal inhibitory concentration

ICH-GCP: International Council for Harmonization of Technical Requirements for Registration of Pharmaceuticals for Human Use and Good Clinical Practice

Ig: immunoglobulin

IgA: immunoglobulin A

IgD: immunoglobulin D

IgE: immunoglobulin E

IgG: immunoglobulin G

IgM: immunoglobulin M

IM: intramuscular

IMGT: The international ImMunoGeneTics information system

IMGT/V-QUEST The international ImMunoGeneTics information system/ V-query and standardization

J: joining region

JEV: Japanese encephalitis virus

ka: association constant

kDa: kilodalton

k_{dis}:	dissociation constant
K_D:	equilibrium dissociation constant
LoD:	limit of detection
mAb:	monoclonal antibody
MHC:	major histocompatibility complex
MNT:	TCID50-based microneutralization test
MMR:	measles, mumps and rubella
mRNA:	messenger ribonucleic acid
MWCO:	molecular weight cut-off
NCBI:	The National Center for Biotechnology Information
NHS:	N-hydroxy-sulfo-succinimide
PBS:	phosphate-buffered saline
PBST:	phosphate-buffered saline plus 0.05% Tween-20
PCR:	polymerase chain reaction
PDB:	Protein Data Bank
PIZV:	purified inactivated Zika vaccine
prM:	precursor membrane protein
QE:	quaternary envelop-protein
RNA:	ribonucleic acid
RT-PCR:	reverse transcription polymerase chain reaction
SA:	streptavidin
SAX:	high precision streptavidin
SC:	subcutaneous
SD:	standard deviation
SDS-PAGE:	sodium dodecyl sulfate-polyacrylamide gel electrophoresis

SHM:	somatic hypermutation
SPR:	surface plasmon resonance
ssDNA:	single-strand DNA
TAK-003:	tetravalent dengue vaccine candidate
V:	variable region
VH:	heavy chain variable region
VL:	light chain variable region
VLP:	virus-like particle
WHO:	The World Health Organization
YF:	Yellow fever
ZIKV:	Zika virus

General introduction

The history of humanity is a battle against microbes, the first endemic of which was reported in 430 BC. A plague that struck the City of Athens reported smallpox and typhus based on the symptoms. Most of the population was infected, and 75,000 - 100,000 people died, which is 25% of the city's population [1]. *Yersinia pestis* is a Gram-negative bacterium that causes plaques. Plague was a pandemic in European countries in the 6th century, with millions of deaths and three pandemics in the region [2]. Cholera is an acute, often fatal gastrointestinal tract disease caused by *Vibrio cholerae*. Six pandemics occurred in Asia in the 19th and 20th centuries [3]. Influenza was also a pandemic in Russia in 1889-1894 [4] and Spain in 1918 [5]. In 2020, coronavirus disease 2019 (COVID-19) became a worldwide pandemic from Wuhan, China [6]. The World Health Organization (WHO) reported 774 million cases and 7 million deaths as of 7 January 2024 (WHO COVID-19 Dashboard, **https://covid19.who.int/**).

Hygiene control is a critical factor for preventing infectious disease outbreaks. Essential elements include clean water supply, sanitation, hand washing, and safe food treatment [7]. Vaccines are also known to prevent these diseases and are preparations for stimulating an immune response against diseases. Edward Jenner discovered the first concept of smallpox in 1796 and immunized cowpox. He found that the milkmaids exposed to cowpox exhibited similar symptoms to smallpox but were not infected with smallpox. Finally, he was inspired to inoculate an 8-year-old boy with cowpox, confirming protection against smallpox [8, 9]. Vaccines for typhoid [10], rabies [11], and diphtheria [12] were developed in the 19th century. Numerous vaccines were developed in the 20th century, such as vaccines for influenza [13], yellow fever [14], pertussis (whooping cough) [15], polio [16], hepatitis B [17], measles mumps and rubella (MMR vaccine) [18], pneumococcal pneumonia [19], *Haemophilus influenzae* type b (Hib) [20],

and rotavirus [21]. Early-developed vaccines were live attenuated or inactivated viruses and toxoid vaccines. However, since recombinant DNA technologies were developed in 1972 [22], recombinant subunit polysaccharides and conjugation vaccines have been developed to reduce side effects and improve efficacy. The human papillomavirus vaccine, recombinant subunits form, was approved in 2006 to treat cervical cancer [23], and the first COVID-19 vaccine was developed using messenger RNA (mRNA) technology only one year after the first case was confirmed [24, 25].

Vaccination has successfully prevented numerous types of childhood-related infections and saved millions of lives [26]. More than 20 million morbidities were reported in the 20th century in the United States, including measles, mumps, pertussis, polio, rubella, and smallpox [27]. However, vaccination reduced the number of infected cases by >90%, and smallpox, diphtheria, and polio were eradicated in the US in 2006 [28]. Smallpox began the inoculation of cowpox in 1796 by Edward Jenner [29] and continued vaccination worldwide. The last such case was reported in Somalia in 1977. WHO declared that smallpox was eradicated in 1980 [30]. Moreover, this was the first virus to be eradicated worldwide.

Antibody function is widely known as neutralizing viruses in the plasma and preventing viral infection. The five primary classes of immunoglobin (Ig) are IgG, IgM, IgA, IgD, and IgE. Furthermore, the functions of the classes differ [31]. IgA protects the intestines against enteric toxins and pathogenic microorganisms [32]. IgE is critical for allergic inflammatory processes such as rhinitis [33]. The function of IgD is not clear; it is expressed on the B-cell surface, regulates the activation of foreign antigens, and is depressed to autoantigens with IgM [34]. IgM and IgG circulate in the blood and play essential roles in protecting against toxins, bacteria, and viral infections.

Vaccines are administered through various routes, including oral, intranasal, subcutaneous (SC), and intramuscular (IM) [35]. Most vaccine programs were immunized via SC or IM administration, and multiple doses are often required to enhance vaccine immunity [36-38]. Dendritic cells (DC) are specialized antigen-presenting cells that are abundant in peripheral tissues such as the skin and function as immune sentinels [39]. Vaccine antigens are internalized into DC through endocytic processes such as receptor-mediated endocytosis, phagocytosis, and macropinocytosis [40]. First, vaccine antigens are decomposed into peptides and displayed on the major histocompatibility complex (MHC) [41]. Next, DC migrates to secondary lymphoid organs in the lymph nodes, spleen, and tonsils, where the peptide/MHC complex in DC activates naïve B cells through the B cell receptor [42]. These activated B cells are converted to short-lived plasma cells and secrete IgM for >one month [43]. The cells are then moved to the lymph node germinal center (GC), where the class switches from IgM to IgG, and antibody affinity maturation is initiated [44]. A booster vaccine dose, typically injected 2 - 6 weeks after the first dose, also activates B cells [45, 46]. GC has been separated into two zones based on histological staining: dark and light zones [47]. The dark zone undergoes affinity maturation induced by somatic hypermutations (SHM). The light zone is where B cells differentiate, activating the affinity-matured B cells through follicular helper T cells, thereby inducing apoptosis of non-affinity mature B cells and differentiation into memory B cells and long-lived secreted plasma cells [48].

Antibody affinity maturation is the process through which antibodies gain increased affinity, avidity, and anti-pathogen activity and is the result of SHM of immunoglobulin genes in B cells coupled with selection for antigen binding [49]. The mutation process is initiated by activation-induced cytidine deaminase (AID), which promotes isotype switching from IgM to IgG by

deaminating deoxycytidines within immunoglobulin genes [50], resulting in SHM and class-switch recombination [51]. AID belongs to the apolipoprotein B mRNA-editing enzyme, a catalytic polypeptide family of cytidine deaminases, and can deaminate deoxy-cytidines to deoxy-uracils in vitro on both single-strand DNA (ssDNA) substrates and ssDNA generated by the formation of RNA-DNA hybrids [52]. Amino acid mutations are more frequently observed in the complementarity-determining regions (CDR) recognized for antigens in the Ig variable region, but lower mutation ratios are observed in the framework region (FWR) located between CDRs. DNA sequences that enhance the deamination of AIDs, referred to as AID overlapping hotspot motifs, WGCW (W=A/T) and AGCT [53], and polymerase eta hotspots (WA/TW) [54] have been reported, and these motif sequences frequently occur in the CDR1 and 2 regions [53, 54].

Neutralizing antibody titers is a standard protective immunity measure [55, 56]. However, neutralizing antibody titers do not always correlate with vaccine effectiveness. Increasing evidence suggests that additional aspects of antiviral immune responses may be critical for disease outcomes. Recent studies have focused on the protective effect of antibody-mediated complement and effector-dependent cytotoxicity on flaviviruses [57-60]. Antibody affinity maturation leads to higher antibody affinity, which optimizes antiviral functions, including virus neutralization [61], antibody-mediated complements and effector-dependent cytotoxicity [57, 62]. This high-affinity matured antibody protects from infection and severe symptoms of the virus [63-66].

Two main approaches are used to assess antibody affinity maturation: genomic and serological approaches. Genomic approaches have been used to confirm antibody DNA sequence mutations in germline sequences. Isolation of B cells is essential for analyzing antibody DNA sequences.

Monoclonal antibodies were generated using hybridoma technology [67, 68]. This technology was used with mouse B cells immunized Balb/c mice with P3X63Ag8U.1 or Sp2/0-Ag 1410 myeloma cells. The genomes of these myelomas lack the hypoxanthine-guanine phosphoribosyltransferase (HGPRT) gene, which is required for nucleotide synthesis. A fused cell referred to as a hybridoma, which harbors HGPRT from B cells, was selected on hypoxanthine-aminopterin-thymidine (HAT) medium to block de novo synthesis or salvage nucleotide synthesis pathways. Unfused myeloma cells do not grow in HAT medium, and unfused B cells die after several days [69]. These established hybridoma cell lines secrete antibodies and select clones using various methods, such as enzyme-linked immunosorbent assay (ELISA) for vaccine antigens [70], flow cytometry of virus-infected cells, and antibody neutralizing assay using virus [71] and reporter virus-like particles [72]. Rabbit monoclonal technology was developed using fusion myeloma, 240E-W, and modified cell lines [73]. Human hybridoma technology is not commonly applied because no versatile cell lines are available [74]. However, through recent advancements in single-cell sorting technology using flow cytometry [75] and nanofluidic chip nanopens, such as Beacons® Optofluidic System [76], and single-cell polymerase chain reaction (PCR) techniques [77], human antibodies have been identified. RNA was extracted from the cell lines, and antibody sequences were read using Sanger sequencing [78]. However, owing to advancements in next-generation sequencing technology, genome-wide antibody sequence analysis has been used to evaluate antibody affinity maturation [79]. An intensive Ig gene allele database is essential for analyzing antibody affinity maturation. The international ImMunoGeneTics (IMGT) information system® is the complete database of all Ig allele sequences [80].

Moreover, The international ImMunoGeneTics information system®/ V-query and standardization (IMGT/V-Quest) is a database that determines the Ig allele, CDR, FWR, DNA and amino acid mutations, SHM ratio, and antibody affinity maturation [81]. The next step is how to assess the antibody functions for affinity maturation. ELISA is widely used to evaluate antibody strength, and the beads-based multiplex assay, Luminex®, has recently been developed to assess multiple antigens [82]. However, these assay results show "static states" of antibody binding as the reaction requires multiple hours to complete, and the antibody binds to the equilibrium state. The evaluation of "dynamic states" is critical for antibody affinity measurement. Surface plasmon resonance (SPR) and bio-layer interferometry (BLI) techniques are used to assess the "dynamic states" of antibody binding and are widely used for monoclonal antibody affinity evaluation [83-85]. This method monitors antibody association and dissociation from the antigen in a time-dependent manner and calculates the association constant, k_a, and the dissociation constant, k_{dis}. The equilibrium dissociation constant K_D is calculated through k_{dis}/k_a, a parameter widely used to evaluate antibody affinity.

Serological approaches have been widely used to assess polyclonal antibodies elicited by vaccine immunization. ELISA for vaccine antigens [70], neutralizing assays using viruses [71], reporter virus-like particle application [72], and complement-fixing antibody assays [57] are commonly used as serological approaches and to evaluate vaccine efficacy. Recently, a new technology for evaluating antibody affinity maturation from serum was developed using the de novo tandem mass spectrometry antibody sequencing technique [86]. However, this technology can only be applied to dominant antibodies and does not analyze all antibodies elicited by immunization. Conventionally, ELISA with chaotropic reagents (8 M urea or 1 M NaSCN) is used to evaluate the strength of the antibody, which is referred to as avidity. Although these methods have high

throughput, they are imprecise [65, 87]. One limitation of the ELISA avidity assay is that it evaluates the static state, not the dynamic state, of antibody binding. The dissociation constant, k_{dis}, is a critical parameter of antibody affinity maturation but cannot be measured using this assay. Recently, SPR and BLI have been used to measure dynamic states, and k_{dis} has been used to evaluate antibody avidity and affinity maturation. [88-91].

Flaviviridae belongs to a family of positive-sense enveloped single-stranded RNA viruses. Yellow fever (YF) [92], Dengue virus (DENV) [93], Japanese encephalitis virus (JEV) [94], West Nile virus [95], and Zika virus (ZIKV) [96] are famous for mosquito-transmitted viruses. These viruses cause widespread morbidity and mortality worldwide [97]. Most common signs and symptoms of these viral infections include skin rash, fever, arthralgia, myalgia, headache, retro-orbital pain, and conjunctivitis. YF is endemic to Africa and South America, whereas JE is endemic to South and Southeast Asia. Viral vaccines for both these diseases were developed in the 1930s and are widely distributed [92]. However, 200,000 cases and 30,000 deaths caused by YF and JE are still reported annually, and 100,308 cases and 25,125 deaths are estimated to occur annually in 2105 [98, 99]. ZIKV does not cause severe symptoms. However, when pregnant women are infected, microcephaly or other developmental abnormalities have been shown to occur in fetuses and newborn babies [100]. DENV has been one of the most significant pandemic Flaviviridae viruses affecting South Asia and Latin America. An estimated 390 million infections occur annually, of which approximately 96 million are symptomatic [101], and 40,000 deaths occur globally [102]. Two DENV vaccines, Dengvaxia® and Qdenga® (TAK003) [103], have been approved with the aim of eradicating the disease.

Antibody affinity maturation after flavivirus vaccine immunization plays a vital role in protection against viruses. However, few reports on the antibody affinity maturation of the flavivirus vaccine have been published using genetic and serological approaches. In this thesis, the antibody affinity maturation of flavivirus vaccination was elucidated. In the first chapter of this text, I elucidate antibody affinity maturation using genetic approaches, focusing on affinity maturation at the molecular level for mutations in the antibody variable regions. Monoclonal antibodies (mAbs) were discovered from ZIKV vaccine candidate-immunized rabbits and characterized through binding epitopes, binding, and neutralizing activity. Finally, I determined correlations between SHM, CDR mutations, and the kinetic parameters of anti-ZIKV neutralizing mAbs, such as K_D and k_{dis}. The second chapter focuses on assessing antibody affinity maturation using serological approaches. I focused on dynamic kinetic assays to overcome the disadvantages of ELISA avidity assays. Collectively, I developed a novel anti-DENV avidity assay platform using BLI and DENV-VLPs to measure the dissociation constant, k_{dis}, which is a critical parameter of antibody affinity maturation. The assay was optimized for human DENV vaccine-immunized serum and the avidity of DENV phase 2 vaccinated volunteers was measured.

Chapter 1 Somatic Hypermutation and Framework Mutations of Variable Region Contribute to Anti-Zika Virus-Specific Monoclonal Antibody Binding and Function.

Abstract

Zika virus (ZIKV) is a global public health concern due to its ability to cause congenital Zika syndrome and the lack of approved vaccine, therapeutic, or other control measures. I discovered eight novel rabbit monoclonal antibodies (mAbs) that bind to distinct ZIKV envelope protein epitopes. The majority of the mAbs were ZIKV-specific and targeted the lateral ridge of the envelope (E) protein domain III, while the mAb with the highest neutralizing activity recognized a putative quaternary epitope spanning E protein domains I and III. One of the non-neutralizing mAbs specifically recognized ZIKV precursor membrane protein (prM). Somatic hypermutation of immunoglobin variable regions increases antibody affinity maturation and triggers antibody class switching. Negative correlations were observed between the somatic hypermutation rate of the immunoglobin heavy chain variable region and antibody binding parameters such as equilibrium dissociation constant, dissociation constant, and half-maximal effective concentration value of mAb binding to ZIKV virus-like particles. Complementarity-determining regions recognize the antigen epitopes and are scaffolded by canonical framework regions. Reversion of framework region amino acids to the rabbit germline sequence decreased anti-ZIKV mAb binding activity of some mAbs. Thus, antibody affinity maturation, including somatic hypermutation and framework region mutations, contributed to the binding and function of these anti-ZIKV mAbs.

Introduction

Zika virus (ZIKV) is a flavivirus that is transmitted to humans through mosquitoes [104] and can also be transmitted between humans through sexual contact [105] and vertically through pregnancy [106]. ZIKV was initially identified in Africa in 1947 [107]. Epidemics were reported in Micronesia in 2007 [108] and French Polynesia in 2013-14, with the virus subsequently spreading to other countries in Oceania [109, 110]. While most ZIKV infections cause mild disease, in 2015, ZIKV spread rapidly in the Americas and caused clusters of microcephaly and other congenital malformations in infants born to women infected during pregnancy [100]. Infection has been associated with microcephaly and other developmental abnormalities in fetuses and newborn babies [111] and Guillain Barre syndrome, brain ischemia, myelitis, and meningoencephalitis in adults [100, 112]. In February 2016, the World Health Organization (WHO) declared ZIKV a Public Health Emergency of International Concern [100, 113, 114]. The number of ZIKV patients subsequently declined [115]. However, ZIKV circulation has also been detected in numerous Asian and African countries [116], including India [117], Thailand [118], Malaysia [119], Myanmar [120], Angola [116], Kenya [121], Mali [122], and Ethiopia [123], thus the virus still poses a public health threat [115]. No vaccines or therapeutics are available to prevent or treat ZIKV infection or disease.

ZIKV is a positive-stranded RNA virus closely related to other flaviviruses. The viral genome is translated into a single polyprotein post-translationally cleaved by cellular and viral proteases into three structural proteins: capsid, precursor membrane (prM), and envelope (E), and seven nonstructural proteins. ZIKV E protein is the primary immunological determinant for inducing

neutralizing antibodies and consists of three domains: a central β-barrel domain (domain I), an extended finger-like dimerization domain (domain II), and an immunoglobulin-like segment (domain III) [124]. The distal end of DII contains the fusion loop (FL), a hydrophobic sequence that inserts into the host cell endosomal membrane during pH-dependent conformational changes that drive fusion of the viral and cellular membrane. In immature virions, ZIKV E protein forms a complex with the prM protein, which is cleaved in the trans-Golgi network, facilitating E protein rearrangement during virion maturation [125].

The human antibody repertoire is highly diverse due to the ability to randomly assemble variable (V), diversity (D), and joining (J) segments of immunoglobulin genes in B cells [126] during antibody affinity maturation. Antibody affinity maturation functions to increase antibody affinity and specificity, generating antibodies capable of effective antiviral activity [79]. Affinity maturation is initiated by AID, which promotes isotype switching by deaminating deoxycytidines within immunoglobulin genes, leading to SHM and class switch recombination [51]. Immunoglobulin binding affinity and specificity are determined by the amino acids in the CDR, which generally form contacts with the antigen. Immunoglobulins contain six CDRs, three on the heavy chain and three on the light chain. The CDRs undergo a high degree of somatic mutation during antibody affinity maturation. Among CDRs, the heavy chain CDR3 (CDRH3), selected from the D allele, contains the highest degree of diversity in sequence and length [127, 128]. The framework region (FWR) sequences, located between CDRs, form β barrel frameworks to stabilize the structure of the CDRs [51, 129, 130]. While the FWR sequences are generally less tolerant of mutations, recently, the accumulation of FWR mutations in anti-human immunodeficiency virus (HIV) antibodies was found to increase the breadth and potency of

neutralizing antibodies, suggesting that the FWR can also contribute to antibody function [131-133].

Rabbit and human antibodies have similar features not shared by mouse antibodies in terms of B-cell ontogeny and diversity of antibody repertoire [134, 135]. From these diverse repertoires, rabbit mAbs possess features such as high specificity [136], high affinity [137], and CDR3 regions that are similar in length to human CDR3s [138].

Here, I describe ZIKV-specific mAbs isolated after the vaccination of rabbits with a combination of a purified inactivated Zika vaccine (PIZV) candidate and ZIKV Virus-Like Particles (ZIKV-VLPs). The results demonstrate that both SHM and FWR mutations of anti-ZIKV mAbs contribute to antibody affinity, specificity, and functionality.

Materials and Methods

Ethics

All procedures were conducted in compliance with the U.S. Department of Agriculture's Animal Welfare Act (9 CFR Parts 1, 2, and 3); the Guide for the Care and Use of Laboratory Animals (Institute of Laboratory Animal Resources, National Academy Press, Washington, D.C., 2011); and the National Institutes of Health, Office of Laboratory Animal Welfare. Whenever possible, procedures in this study were designed to avoid or minimize discomfort, distress, and pain to animals. The animal immunization experiment protocols were approved by the International Animal Care & Use Committee (IACUC) committee at LabCorp (Denver, PA, USA).

Antigens and other reagents

ZIKV (Strain: PRVABC59, Centers for Disease Control and Prevention (CDC), Fort Collins, USA) was grown in Vero cells, harvested, purified, and formalin-inactivated. These purified inactivated Zika virus (PIZV) were formulated with aluminum hydroxide. DENV-1 VLP (Nauru/Western Pacific/1974), DENV-2 VLP (Thailand/16681/84), DENV-3 VLP (Sri Lanka D3/H/IMTSSA-SRI/2000/1266), DENV-4 VLP (Dominica/814669/1981), ZIKV-VLP (Suriname Z1106033), and ZIKV E protein (Suriname Z1106033) were purchased from The Native Antigen Company (Oxford, UK). DENV-1 (Nauru/Western Pacific/1974), DENV-2 (Thailand/16681/84), DENV-3 (CH53489), and DENV-4 (TVP/360) inactivated viruses were obtained from Microbix Biosystems (Mississauga, ON, Canada). Anti-Flavivirus group antigen-antibody clone D1-4G2-4-15 (4G2) [139] was obtained from Absolute Antibodies (Oxford, UK).

Rabbit immunization and spleen cell preparation

Two New Zealand White female rabbits (LabCorp, Denver, PA, USA) were immunized intramuscularly (IM) with 5 µg of PIZV plus aluminum hydroxide on days 0, 14, 28, 56, and 95. Both rabbits were boosted IM with five µg ZIKV-VLP in Freund's incomplete adjuvant on Day 109, followed by an intravenous injection of 5 µg ZIKV-VLP on Day 130. Splenocytes from rabbits were isolated four days after the final boost. The spleen cells were dispersed, and red cell lysis. The cells were frozen in a freezing medium (90% fetal bovine serum and 10% dimethyl sulfoxide) in liquid nitrogen.

Anti-ZIKV mAb hybridoma generation and clone selection

Eight hundred million rabbit splenocytes were fused with 400 million fusion partner cells (240E-W2 cells) [140] and plated into eighty 96-well plates. The hybridomas were cultured at 37ºC, 5% CO_2. After 14 days, 7,680 multiclonal supernatants were screened by enzyme-linked immunosorbent assay (ELISA) using ZIKV-VLP and ZIKV E Protein. 384 clones were positive for ZIKV-VLP alone, and 19 positive multi clones were selected by both ZIKV-VLP and E protein positive. These multi clones were subcloned by limit dilution, and 155 sub mono clones were determined by mAb production, ZIKV neutralizing activity, ELISA, against DENV1-4 inactivated virus, ZIKV-VLP, and ZIKV E protein, and k_{dis} ranking against ZIKV-VLP using Octet-96 Red (Sartorius, Fremont, CA, USA). I selected fourteen clones with high antibody expression for further characterization, nine with neutralizing activity, and five without neutralizing activity.

DNA sequence analysis of anti-ZIKV mAbs

Hybridoma cells were collected and lysed for poly(A) + mRNA isolation using Poly(A) + RNA isolation kit. RT-PCR reactions were conducted using RNA products and then synthesized cDNA. First, the rabbit IgG variable region of heavy chain and full-length light chain were individually PCR amplified using gene-specific primers. Following gel purification of PCR products, the entire light chain fragment was cloned into a mammalian light chain expression vector. Next, the heavy chain variable fragment was fused with a rabbit heavy chain constant region expression vectors.

Anti-ZIKV mAb expression and purification

To express recombinant rabbit monoclonal antibodies (RabMAb®), the light and heavy chain mammalian expression plasmids were co-transfected into exponentially growing 293-6E cells using lipid-mediated transfection reagent [141]. The serum-free culture supernatant was harvested five days after transfection by centrifugation. The harvested culture medium was centrifuged to remove cell debris, and the clear supernatant containing secreted monoclonal antibodies was purified through MabSelect SuRe protein A column chromatography (Cytiva, Marlborough, MA, USA). The eluted antibody was dialyzed in phosphate-buffered saline (PBS) buffer, sterile filtered, and adjusted to pH 7.4.

Antibody expression and purification of anti-ZIKV allele reverted mAbs

The light and heavy chain of rabbit mAb mammalian expression plasmids were co-transfected into Expi 293 cells systems (Thermo Fisher, Waltham, MA, USA) [142], and the transfected medium was harvested five days after transfection with centrifuging. Monoclonal antibodies were purified through rProtein A Sepharose (Cytiva, Marlborough, MA, USA). The eluted antibody was exchanged to Dulbecco's phosphate-buffered saline, D-PBS (Gibco, Waltham, MA, USA), using Amicon Ultra (Merck Millipore, Burlington, MA, USA).

Allele analysis

Anti-ZIKV mAb allele and CDR3 regions were analyzed by IMGT/V-QUEST (**http://www.imgt.org/IMGT_vquest/analysis**) and NCBI IGBLAST (**https://www.ncbi.nlm.nih.gov/igblast/**). SMH rate, FWR mutation, and CDR mutation were calculated by mutated DNA and proteins in the variable region from the allele sequence.

Neutralization assay

A TCID50-based microneutralization test (MNT) was used for the virus-neutralizing activity of mAbs in 96-well plates. ZIKV (Strain: PRVABC59, CDC, Fort Collins, USA) grown in Vero cells was used as the challenge virus in the neutralization assay. First, hybridoma supernatants or diluted purified mAbs were incubated with 100 TCID50/well of ZIKV infectivity for 1.5 hours at 37ºC 5% CO_2. Next, the ZIKV-mAb mixture was added to Vero cell monolayers in 96-well plates. The plates were incubated at 37ºC 5% CO_2 for five days, and the cytopathic effect was scored under light microscopy. Relative infectivity was plotted against mAb concentration, and IC_{50} values were determined as described previously [143].

Western analysis

Western blot analysis was conducted by a capillary-based electrophoresis system [144] (Wes, ProteinSimple, Santa Clara, CA, USA). In brief, 27 or 240 ng ZIKV-VLP were denatured at 70ºC without reducing agent for 5 minutes, loaded on a Wes assay plate, and electrophoresed. Next, 10 µg/mL of Anti-ZIKV mAb was charged, followed by Wes horseradish peroxidase-conjugated

anti-rabbit secondary antibody. The sample run was analyzed by examining the electropherogram and digital gel image.

Luminex assay

The Luminex assay was conducted by FlexMap 3D (Luminex, Austin, TX, USA), and the conjugation of VLP was previously reported [57]. Briefly, 65 µg ZIKV and DENV-VLP were conjugated to 1-ethyl-3-[3-dimethylaminopropyl] carbodiimide hydrochloride, (ECD)/ N-hydroxy-sulfo-succinimide, (NHS) (Thermo Fisher, Waltham, MA, USA) activated 12.5 million MagPlex beads (Luminex, Austin, TX, USA) at 50 mM 2-(N-morpholino) ethane sulfonic acid buffer pH 7.0 or 6.0 for 120 minutes at room temperature. After conjugation, excess active residues were blocked by Sample buffer (1% bovine serum albumin (BSA) in Dulbecco's phosphate-buffered saline, D-PBS) overnight at 4^{o}C. 10,000 ZIKV and DENV-VLP conjugated beads/mL and anti-ZIKV mAb were incubated at room temperature in sample buffer for 90 minutes and washed with phosphate-buffered saline plus 0.05% Tween-20 (PBST). After washing, the beads were incubated at 10 µg/mL phycoerythrin-labeled anti-rabbit IgG (Thermo Fisher, Waltham, MA, USA) for 60 minutes. The beads were washed and mixed with sheath fluid (Luminex, Austin, TX, USA). The plates were measured fluorescence intensity by FlexMap 3D.

Equilibrium dissociation constant, K_D, measurement

Antibody kinetic analyses were conducted by Octet HTX systems (Sartorius, Fremont, CA, USA). Briefly, 0.1 - 0.3 µg/ml anti-ZIKV mAb were conjugated to amine-reactive second-generation biosensor (AR2G: Sartorius, Fremont, CA, USA) using EDC/ NHS at pH 4.0 or 5.0 acetic buffer. 0.1 - 1.0 µg/mL ZIKV-VLP or 0.2 - 2.0 µg/ml ZIKV E protein in 1x kinetic buffer (Sartorius, Fremont, CA, USA) were associated with anti-ZIKV mAb for 900 seconds and dissociated for 1200 seconds. Kinetic parameters, antibody association constant (k_a), and dissociation constant (k_{dis}) were analyzed by Octet Data Analysis Software HT (ver. 11.1.2.48 Sartorius, Fremont, CA, USA) with the Langmuir 1:1 binding model.

Shotgun Mutagenesis Epitope Mapping

Epitope mapping by shotgun mutagenesis alanine-scanning mutagenesis [145] was performed as described previously [146]. A ZIKV (strain; ZIKV SPH2015) prM/E alanine scanning mutation library was created, individually changing residues to alanine (or alanine residues to serine). A total of 672 ZIKV prM/E mutants (100% coverage of prM/E) were generated and transfected into HEK-293T cells. Cells were fixed in 4% (v/v) paraformaldehyde (Electron Microscopy Sciences, Hatfield, PA, USA) and permeabilized with 0.1% (w/v) saponin in D-PBS plus calcium and magnesium (D-PBS++) before incubation with mAbs diluted in D-PBS++, 10% normal goat serum, and 0.1% saponin. Antibodies were detected using 3.75 µg/mL of AlexaFluor488-conjugated secondary antibody (Jackson ImmunoResearch Laboratories, West Grove, PA, USA) in 10% normal goat serum with 0.1% saponin. Cells were washed three times with D-PBS++/ 0.1% saponin followed by two washes in D-PBS, and mean cellular fluorescence was detected using a high-throughput iQue flow cytometer (Sartorius, Fremont, CA, USA). mAb

reactivities against each mutant prM/E clone were calculated relative to wildtype prM/E reactivity by subtracting the signal from mock-transfected controls and normalizing the wildtype prM/E-transfected controls. The counter-screen strategy facilitates the exclusion of mutants locally misfolded or have an expression defect [147].

Correlation analysis

All data were analyzed by GraphPad Prism (Ver.8.0.0, San Diego, CA, USA). Eight anti-ZIKV mAbs characteristics (102-1, 242-3, 270-12, 289-3, 306-2, 78-2, 278-11, and 11-3) and five neutralizing anti-ZIKV mAbs bound to E protein domain III and I-III characteristics (102-1, 242-3, 270-12, 289-3, and 306-2) were selected for the analysis. I analyzed the correlation between anti-ZIKV mAb variable region mutations (SHM, FWR mutations, CDR mutations), CDR3 length, and antibody functions (EC_{50} of Luminex assay, K_D, k_a, k_{dis} of ZIKV-VLP and IC_{50} of neutralization). All parameters were converted into $\log_{10}$, and the correlations were compared.

Association/ dissociation analysis of FWR mutation reverted anti-ZIKV mAb

Evaluation of anti-ZIKV mAb allele mutation reverted mAb was conducted by Octet HTX (Sartorius, Fremont, CA, USA). Briefly, anti-ZIKV mAbs were diluted to 2 μg/mL in 0.1% BSA-PBST buffer and captured by Protein G biosensor (Sartorius, Fremont, CA, USA). Then, 3 μg/mL ZIKV E protein was associated for 600 seconds and dissociated for 900 seconds in the same buffer.

Results

Binding and neutralization activity of anti-ZIKV mAbs

Fourteen anti-ZIKV mAb clones were isolated from rabbits vaccinated with Takeda's candidate PIZV and boosted with ZIKV-VLP. Based on preliminary screening and characterization, I selected eight mAbs with diverse characteristics (102-1, 242-3, 270-12, 289-3, 306-2, 78-2, 278-11, and 11-3) for further characterization.

Seven mAbs (102-1, 242-3, 270-12, 289-3, 306-2, 11-3, and 278-11) bound specifically to ZIKV-VLP, and one mAb (78-2) was cross-reactive, binding to both to ZIKV and DENV-VLP (**Figure 1A and Table 1**). One mAb (278-11) bound only weakly to ZIKV-VLP. The binding of all mAbs to ZIKV-VLP was at levels greater than a control cross-reactive DENV mAb 4G2 (**Figure 1A**). Five ZIKV-specific mAbs (102-1, 242-3, 270-12, 289-3 and 306-2) demonstrated ZIKV neutralizing activity (Table 1), with mAb289-3 displaying the lowest half maximal inhibitory concentration (IC_{50}) values of ZIKV neutralizing antibody titer (7.8 ng/mL).

Four mAbs (102-1, 242-3, 270-12, and 306-2) bound to ZIKV E protein, as determined by Western analysis, while one mAb (278-11) did not bind to ZIKV E protein but bound to a 30kDa protein, identified as ZIKV prM protein (**Figure 1B and Table 1**). Three mAbs (289-3, 78-2, and 11-3) did not bind to any ZIKV protein on Western analysis, suggesting they might bind quaternary epitopes. The equilibrium dissociation constant (K_D) ranged from 0.19 to 0.57 nM for mAb binding to ZIKV-VLPs and 0.10 to 1.78 nM for mAb binding to soluble ZIKV E protein. For mAbs 102-1, 242-3, 270-12, and 11-3, K_D for ZIKV-VLPs was lower than K_D for ZIKV E protein. (**Figure 2 and Table 1**).

Epitope mapping of anti-ZIKV mAbs

The epitopes recognized by mAbs 102-1, 242-3, 270-12, 289-3, 306-2, 78-2, and 278-11 were mapped by screening for binding against a comprehensive shotgun mutagenesis alanine scanning mutant library covering ZIKV prM/E (**Figure 3 and Table 2**). Three ZIKV neutralizing mAbs (102-1, 242-3, and 270-12) bound epitopes in the lateral ridge of domain III. mAb 102-1 recognized an epitope covering residues T309, T335, G337, S368. The epitope of mAb 270-12 also included residues T335 and S368. mAb 242-3 and 270-12 also recognized domain III lateral ridge, including residues T369 and E370, in addition to residues T335 and S368. mAb 306-2 bound to an epitope including residues I317, T397, H398, H399 at the distal end of domain III. Consistent with its cross-reactivity with DENV, mAb 78-2 bound to residues G100 and L107 in the highly-conserved fusion loop. The shotgun mutagenesis analysis demonstrated that mAb 289-3 recognized a conformational quaternary epitope spanning domains I and III, including amino acid residues E162, G182, K301, G302, and S368. In addition, mAb 278-11 was confirmed to bind prM protein with a linear epitope, including residues D57, E58, G59, and V60.

Antibody allele analysis of anti-ZIKV mAbs

The rabbit anti-ZIKV mAbs all utilized one of two heavy chain variable region alleles, IGHV1S40*01 for mAbs 102-1, 289-3, 306-2, 78-2, and 278-11 and IGHV1S45*01 for mAbs 11-3, 242-3 and 270-12 (**Table 3A**). 242-3 and 270-12 recognize the same two amino acids on the domain III lateral ridge (**Figure 3 and Table 2**). Four alleles for the D region were utilized IGHD1-1*01, 4-1*01, 7-1*01, and 8-1*01, and two alleles for J region, IGHJ4*01 and IGHJ6*01 (Table 3A). The mAbs utilized six alleles of light chain variable region: five kappa chain: IGKV1S10*01 for mAb 289-2 and 11-3, IGKV1S32*01 for 278-11, IGKV1S34*01 for

242-3 and 270-12, IGKV1S36*01 for 306-2, and IGKV1S37*01 for 102-1: one lambda chain IGLV5S3*01 for 78-2. The J region alleles utilized were IGKJ1-2*01 for kappa and IGLJ5*01 for lambda chain (**Table 3B**).

Mutation analysis and CDR3 length of anti-ZIKV mAbs

The protein SHM rate for the mAbs varied from 8.2% to 20.6% for heavy chain and 8.4% to 22.7% for light chain. The CDR mutation rate ranged from 20.0% to 57.9% for the heavy chain CDR1 and 2 and 14.8% to 68.8% for the light chain CDR1-3. The FWR was mutated from 3.8% to 15.2% for heavy chain and 6.3% to 17.7% for light chain (**Figure 4A, B and Table 3A, B**). The CDRH3 lengths ranged from 10 - 18 amino acids for heavy chain and 12 - 16 amino acids for light chain. I analyzed the neutralizing mAbs to understand the contribution of the heavy chain mutations and CDRH3 length to specificity and neutralization activity. The two ZIKV-specific neutralizing mAbs that demonstrated the highest SHM/ FWR mutation rates were mAb 102-1 (20.6%/ 11.5%) and mAb 289-3 (18.6%/ 15.2%) which recognizes a quaternary epitope. On the other hand, the neutralizing mAb 306-2, which recognizes an epitope at the distal end of domain III, had the lowest SHM/ FWR mutation rate, 8.2%/ 3.8%. (**Figure 4A and Table 3A**). Consistent with the high SHM/ FWR mutation rates, the quaternary mAb 289-3 had the most extended CDR3 length at 18 amino acids. The CDR1,2 mutation rate of mAb 289-3 was 33.3%. The CDR3 length of the mAb 102-1 was 12 amino acid residues, with a high CDRH1,2 mutation rate of 57.9%. The CDR3 length of mAb 306-2 was the shortest among the mAbs at ten amino acids, with a CDRH1,2 mutation rate of 26.3%. (**Figure 4A and Table 3A**). The other two neutralizing mAbs 242-3 and 270-12 had similar sequences with an amino acid identity of 99% and similar epitope recognition in the lateral ridge of domain III, SHM/ FWR mutation rates (mAb 242-3: 12.1%/ 6.3%, mAb 270-12: 11.1%/ 5.1%) and CDR3 lengths, (17 amino acids for

both) that were intermediate between mAbs 289-3 and 306-2. Interestingly, the ZIKV prM-specific non-neutralizing mAb 278-11 also had a high SHM/ FWR mutation rate of 17.9%/ 11.5% and a high CDRH1,2 mutation rate of 47.1%. The CDR3 length of mAb 278-11 was 12 amino acids. In conclusion, among ZIKV-specific neutralizing mAbs, I observed higher somatic mutation and the longest CDR3 length in the mAb recognizing a quaternary epitope. There was no clear trend between epitope mapping information and SHM, FWR mutation, and CDR information for the light chain variable region, except that the longest CDR3 length (16 amino acids) was also observed in mAb 289-3, which recognizes a quaternary epitope (**Figure 4B and Table 3B**).

Correlations among anti-ZIKV mAb variable region mutations, CDR3 length, and antibody binding parameters in ZIKV neutralizing antibodies

I analyzed the correlation between binding parameters and SHM, CDR and FWR mutation, and CDR3 length for all eight neutralizing and non-neutralizing anti-ZIKV mAbs (**Figure 5A, B and Table 4A, B**). Two parameters were negatively correlated: heavy chain CDR mutation/ K_D ($r = -0.722$, $p = 0.043$, **Figure 5E**) and light chain CDR mutation/ association constant (k_a) ($r = -0.708$, $p = 0.050$, **Figure 5F**). There were weak negative to no correlations for other parameters (r: -0.546 - 0.427). Focusing on the five ZIKV- neutralizing mAbs, 102-1, 242-3, 270-12, 289-3, and 306-2, I observed negative correlations between binding parameters and heavy chain SHM, CDRH, and FWR mutation rates (r: -0.985 - -0.264, **Figure 5C and Table 4C**). There were significant negative correlations between SHM and VLP binding Luminex EC_{50} ($r = -0.971$, $p = 0.006$, **Figure 5G**), FWR mutations and VLP binding Luminex EC_{50} ($r = -0.924$, $p = 0.025$, **Figure 5H**), CDR mutations and K_D, ($r = -0.920$, $p = 0.027$, **Figure 5I**) and CDR mutations and k_{dis} ($r = -0.985$, $p = 0.002$, **Figure 5J**). While correlations between CDRH3 length and binding

parameters were low, there was a trend for correlation between CDRH3 length and neutralizing antibody EC_{50} values (r = -0.831, p = 0.081, **Figure 5K**). Overall, correlations were weaker between binding and light chain parameters, SHM, FWR mutation, and CDR length (r: -0.825 - 0.186: **Figure 5D and Table 4D**). Contrary to the other observations, CDR mutation parameters showed positive correlations (r: 0.049- 0.826).

Impact of framework amino acids on the binding activity of anti-ZIKV mAbs

To understand the impact of the FWR mutations on mAb binding, all FWR amino acids of anti-ZIKV domain I-III and III mAb 102-1, 270-12, 289-3, and 306-2 were reverted to the germline amino acids of the allele and characterized (**Figure 6 and Table 5**). Reversion of 4 FWR H chain and 12 FWR L chain amino acids in mAb 270-12 resulted in the loss of binding activity to ZIKV E protein and reduced binding to ZIKV-VLPs (**Figure 6B and F**). Reversion of 9/ 9 and 3/ 5 amino acids of FWRH/ FWRL chains of mAb 102-1 and 306-2 increased the dissociation rate of ZIKV E protein binding. However, there were no differences in binding to ZIKV-VLPs (**Figure 6A, D, E, and H**). Although the highest rate of mutation of FWR H and L chains was observed in mAb 289-3, reversion of 13 FWRH and 9 FWRL amino acids of mAb 289-3 did not alter binding to either ZIKV E protein or ZIKV-VLPs (**Figure 6C and G**).

Discussion

I identified and characterized eight unique ZIKV-specific rabbit mAbs with diverse qualities, including epitope specificity, neutralizing activity, and degree of affinity maturation. Rabbits represent an alternative species to generate mAbs with properties similar to human mAbs.

Rabbits are evolutionarily distinct from mice and other rodents, and rabbit and rodent antibody ontogeny also differ [135]. Rabbit antibodies have a long average CDRH3 of 14.8 ± 3.6 amino acids, similar to the average human CDRH3 length, 15.3 ± 4.0 amino acids, and longer than the average mouse CDRH3 length of 11.1 ± 2.0 [138]. The rabbit CDRH3 length likely contributed to the neutralizing properties of anti-ZIKV mAbs directed to conformational and quaternary epitopes. Human conformational anti-ZIKV neutralizing antibodies have been described with CDRH3 lengths of 15 - 26 amino acids [138, 148-150]. The CDRH3 length of the rabbit anti-ZIKV neutralizing mAbs recognizing conformational epitopes described herein had 12 - 18 CDRH3 amino acids. Rabbit immunoglobulin genes also undergo a high degree of variable region rearrangement [138]. The SHM rates of the identified rabbit anti-ZIKV mAb genes ranged from 5.4% to 10.5%, compared to SHM rates of published human and mouse anti-ZIKV mAbs of 2.7% to 10.4% [151, 152].

Potently neutralizing ZIKV-specific human mAbs have been described that map to the domain III lateral ridge [143, 146, 151, 153], domain II [146, 154], or to complex epitopes spanning multiple domains [155, 156], while fusion loop-specific mAbs are more likely to be cross-reactive with DENV [150]. Three of the rabbit mAbs described here map to the domain III lateral ridge. This region is also targeted by several mouse and human mAbs that have demonstrated ZIKV-neutralizing activity and protective immunity in mouse models, suggesting that this is an immunodominant region for ZIKV-specific neutralizing antibodies in multiple species [146, 153, 154, 157]. The epitopes recognized by mAbs 102-1 and 270-12 include residue S368 in the domain III lateral ridge, which has been determined to be an important residue for human ZIKV-specific neutralizing antibodies [158]. mAb 242-3 also recognized the domain III lateral ridge, but while S368 was not identified as a critical residue, the adjacent

residues T369 and E370 were identified as critical. Other human ZIKV-specific neutralizing antibodies, including ZIKV-116, 7B3, and ZK2B10 recognize domain III lateral ridge epitopes [146, 154, 159] whose residues are overlapping but distinct from those of the rabbit mAbs described herein. These results suggest that domain III immunodominant ZIKV-specific epitopes recognized by neutralizing rabbit mAbs are similar to epitopes recognized by human ZIKV-specific mAbs, with the exception of ZIKV-specific neutralizing mAb, 306-2, which recognizes a novel conformational epitope at the distal end of domain III.

Potently neutralizing antibodies recognizing complex and quaternary epitopes have been described for a number of viruses, including ZIKV, DENV, and HIV [152, 155, 160, 161]. Among the mAbs described herein, mAb 289-3 had the most potent neutralizing activity and recognized a quaternary epitope, including critical amino acids in both domains I and III. Previously, a rationally engineered mAb designed to target a quaternary epitope spanning an epitope proximal to the fusion loop could broadly neutralize ZIKV strains and conferred protection against vertical transmission and fetal mortality in mice [155]. Modeling studies suggest that mAbs targeting this region may constrain the E protein structure and block fusion [155]. Further studies will be required to determine the structure of mAb 289-3 complexed with ZIKV E protein. Three ZIKV-specific human mAbs that also span an epitope in domains I and III have recently been described [152, 156]. Alanine-scanning mutagenesis identified the critical residues recognized by two of these mAb, B11F, and A9E, as mapping within domain I alone. Two critical domain I residues of mAb 289-3, E162 and G182, are described as escape mutation sites for mAb A9E [156, 162]. I also note that the critical residues K301 (domain III) and G182 (domain I) were also identified by shotgun mutagenesis analysis as critical for binding by the

third mAb, protective anti-ZIKV mAb, MZ4, which binds a site centered on the E protein domain I/III linker region [152].

CDRH3 length was associated with increased neutralizing antibody activity. A high degree of SHM and relatively long CDRH3 have been associated with the evolution of potent neutralization activity as well as with the recognition of complex quaternary epitopes [163]. Among the mAbs with ZIKV neutralizing activity, the binding strength was associated with higher heavy chain SHM, CDRH, and FWR mutation rates. My findings were consistent with those for anti-ZIKV EDE1 mAbs C8 and C10, which bind across E protein dimers to strongly neutralize ZIKV [164] and show a high rate of heavy chain gene SHM, 6.9%, and 2.8%, and longer CDRH3 length, 15 and 21 amino acid residues, respectively [150]. The association between somatic mutation rate and increased antibody affinity is well established [49, 127, 165]. Characterization of mAb 289-3 demonstrates that a high degree of SHM and long CDRH3 can be achieved by ZIKV vaccination and can lead to the evolution of antibodies with potent ZIKV-specific neutralizing activity.

As expected, strong correlations were observed between antibody binding parameters and heavy chain CDR mutation rate since CDRs comprise the antigen-binding site. Strong correlations were also observed between antibody binding parameters and FWR mutation rate, which was less expected as FWRs likely do not directly bind but provide structural support for the CDR regions. FWR mutations may increase antibody flexibility, facilitating CDR contact with epitopes [132, 133]. The role of FWR mutations in the potency and neutralization of anti-HIV mAbs depends on the specific antibody [166]. FWR mutations are important for mAbs against anti-vascular endothelial growth factor [133], and FWR mutations have been widely applied to stabilize the structure of humanized mAbs derived from mice [167]. I found that the binding activity of mAbs

102-1, 306-2, and 270-12 were impacted by the reversion of FWR mutations but that FWR mutations were not essential for the binding activity of the most potent mAb, 289-3. This result for mAb 289-3 was different from my expectations since eight amino acids, the highest number among four mAbs, were changed in heavy chain FWR3 regions supporting CDR3, and the threonine residue at position 92 (in the international ImMunoGeneTics information system, IMGT numbering) [168] was mutated to proline. Although the introduction of proline residue might be thought likely to perturb the FWR structure, a proline at position 61 was critical for the thermal stability of a broadly neutralizing anti-HIV mAb 3BNC60 [131]. Further studies are required to fully understand the role of FWR amino acids in anti-flavivirus mAb specificity and activity.

In summary, I discovered eight ZIKV-specific mAbs against distinct regions of envelope and prM proteins, including a potent neutralizing mAb that recognized a quaternary epitope spanning domains I and III and a non-neutralizing mAb that recognized a linear epitope on the ZIKV prM protein. Detailed characterization of the rabbit mAbs demonstrated that ZIKV-specific mAbs recognizing conformational and quaternary epitopes on the ZIKV E protein bind with high affinity and are neutralizing. There were significant correlations between the SHM rate, FWR mutation rate, and antibody binding parameters. The higher degree of CDR mutation and SHM, and longest CDRH3 were found in a mAb recognizing a quaternary epitope spanning ZIKV E domains I and III. For some mAbs, reversion of FWR mutations to the germline allele reduced the affinity of antigen-binding. Thus, I conclude that both SHM and FWR mutations of anti-ZIKV mAbs contribute to antibody affinity, specificity, and functionality.

Figures

Figure 1 Reactivity of anti-ZIKV mAbs

A: reactivity of anti-ZIKV mAbs with ZIKV and DENV virus-like particles (VLP) using Luminex assay. ZIKV and DENV-VLP were conjugated to MagPlex beads (Luminex) and 10,000 beads/mL of these beads mixed with 0.2 pg/mL to 10 µg/mL of anti-ZIKV mAbs clones, mAb 102-1, 242-3, 270-12, 289-3, 306-2, 11-3, 278-11, 78-2 and 4G2 for 90 min at room temperature. B. Western blot analysis of anti-ZIKV mAbs. ZIKV-VLP were heat-denatured in non-reduced conditions at 70°C for five min. 27 ng for left and 240 ng for right, were electrophoresed by Wes capillary and detected by 10 µg/mL of anti-ZIKV mAb clones, left mAb 102-1, 242-3, 270-12, 289-3, 306-2, 78-2 and 11-3, right mAb 278-11. M: molecular weight marker. The estimated molecular weight of ZIKV E protein is 55 kDa, and prM protein is 23 kDa.

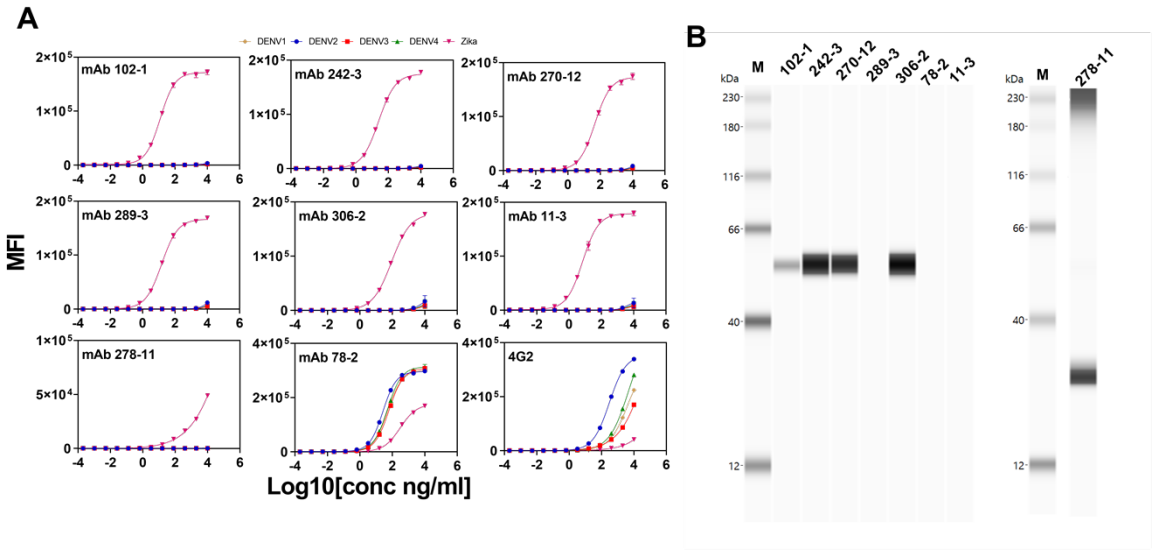

Figure 2 Kinetic analysis of anti-ZIKV mAbs

Kinetic analysis was conducted by Octet HTX (Sartorius). Anti-ZIKV mAbs were conjugated to amine-reactive 2nd generation, AR2G, biosensor at 0.1 to 0.3 μg/mL, and the association constant (k_a) measured over 0 to 900 seconds, and dissociation constant (k_{dis}) for 1200 seconds for ZIKV-VLP or E proteins in various concentrations. A: mAb 289-3 and 102-1 to ZIKV-VLP 3.3 - 16.7nM, B: mAb 289-3 and 102-1 to ZIKV E proteins 6.67 - 33.3 nM, red line: fitting pattern. C: k_a/k_{dis} plot for anti-ZIKV mAbs to ZIKV-VLP and ZIKV E proteins: Blue: mAb 78-2, 289-3, 306-2 and 278-11, Red: mAb 102-1, 242-3. 270-12 and 11-3. k_a and k_{dis} values were calculated by two runs, and the average values were shown. Values (nM) for equilibrium dissociation constant (K_D) are shown for each dotted line.

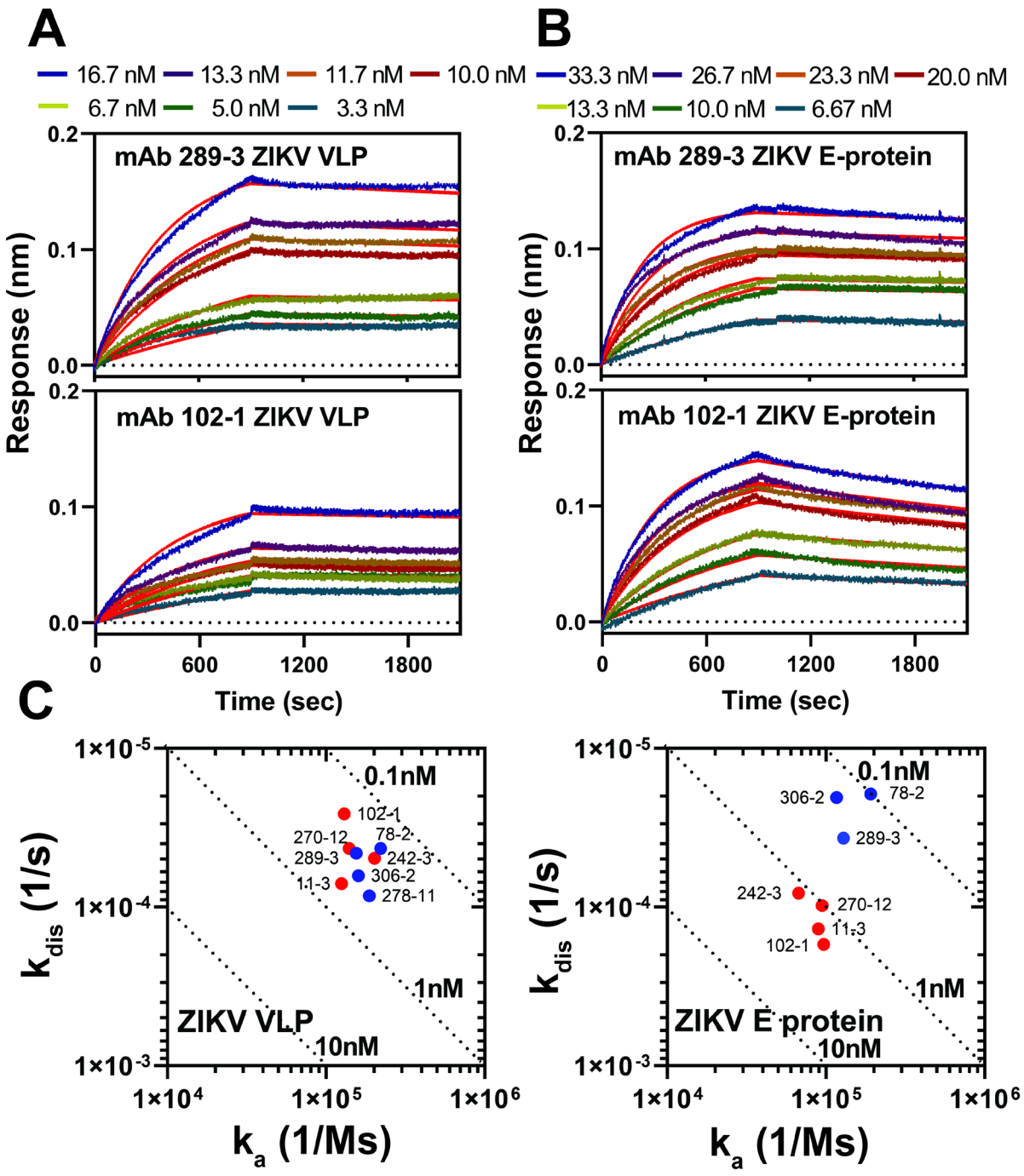
A
16.7 nM
13.3 nM
11.7 nM
10.0 nM
6.7 nM
5.0 nM
3.3 nM
mAb 289-3 ZIKV VLP
mAb 102-1 ZIKV VLP
Response (nm)
Time (sec)
B
33.3 nM
26.7 nM
23.3 nM
20.0 nM
13.3 nM
10.0 nM
6.67 nM
mAb 289-3 ZIKV E-protein
mAb 102-1 ZIKV E-protein
C
0.1nM
1nM
10nM
ZIKV VLP
ZIKV E protein
102-1
270-12
78-2
289-3
242-3
11-3
306-2
278-11
k_dis (1/s)
k_a (1/Ms)

Figure 3 Epitope mapping of anti-ZIKV mAbs

Critical residues (green spheres) for antibody binding are visualized on a crystal structure of the ZIKV E protein dimer (Protein Data Bank (PDB) ID: 5IRE, Sirohi et al., 2016) or on a cryo-electron microscopy (EM) structure of ZIKV precursor membrane prM protein, for 278-11 (PDB ID: 5U4W, Prasad et al., 2016). Secondary residues (grey spheres) that may contribute to binding are also shown. Red: E protein domain I, Yellow: domain II, Blue: domain III. Detailed data are shown in **Table 2**.

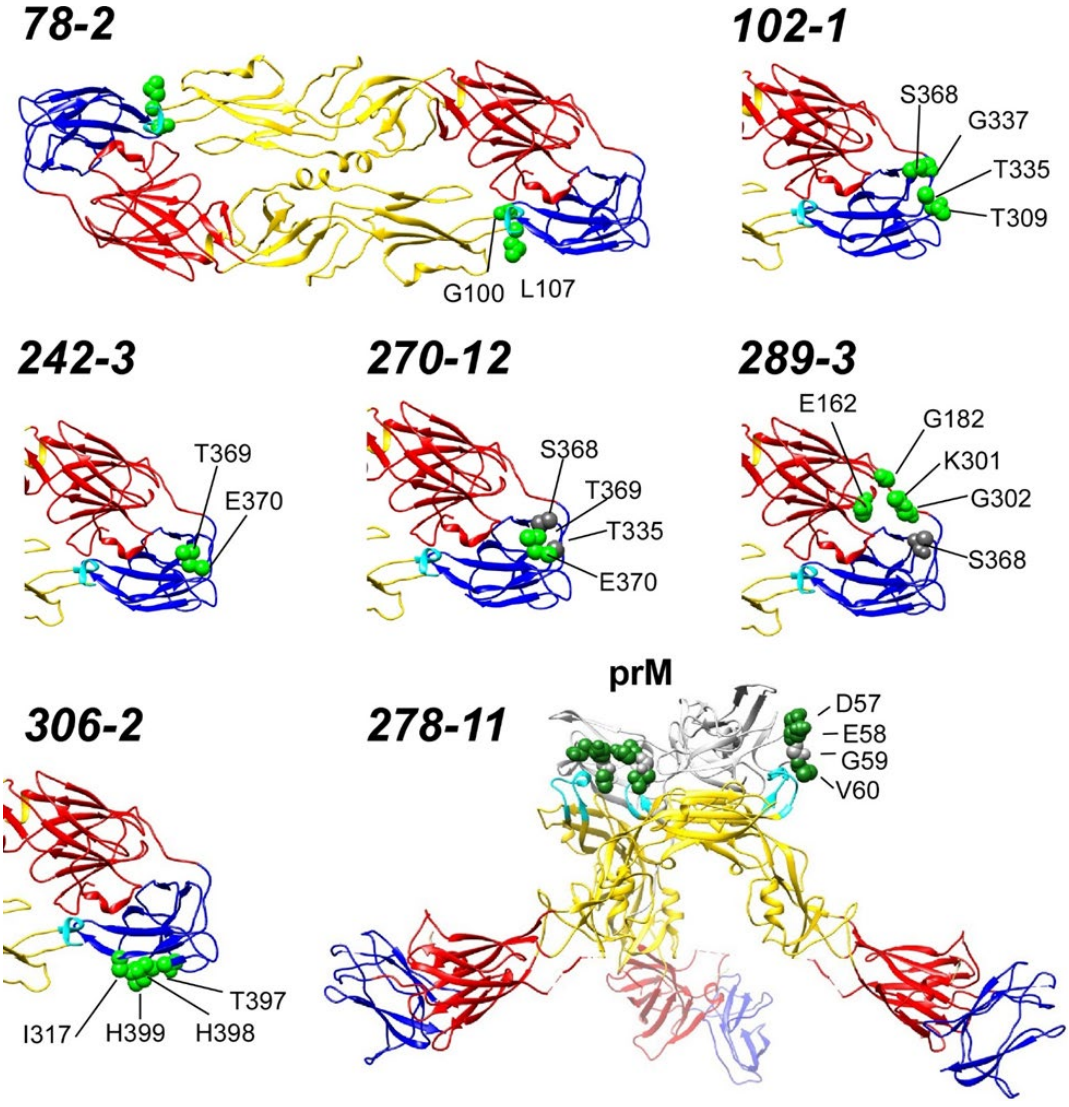

Figure 4 Variable region mutations and CDR 3 length of anti-ZIKV mAbs

Somatic hypermutation (SHM), framework region (FWR) mutations, CDR mutations, and CDR3 amino acid length of anti-ZIKV mAbs. A: Heavy chain variable region, B: Light chain variable region. Binding ZIKV amino acid residues and ZIKV domains were shown for each mAb (detailed data were in Table 3). Blue bar: mAb epitopes: ZIKV E protein domain III or domain I-III, Green bar: mAb epitope: ZIKV E protein Fusion loop (FL), Yellow bar: mAb epitope: ZIKV precursor membrane (prM) protein. Bolded amino acid residues: critical amino acid of ZIKV E protein and prM protein for anti-ZIKV mAb binding (Table 2).

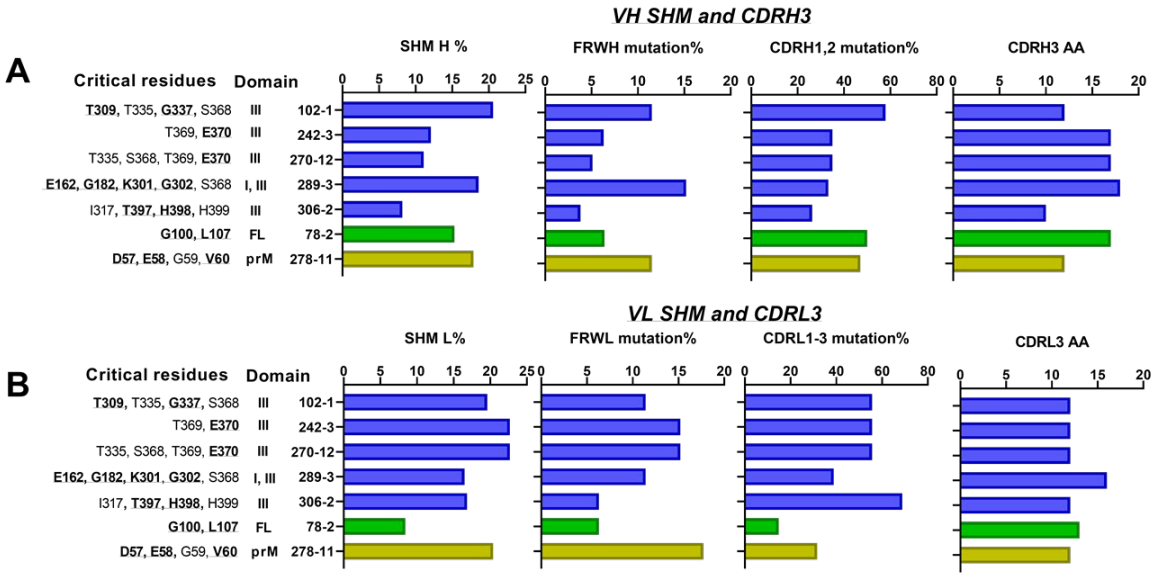

Figure 5 Correlation analysis of anti-ZIKV MAb somatic hypermutations, CDR length, and antibody binding parameters.

A - D: r values of correlation analysis between anti-ZIKV mAb somatic hypermutation (SHM), CDR mutation, Framework region (FWR) mutation, CDR3 amino acid length, and antibody binding parameters. A, B: Binding parameters of eight all anti-ZIKV mAbs: mAb102-1, 242-3, 270-12, 306-2, 289-3, 78-2, 278-11, and 11-3. C, D: anti-ZIKV neutralizing mAbs: mAb 102-1, 242-3, 270-12, 306-2, and 289-3. E - K: Correlation analysis of anti-ZIKV mAb SHM, CDR, FWR mutations and CDR3 length, and binding parameters. E: Correlation between heavy chain CDR mutations and equilibrium dissociation constant (K_D) for all anti-ZIKV mAbs, F: Correlation between light chain CDR mutations and association constant (k_a) for all anti-ZIKV mAbs, G: Correlation between heavy chain SHM rate and Luminex assay EC_{50} value for anti-ZIKV neutralizing mAbs, H: Correlation between heavy chain FWR mutation rate and Luminex assay EC_{50} value for anti-ZIKV neutralizing mAbs, I: Correlation between heavy chain CDR mutation rate and K_D for anti-ZIKV neutralizing mAbs, J: Correlation between heavy CDR mutation rate and dissociation constant (k_{dis}) for anti-ZIKV neutralizing mAbs, K: Correlation between heavy chain CDR3 length and microneutralization test (MNT) IC_{50} value for anti-ZIKV neutralizing mAbs. Plot and linear regression curves: Red; $p < 0.05$, Blue: $p > 0.05$

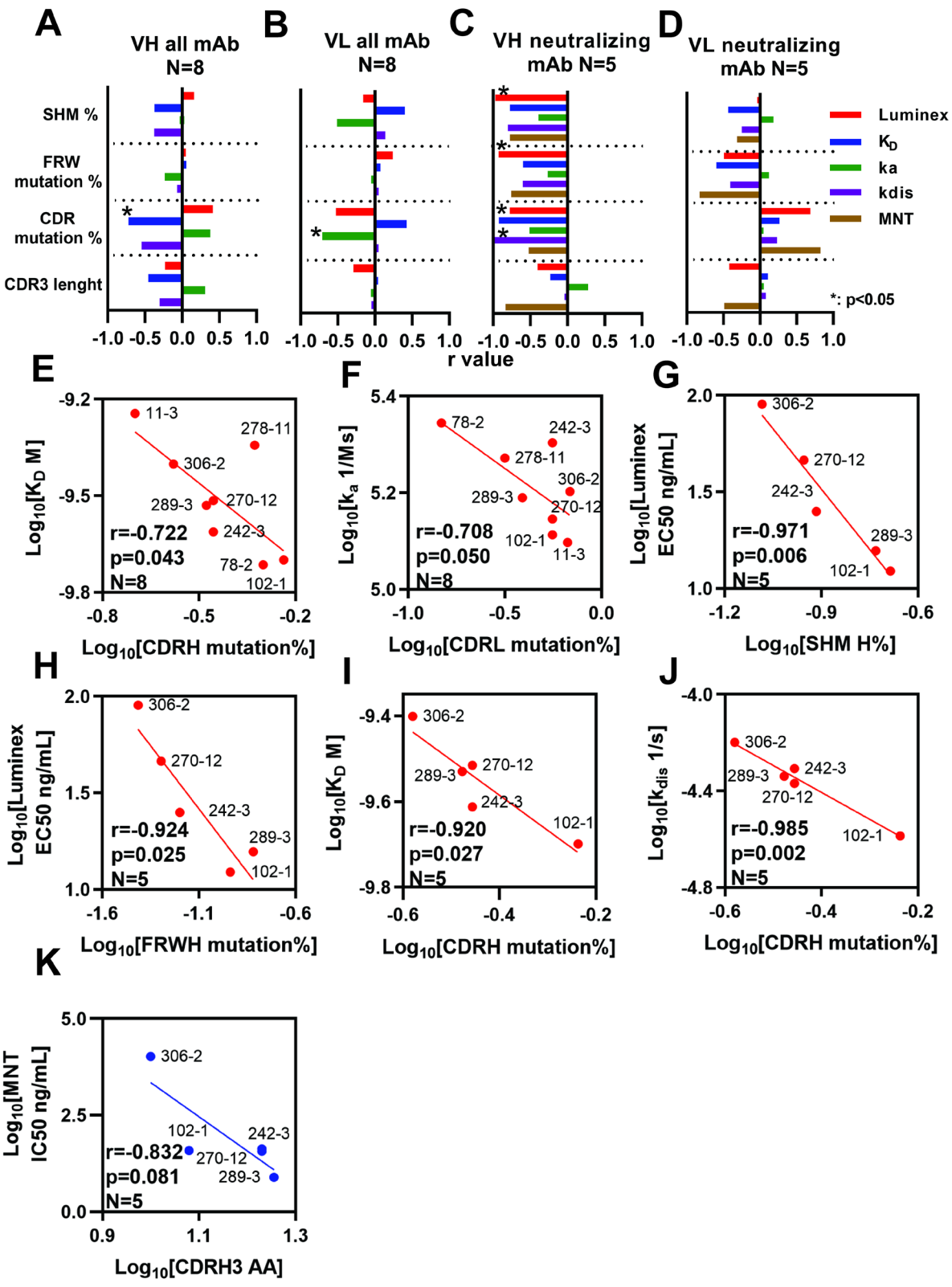
A
VH all mAb N=8
B
VL all mAb N=8
C
VH neutralizing mAb N=5
D
VL neutralizing mAb N=5
SHM %
FRW mutation %
CDR mutation %
CDR3 lenght
Luminex
KD
ka
kdis
MNT
*: p<0.05
r value
E
Log10[KD M]
r=-0.722
p=0.043
N=8
Log10[CDRH mutation%]
F
Log10[ka 1/Ms]
r=-0.708
p=0.050
N=8
Log10[CDRL mutation%]
G
Log10[Luminex EC50 ng/mL]
r=-0.971
p=0.006
N=5
Log10[SHM H%]
H
Log10[Luminex EC50 ng/mL]
r=-0.924
p=0.025
N=5
Log10[FRWH mutation%]
I
Log10[KD M]
r=-0.920
p=0.027
N=5
Log10[CDRH mutation%]
J
Log10[kdis 1/s]
r=-0.985
p=0.002
N=5
Log10[CDRH mutation%]
K
Log10[MNT IC50 ng/mL]
r=-0.832
p=0.081
N=5
Log10[CDRH3 AA]

Figure 6 Binding activity of framework region (FWR) amino acid reverted anti-ZIKV mAb

A - D: Association and dissociation analysis of FWR amino acid reverted anti-ZIKV mAbs by Octet HTX (Sartorius), 2 μg/mL mAbs were captured to Protein G biosensor (Sartorius), and 3 μg/mL of ZIKV E protein were associated for 600 seconds and dissociated for 900 seconds. E - H. Reactivity of anti-ZIKV mAbs of ZIKV-VLP using Luminex assay. Blue: anti-ZIKV mAbs with matured amino acid, Red: anti-ZIKV mAbs with revert amino acid to allele. A and E: mAb 102-1, B and F: mAb 270-12, C and G: mAb 289-3, D and H: mAb 306-2

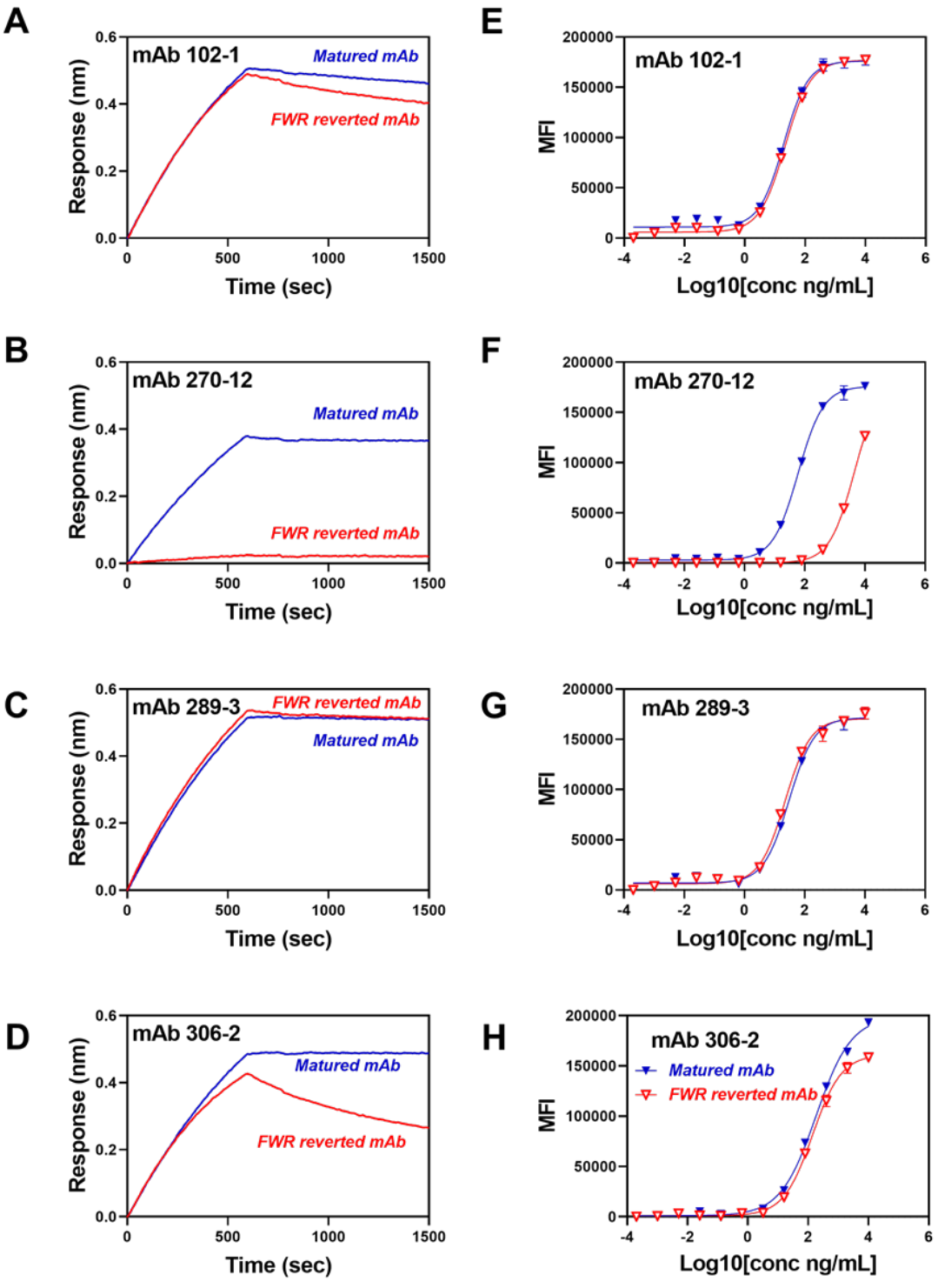
A
mAb 102-1
Matured mAb
FWR reverted mAb
Response (nm)
Time (sec)
B
mAb 270-12
Matured mAb
FWR reverted mAb
Response (nm)
Time (sec)
C
mAb 289-3
FWR reverted mAb
Matured mAb
Response (nm)
Time (sec)
D
mAb 306-2
Matured mAb
FWR reverted mAb
Response (nm)
Time (sec)
E
mAb 102-1
MFI
Log10[conc ng/mL]
F
mAb 270-12
MFI
Log10[conc ng/mL]
G
mAb 289-3
MFI
Log10[conc ng/mL]
H
mAb 306-2
Matured mAb
FWR reverted mAb
MFI
Log10[conc ng/mL]

Tables

Table 1 Summary of characterization of anti-ZIKV mAbs

clone	Luminex assay			MNT titer	Kinetic analysis VLP			Kinetic analysis E protein		
	Specificity [a]	EC_{50} ng/mL	Western reactivity [b]	IC_{50} ng/mL[c]	K_D nM	k_a 1/Ms	k_{dis} 1/s	K_D nM	k_a 1/Ms	k_{dis} 1/s
102-1	ZIKV	12.3	E	38.4	0.20	1.30×10^5	2.59×10^{-5}	1.78	9.67×10^4	1.72×10^{-4}
242-3	ZIKV	25.1	E	42.8	0.24	2.02×10^5	4.93×10^{-5}	1.22	6.71×10^4	8.16×10^{-5}
270-12	ZIKV	46.2	E	37.2	0.31	1.40×10^5	4.27×10^{-5}	1.04	9.45×10^4	9.80×10^{-5}
289-3	ZIKV	15.7	ND	7.8	0.30	1.55×10^5	4.58×10^{-5}	0.29	1.29×10^5	3.68×10^{-5}
306-2	ZIKV	89.9	E	10547	0.40	1.60×10^5	6.34×10^{-5}	0.17	1.17×10^5	2.04×10^{-5}
78-2	CR	303	ND	ND	0.19	2.21×10^5	4.28×10^{-5}	0.10	1.92×10^5	1.94×10^{-5}
278-11	ZIKV	23800	prM	NT	0.45	1.87×10^5	8.49×10^{-5}	NT	NT	NT
11-3	ZIKV	6.93	ND	ND	0.57	1.25×10^5	7.13×10^{-5}	1.53	8.98×10^4	1.37×10^{-4}

a:Specificity: ZIKV: ZIKV specific, CR: cross-reactive, b: Western reactivity: E: envelope protein, prM: precursor membrane protein, ND: not detected, c: MNT: microneutralization test, NT: not tested, ND: not detected.

Table 2 Critical amino acid residues on ZIKV E/prM protein important for anti-ZIKV mAb binding

	Antibody Binding Reactivity (% WT)							
	Mutation	**278-11[a]**	**78-2**	**102-1**	**242-3**	**270-12**	**289-3**	**306-2**
prM	D57A	**0.8 (1)**	123.3 (8)	84.5 (1)	91.9 (0)	105.1 (3)	97.92 (0)	122.1 (38)
	E58A	**14.7 (3)**	129.5 (3)	84.0 (9)	96.8 (9)	93.1 (6)	83.9 (18)	117.1 (36)
	G59A	28.5 (3)	116.7 (10)	99.4 (3)	94.9 (0)	99.3 (1)	93.6 (2)	127.6 (6)
	V60A	**19.9 (5)**	113.1 (3)	77.6 (4)	97.2 (7)	85.9 (4)	96.7 (16)	100 (36)
E	G100A	95.1 (0)	**18.9 (1)**	72.7 (9)	70.3 (4)	63.6 (2)	72.7 (9)	105.4 (34)
	L107A	-	**17.3 (0)**	97.1 (19)	121.9 (6)	89.8 (4)	96.8 (27)	98.8 (9)
	E162A	77.8 (21)	101.3 (1)	89.9 (10)	79.6 (11)	84.5 (0)	**4 (0)**	83 (18)
	G182A	85.9 (5)	110.5 (3)	93.2 (8)	85.6 (6)	75.5 (9)	**2.8 (0)**	122.1 (39)
	K301A	-	82.5 (4)	91.3 (7)	78.7 (14)	79.1 (3)	**7.2 (1)**	64.8 (7)
	G302A	-	69.2 (14)	89.1 (2)	68.3 (13)	79.1 (0)	**11.5 (2)**	58.8 (10)
	T309A	-	96.2 (17)	**2.9 (2)**	103.9 (6)	78 (7)	65.2 (8)	72.5 (7)
	I317A	-	61.2	85.7 (6)	111.8 (40)	106.8 (5)	106.8 (25)	17.6 (4)
	T335A	-	71.6 (13)	21.5 (2)	36.2 (15)	30.1 (1)	54 (4)	25.5 (25)
	G337A	-	59.7 (32)	**2.5 (0)**	48.3 (20)	45.1 (1)	40 (11)	127 (0)
	S368A	-	87.5 (0)	26.3 (3)	89.1 (15)	39.8 (4)	23.8 (10)	71.4 (21)
	T369A	-	113.0 (2)	66.4 (4)	34.5 (13)	20.8 (7)	73.6 (7)	79.2 (7)
	E370A	-	92.7 (6)	84.4 (8)	**12.6 (3)**	**5 (2)**	109.6 (2)	101.6 (5)
	T397A	-	147	97.3 (6)	110.9 (11)	78.6 (3)	94.7 (20)	**0.9 (2)**
	H398A	-	92.9 (13)	80.3 (3)	77.2 (9)	76.3 (1)	55 (7)	**3.9 (3)**
	H399A	-	97.2 (0)	110.1 (1)	127.1 (24)	99.2 (11)	80.2 (10)	23 (2)

mAb binding data for all prME clones identified as critical for mAb binding. mAb reactivities for each mutant are expressed as percent of binding to wildtype prME, with ranges (half of the maximum minus minimum values) in parentheses. Values are bold and shaded in grey for critical residues and shaded in grey for secondary residues. At least two replicate values were obtained for each experiment. a: mAb 278-11 was screened only on a subset of the prME library clones that contained the mutations covering the prM protein. Abbreviation: E: envelope protein, prM: precursor membrane protein, WT: wild type, prME: precursor membrane and envelope protein

Table 3 Summary of anti-ZIKV mAb allele and analysis

A: Heavy Chain

clones	V region	VH SHM(%)		FWR AA mutation (%)	CDR1,2 AA mutation (%)	CDR3 AA (N)	CDR3 Amino acid sequences	D region	J region
		DNA (%)	Protein (%)						
102-1	IGHV1S40*01	9.4%	20.6%	11.5%	57.9%	12	IISTGGSHRFNL	IGHD1-1*01	IGHJ4*01
242-3	IGHV1S45*01	5.7%	12.1%	6.3%	35.0%	17	ARSSYPDSSGYSYGMDL	IGHD1-1*01	IGHJ6*01
270-12	IGHV1S45*01	5.4%	11.1%	5.1%	35.0%	17	ARSSYPDSSGYSYGMDL	IGHD1-1*01	IGHJ6*01
289-3	IGHV1S40*01	10.4%	18.6%	15.2%	33.3%	18	ARAIAVGAGYGVGNYFTL	IGHD7-1*01	IGHJ4*01
306-2	IGHV1S40*01	5.8%	8.2%	3.8%	26.3%	10	ARHPGTYFTL	IGHD8-1*01	IGHJ4*01
78-2	IGHV1S40*01	8.1%	15.3%	6.4%	50.0%	17	ARDLPSFTAPYAGYLRL	IGHD7-1*01	IGHJ4*01
278-11	IGHV1S40*01	10.5%	17.9%	11.5%	47.1%	12	ARYNTGGFYYDL	IGHD4-1*01	IGHJ4*01
11-3	IGHV1S45*01	5.4%	12.1%	10.1%	20.0%	13	ARGGSTAAAGFNL	IGHD7-1*01	IGHJ4*01

B: Light Chain

clones	V region	VL SHM(%)		FWR AA mutation (%)	CDR1-3 AA mutation (%)	CDR3 AA (N)	CDR3 Amino acid sequences	J region
		DNA (%)	Protein (%)					
102-1	IGKV1S37*01	10.7%	19.6%	11.4%	55.6%	12	QATDVGGSGRGA	IGKJ1-2*01
242-3	IGKV1S34*01	10.9%	22.7%	15.2%	55.6%	12	QTYYDISNYGYA	IGKJ1-2*01
270-12	IGKV1S34*01	11.3%	22.7%	15.2%	55.6%	12	QTYYDISNYGYA	IGKJ1-2*01
289-3	IGKV1S10*01	8.2%	16.5%	11.4%	38.9%	16	QSYYTSSSNADGSENA	IGKJ1-2*01
306-2	IGKV1S36*01	8.4%	16.8%	6.3%	68.8%	12	QTYYYYNKIING	IGKJ1-2*01
78-2	IGLV5S3*01	5.3%	8.4%	6.3%	14.8%	13	YTVHATESSLHYV	IGLJ5*01
278-11	IGKV1S32*01	11.2%	20.4%	17.7%	31.6%	12	QQGYSSNDADNT	IGKJ1-2*01
11-3	IGKV1S10*01	10.3%	19.6%	8.9%	66.7%	13	QCNDYGGTYVPNA	IGKJ1-2*01

Abbreviation V region: variable region, VH: heavy chain variable region, VL: light chain variable region, SHM: somatic hypermutation, CDR: complementarity-determining region, FWR: framework region, D: diversity region, J region: joining region, AA: amino acid.

Table 4 Summary of Correlation analysis of anti-ZIKV mAb

A; Heavy chain All mAbs [a]		SHMH %		FWRH mutation %		CDRH 1,2 mutation %		CDRH3 AA Length	
	N	r value	p-value	r value	p-value	r value	p-value	r value	p-value
Luminex EC_{50} (ng/ mL)	8	0.161	0.704	-0.009	0.983	0.414	0.309	-0.229	0.586
K_D (nM)	8	-0.372	0.365	0.059	0.889	**-0.722***	0.043	-0.456	0.257
k_a (1/Ms)	8	0.027	0.949	-0.231	0.583	0.379	0.355	0.308	0.458
k_{dis} (1/s)	8	-0.375	0.359	-0.068	0.873	-0.546	0.161	-0.303	0.465
B Light chain All mAbs [a,]		SHML %		FWRL mutation %		CDRL 1-3 mutation %		CDRL3 AA Length	
	N	r value	p-value	r value	p-value	r value	p-value	r value	p-value
Luminex EC_{50} (ng/mL)	8	-0.158	0.709	0.240	0.567	-0.525	0.181	-0.288	0.489
K_D (nM)	8	0.402	0.323	0.075	0.860	0.427	0.291	-0.017	0.968
k_a (1/Ms)	8	-0.507	0.200	-0.051	0.905	**-0.708***	0.050	-0.054	0.900
k_{dis} (1/s)	8	0.137	0.747	0.051	0.905	0.049	0.909	-0.047	0.913
C Heavy chain Neutralizing mAb[b]		SHMH %		FWRH mutation %		CDRH 1,2 mutation %		CDRH3 AA Length	
	N	r value	p-value	r value	p-value	r value	p-value	r value	p-value
Luminex EC_{50} (ng/mL)	5	**-0.971***	0.006	**-0.924***	0.025	-0.776	0.123	-0.402	0.502
K_D (nM)	5	-0.772	0.126	-0.597	0.287	**-0.920***	0.027	-0.233	0.706
k_a (1/Ms)	5	-0.388	0.519	-0.264	0.668	-0.511	0.379	0.277	0.652
k_{dis} (1/s)	5	-0.803	0.101	-0.603	0.282	**-0.985***	0.002	-0.040	0.950
MNT titer IC_{50} (ng/mL)	5	-0.773	0.126	-0.756	0.139	-0.521	0.368	-0.831	0.081
D Light chain Neutralizing mAb[b]		SHML %		FWRL mutation %		CDRL 1-3 mutation %		CDRL3 AA Length	
	N	r value	p-value	r value	p-value	r value	p-value	r value	p-value
Luminex EC_{50} (ng/mL)	5	-0.037	0.953	-0.494	0.397	0.689	0.198	-0.421	0.481
K_D (nM)	5	-0.435	0.464	-0.598	0.287	0.265	0.667	0.107	0.864
k_a (1/Ms)	5	0.186	0.764	0.120	0.847	0.049	0.937	-0.009	0.988
k_{dis} (1/s)	5	-0.247	0.689	-0.407	0.496	0.231	0.709	0.082	0.896
MNT titer IC_{50} (ng/mL)	5	-0.316	0.605	-0.825	0.085	0.826	0.085	-0.487	0.406

***: p<0.05 for p-value.**

All mAbs: 102-1, 242-3, 270-12, 289-3, 306-2, 78-2, 278-11, and 11-3. b: neutralizing mAbs: 102-1, 242-3, 270-12, 289-3 and 306-2. Abbreviation: K_D: equilibrium dissociation constant, k_a: association constant, k_{dis}: dissociation constant, MNT: microneutralization test, SHM: somatic hypermutation, FWR: framework region, AA: amino acid, SHM: somatic hypermutation, CDR: complementarity-determining region, FWR: framework region,.

Table 5 Summary of anti-ZIKV mAb framework amino acid mutations

A: Heavy chain

clones	VH allele	FWRH AA mutation (%)	FWRH1 AA mutation (N)	mutated AA allele AA IMGT No>mutated AA	FWRH2 AA mutation (N)	mutated AA allele AA IMGT No>mutated AA	FWRH3 AA mutation (N)	mutated AA allele AA IMGT No>mutated AA
102-1	IGHV1S40*01	11.5%	3	C23>S, T24>K, A25>V	2	M39>I, A54>G	4	S69>N, A71>V, T81>P, Q90>E
270-12	IGHV1S45*01	5.1%	1	E2>A	1	I39>M	2	K72>R, Q90>R
289-3	IGHV1S40*01	15.2%	3	X2>E, S3>E, T24>K	2	M39>I, L50>P	8	S69>N, G74>R, K80>S, T81>S, T88>A, Q90>E, T92>P, A96>D
306-2	IGHV1S40*01	3.8%	0	ND	1	A54>G	2	K80>R, R93>S

B: Light chain

clones	VL allele	FWRL AA mutation (%)	FWRL1 AA mutation (N)	mutated AA allele AA IMGT No>mutated AA	FWRL2 AA mutation (N)	mutated AA allele AA IMGT No>mutated AA	FWRL3 AA mutation (N)	mutated AA allele AA IMGT No>mutated AA
102-1	IGKV1S37*01	11.4%	4	S9>A, P10>S, S12>E, N22>K	0	ND	5	E68>D, K77>S, Q86>E, E95>D, T101>S
270-12	IGKV1S34*01	15.2%	5	V2>I, S9>A, P10>S, S12>E, N22>K	4	S40>A, P49>R, L52>F, I54>M	3	T69>S, S77>R, E86>Q
289-3	IGKV1S10*01	11.4%	5	V2>I, K11>V, D17>G, K22>N, Q24>H	0	ND	4	E68>A, S83>A, S92>T, D93>A
306-2	IGKV1S36*01	6.3%	1	P10>S	2	S40>A, K45>R	2	N66>T, R80>G

Abbreviation: AA: amino acid, VH: heavy chain variable region, FWRH: heavy chain framework region, VL: light chain variable region, FWRL: light chain framework region, FWR(H or L) 1: framework region 1 of the heavy chain or light chain (framework from N terminal to CDR1), FWR(H or L) 2: framework region 2 of the heavy chain or light chain (framework between CDR1 and CDR2), FWR(H or L) 3: framework region 3 of the heavy chain or light chain (framework between CDR2 and CDR3), ND: no mutation detected, X: no amino acid residues from IMGT unique numbering.

All amino acid numbers were displayed IMGT unique numbering.

Chapter 2 Development of a novel assay to assess the avidity of dengue virus-specific antibodies elicited in response to a tetravalent dengue vaccine

Abstract

Antibody affinity maturation is a critical step in developing functional antiviral immunity. However, accurate measurement of affinity maturation of polyclonal serum antibody responses to particulate antigens such as virions is challenging. I describe a novel avidity assay employing bio-layer interferometry and dengue virus-like particles. After validation using anti-dengue monoclonal antibodies, the assay was used to assess the avidity of antibody responses to a tetravalent dengue vaccine candidate (TAK-003) in children, adolescents, and adults during two Phase 2 clinical trials conducted in dengue-endemic regions. Vaccination increased the avidity index, and avidity remained high through one year post-vaccination. Neutralizing antibody titers and avidity index did not correlate overall. However, a correlation was observed between neutralizing antibody titer and avidity index in those subjects with the highest degree of antibody affinity maturation. Therefore, vaccination with TAK-003 stimulates polyclonal affinity maturation and functional antibody responses, including neutralizing antibodies.

Introduction

Affinity maturation leads to higher antibody affinity, which optimizes antiviral functions, including virus neutralization and antibody-dependent cell-mediated cytotoxicity [49]. Several methods have been developed to measure affinity maturation of the antibody repertoire, including deep sequencing of B cells and whole genome phage display libraries [169, 170]. These methods are low throughput and, therefore, unsuitable for vaccine or natural infection history studies. Other techniques, such as ELISA with chaotropic reagents (8 M urea or 1 M NaSCN), are higher throughput, but the dissociation constant, a critical parameter to assess affinity maturations, cannot be calculated [65, 87]. To overcome the issues for ELISA, SPR and BLI are techniques commonly used to measure monoclonal antibody affinity [83, 84] and recently applied to evaluate the affinity maturation for vaccines and virus infection [88-91]. BLI is the technology to assess the protein/ protein interaction, antibody/ antigen binding kinetics, and quantified protein concentration [171]. BLI measures the shifts in reflected white light upon changes in the thickness of the bio-layer. The measured shift depends on the interactors' size and affinity. Bio-layers are coated with molecules (e.g., streptavidin) that allow the immobilization of one of the interactors [172]. The technology is widely used in vaccine research [171]. SPR is also known as the technology to assess various antibody antigens interactions, and both technologies apply to vaccine research [173]. However, the advantages of BLI apply to a high throughput platform: to measure 96 samples simultaneously for Octet HTX [174] and only 16 samples for Biocore 4000 [174, 175]. Extending these methods to particulate antigens such as virions or virus-like particles (VLPs) is essential because, unlike peptides and proteins, they preserve the conformational and quaternary epitopes, which are the target of many potent neutralizing antibodies [176, 177].

Dengue virus (DENV) is a flavivirus that is transmitted to humans through mosquitoes. Four distinct serotypes (DENV-1, DENV-2, DENV-3, and DENV-4) have been reported worldwide, showing different antigenicity. With an estimated 390 million infections annually, of which approximately 96 million are symptomatic [101], 40,000 deaths occur globally [102]. The first dengue outbreak was reported in 1779 in Jakarta, Indonesia, and Cairo, Egypt [178], and in 1780, North American outbreaks were confirmed in Philadelphia. [179] The first isolation of dengue pathogens was done by a Japanese scientist in 1943 [180], and the virus was isolated from Southeast Asian countries, Caribbean and South American countries [181]. Dengue fever is the most rapidly spreading mosquito-borne viral disease globally. The dengue outbreak was reported in Latin American countries, Venezuela, Brazil, Costa Rica, Colombia, Honduras, and Mexico [182, 183], African countries, Seychelles, Reunion Island, Djibouti, Comoros, and Cape Verde [184, 185] and Asia countries, Philippines [186], Thailand, Singapore, Indonesia [187], Malaysia [188], Vietnam [189], Sri Lanka [190] and India [191]. DENV infection presents clinical symptoms from mild fever to severe physiological conditions. Biphasic fever, myalgia, headache, joint pain, retro-orbital pain, body rash, thrombocytopenia, lymphadenopathy, and leukopenia were dengue symptoms, and high dengue fever continued for two to seven days [192]. Dengue hemorrhagic fever (DHF) is a symptom of high fever with homeostasis malfunction. Severer increased vascular leakage may cause dengue shock syndrome (DSS) [193]. Secondary dengue-infected patients have severe symptoms: high fever, lower platelet counts, and a high risk of DHF and DSS [194]. The mechanism of severe dengue secondary infection proposes that anti-dengue antibodies in the blood enhance the virus cell entry via cell surface Fcγ receptor, called Antibody-dependent enhancement [195]. Dengue vaccine is

approved for two products: Dengvaxia® (Sanofi Pasteur, Lyon, France) and Qdenga ® (Takeda, Osaka, Japan). Dengvaxia is limited to individuals nine years of age and above with evidence of prior infection. Besides, Qdenda® can be applied to individuals four years old and has no limitation of dengue infection histories.

Here, I report the development of a high-throughput, low-volume avidity assay based on BLI and capable of measuring polyclonal serum antibody avidity to particulate DENV-1, -2, -3, and -4 antigens. Using sera from two phase 2 trials, I demonstrate that polyclonal antibody avidity to all four DENV serotypes increases over time following vaccination of seronegative volunteers with TAK-003, and high avidity antibodies persist through 360 days.

Materials and methods

Ethics Statement

DEN-203 (ClinicalTrials.gov Identifier NCT01511250) and DEN-204 (NCT02302066) were conducted in accordance with the Declaration of Helsinki, International Council for Harmonization of Technical Requirements for Registration of Pharmaceuticals for Human Use and Good Clinical Practice (ICH-GCP) guidelines, and applicable regulatory requirements. Informed consent forms and study protocols were reviewed and approved by institutional review boards, independent ethics committees, or health authorities. Written informed assent or consent was obtained from all participants or their parents or legal guardians before enrollment.

Reagents

DENV-VLPs for serotypes 1, 2, 3, and 4 were purchased from The Native Antigen Company Ltd (Oxford, UK). Streptavidin (SA) and high precision streptavidin (SAX) biosensors were purchased from Sartorius Inc (Fremont, CA, USA). Protein A and Protein G Sepharose were obtained from Cytiva (Marlborough, MA, USA). Anti-dengue monoclonal antibody clones, 4G2 [139], WNV-E60 [196], 1M7 [197], DENV1-E106 [198], 2D22 [199], 5J7 [200], and DV4-75 [201] were purchased from various vendors or provided by collaborators.

Clinical serum samples

Sera from 56 TAK-003 vaccinated volunteers, 37 baseline seronegative and 19 seropositive, from trial DEN-203 [202] and 36 vaccinated volunteers, 21 baseline seronegative and 15 seropositive from trial DEN-204 [203] were tested for antibody avidity. DEN-203 was conducted in Puerto Rico, Colombia, Singapore, and Thailand among 1.5 - 45-year-olds. DEN-204 was conducted in the Dominican Republic, Panama, and the Philippines among 2 - 17-year-olds.

Preparation of biotinylated dengue virus-like-particles

Biotinylation of DENV-VLPs was conducted to incubate 50 - 200 µg of DENV-VLPs (serotypes 1 - 4) and 50 excess moles of EZ-Link™ Sulfo-NHS-Biotin (ThermoFisher Scientific, Waltham, MA, USA) at room temperature for 60 minutes. After the reaction, biotinylated VLPs were buffer-exchanged to Dulbecco's phosphate-buffered saline (D-PBS) by Amicon® Ultra-4 centrifugal filter units, molecular weight cut off (MWCO) 30 kDa (Merck Millipore, Burlington,

MA, USA). Protein contents were measured by BCA protein quantification kit using immunoglobulin protein as a standard protein (ThermoFisher Scientific, Waltham, MA, USA).

SDS-PAGE analysis

Antibodies and DENV-VLP purity were confirmed by NuPAGE 4 - 12% Bis-Tris gel and 10 - 20% Tricine gel (ThermoFisher Scientific, Waltham, MA, USA), respectively. Reduced/ heat denaturation was conducted to the proteins and 1 μg of IgG or 20 μg of DENV-VLPs and applied to the gel and running for 50 and 90 minutes, respectively. Gels were stained by SimplyBlue Safe stain (ThermoFisher Scientific, Waltham, MA, USA), and band intensities were analyzed by ChemiDoc Touch Imaging System (Bio-Rad, Hercules, CA, USA) and the purity of proteins was calculated.

Reactivity of anti-dengue antibodies to dengue virus-like-particles

The reactivity of anti-dengue antibodies to DENV-VLPs was measured using the Octet RED or Octet HTX system equipped with Octet Acquisition Software ver. 9.0.0.26 and 11.1.2.24, respectively (Sartorius Fremont, CA, USA). For binding between anti-dengue antibody panels and DENV-VLPs to occur, biotinylated DENV-VLPs were diluted to 5 μg/mL in 0.1% bovine serum albumin-phosphate-buffered saline + Tween (BSA-PBST) and bound to the SA or SAX Biosensor for 600 seconds. The antibody solution was then diluted to 0.01 - 10.0 μg/mL in 0.1% BSA-PBST. Antibodies were associated with DENV-VLPs for 600 seconds and dissociated in the same buffer for 900 seconds. The assay was conducted at 30°C with agitation (plate shaker,

1000 rpm). Response data at 600 sec association of each monoclonal antibody were used for reactivity data.

Optimization of antibody purification

Dengue standard serum, DEN-203 serum (1044010 Day 90) or human serum (GeneTex, Irvine, CA, USA): 30 - 200 µL, were mixed with 3 mL D-PBS and 0.6 mL 50% Protein G Sepharose or 3mL Protein A MAPSII Binding buffer (Bio-Rad, Hercules, CA, USA) and 0.6mL 50% Protein A Sepharose in 15 mL centrifuge tubes for 90 minutes at room temperature. Protein G Sepharose or Protein A Sepharose slurry was washed with D-PBS or Protein A MAPSII Binding buffer and eluted with 0.1 M Glycine HCl pH 3.0, 2.7, and 2.5. Eluate was immediately neutralized to pH 7.0 - 7.5 with 1M Tris HCl (pH 8.0). The solution was buffer-exchanged to D-PBS using Amicon® Ultra-4 centrifugal filter units, MWCO 30 kDa. Antibody concentrations were calculated using the NanoDrop™ 2000 (ThermoFisher Scientific, Waltham, MA, USA): Protein A280 (E1% A280 = 13.8). All purified antibodies' purity was measured by SDS-PAGE and evaluated for avidity index followed by *Biosensorgram of dengue vaccine recipients and avidity assay parameters*.

Optimization of avidity assay -association and VLP concentration-

SAX Biosensor captured 1, 3, and 5 µg/mL biotinylated DENV-VLPs in 0.1% BSA-PBST for 600 seconds, then 50 µg/mL biocytin (ThermoFisher Scientific, Waltham, MA, USA) was blocked with excess SA for 200 seconds. Anti-dengue polyclonal antibodies purified from DEN-203 volunteer's serum (DENV-1: 1071001 Day 90, DENV-2: 1071009 Day 90, DENV-3:

1083005 Day 0, DENV-4 1093001 Day 90) were diluted to125 μg/mL in 0.1% BSA-PBST and bound to the SAX Biosensor for 600, 900 and 1800 seconds. The sensors were then incubated in 0.1% BSA-PBST 0.35 M NaCl for 1200 seconds to dissociate the bound antibody. Avidity assay was conducted by *Avidity assay of DEN-203 and DEN-204 subjects,* and data analysis was followed by *Data analysis of avidity assay for DEN-203 and DEN-204 subjects.*

Optimization of avidity assay -dissociation simulation -

Biosensorgram of anti-dengue polyclonal antibodies purified from DEN-203 volunteers serum (1081001 Day 0: 250 μg/mL) were generated by Octet RED systems (Sartorius, Fremont, CA, USA) with 5 μg/mL DENV-3 VLPs followed by *Biosensorgram of dengue vaccine recipients and avidity assay parameters*. Antibody dissociation constants were calculated by Octet Data Analysis Software (version 9.0.0.10, Sartorius) from 30 to 600 sec and from 30 to 1200 sec for nine independent assays.

Optimization of avidity assay - Difference of biotinylated dengue 1 VLP-

Five lots of DENV-1 VLPs (Lot No: 15062616, 18011816, 18042710, 19040109, and 20012911: 50 - 100 μg; Native Antigen, Oxford, UK) were biotinylated followed by *Preparation of biotinylated dengue virus-like particles*. Seven anti-dengue polyclonal antibodies purified from DEN-203 volunteers serum (1044010 Day 90, 1053009 Day 90, 1053011 Day 120, 1071001 Day 90, 1071009 Day 90, 1083005 Day 0 and 1093001-Day 90: 125 μg/mL) were measured for avidity using these five biotinylated DENV-1 VLPs followed by *Avidity assay of DEN-203 and DEN-204 subjects.*

Optimization of avidity assay - dose dependence of Avidity assay -

Anti-dengue polyclonal antibodies purified from DEN-203 volunteer serum (1053005 Day 90) were diluted from 4.0 to 250 μg/mL and measured for response, followed by *Biosensorgram of dengue vaccine recipients and avidity assay parameters.*

Optimization of avidity assay -linearity of Avidity assay-

Three anti-dengue polyclonal antibodies purified from DEN-203 volunteers serum (DENV-1: 1053005 Day 90, DENV-2 and DENV-4: 1053011 Day 120, DENV-3: 1053011 Day 90) were diluted from 5.0 - 70 μg/mL in 0.1% BSA-PBST and conducted avidity assay followed by *Avidity assay of DEN-203 and DEN-204 subjects.* Assays were run six times with triplicated data points.

Intra-plate differences and inter-assay differences of Avidity assay

Anti-dengue polyclonal antibodies purified from DEN-203 volunteers serum (DENV-1, -2, -3: 1053005 Day 90 and DENV-4: 1053011 Day 90) were diluted to 50 μg/mL for DENV-1 and -2, and 75 μg/mL for DENV-3 and -4 in 0.1% BSA-PBST and conducted avidity assay followed by *Avidity assay of DEN-203 and DEN-204 subjects.* Mean ± Standard Deviation (SD) and Coefficient of Variation (CV) of Response and $\log_{10}$[Avidity index] within the plate were calculated, and these data between the two runs were compared.

Determination of limit of detection (LoD)

Noise of each dengue serotype was monitored for 1800 sec using 125 µg/mL of three negative antibodies purified from DEN-203 volunteer's serum (1044008 Day 0, 1044010 Day 0, and 1053005 Day 0) in 0.1% BSA-PBST with 5 µg/mL biotinylated DENV-VLPs captured with SA biosensor. Noise was defined as the differences in response in 60 sec (**Table 6**)**.** LoD was determined by three times of noise (**Table 7**).

Biosensorgram of dengue vaccine recipients and avidity assay parameters.

Antibody avidity was measured using the Octet RED systems and the SA Biosensor (**Figure 7A**). Biotinylated DENV-VLPs (5 µg/mL) in 0.1% BSA-PBST were captured with the SA Biosensor for 600 sec, and then 50 µg/mL Biocytin was blocked with excess SA for 200 sec (**Figure 7B**). Anti-dengue polyclonal antibodies (250 µg/mL) purified from the serum of DEN-203 volunteers (1022005 and 1044010 at Day 0, 28, 90, 120, 180 and 360) in 0.1% BSA-PBST was bound to the SA Biosensor for 1800 seconds (**Figure 7C**), the sensors were then incubated in 0.1% BSA-PBST 0.35 M NaCl for 1200 seconds to dissociate bound antibody (**Figure 7D**). This assay was conducted at 30°C with agitation (plate shaker, 1000 rpm). Data were analyzed by double subtraction and using Octet Data Analysis Software (version 9.0.0.10; Sartorius). Response values were measured at 1800 seconds association time. Dissociation constant (k_{dis}) was measured by the Langmuir 1:1 binding model, with 30 - 600 seconds for the dissociation phase. Avidity index was calculated as avidity index = response/k_{dis}. All samples were analyzed in duplicate, and average values are shown.

Antibody purification of DEN-203 and DEN-204 subjects

DEN-203 and DEN-204 serum, 100 - 200 µL, were mixed with 3.0 mL D-PBS and 0.6 mL 50% Protein G Sepharose in 15 mL centrifuge tubes for 90 min at room temperature. Protein G Sepharose slurry was washed with D-PBS and eluted with 0.1 M Glycine HCl pH 2.7. Eluate was immediately neutralized to pH 7.0 - 7.5 with 1M Tris HCl (pH 8.0). The solution was buffer-exchanged to D-PBS using Amicon® Ultra-4 centrifugal filter units, MWCO 30 kDa. Antibody concentrations were calculated using the NanoDrop™ 2000: Protein A280 (E1% A280 = 13.8). All antibodies' purity was confirmed to be more than 80% by SDS-PAGE prior to antibody avidity assay.

Avidity assay of DEN-203 and DEN-204 subjects

Antibody avidity was measured using the Octet HTX systems with Octet Acquisition Software (version 11.1.2.24). Biotinylated DENV-VLPs (5 µg/mL) in 0.1% BSA-PBST were captured with the SA or SAX Biosensor for 600 sec, then 50 µg/mL Biocytin was blocked with excess SA for 200 sec. Anti-dengue polyclonal antibodies (125 µg/mL) purified from the serum of DEN-203 volunteers in 0.1% BSA-PBST were bound to the SA or SAX Biosensor for 1800 seconds, the sensors were then incubated in 0.1% BSA-PBST 0.35 M NaCl for 1200 seconds to dissociate bound antibody. This assay was conducted at 30°C with agitation (plate shaker, 1000 rpm).

Data analysis of avidity assay for DEN-203 and DEN-204 subject

Data were analyzed by double subtraction and using Octet Data Analysis Software HT (version 11.1.2.48). Response values were measured at 1800 seconds association time. Dissociation

constant (k_{dis}) was measured by the Langmuir 1:1 binding model, with 30 - 600 seconds for the dissociation phase. The k_{dis} for some serum samples could not be measured due to strong binding; in this case, k_{dis} was extrapolated to 2 x 10^{-5} 1/s (detectable dissociation from 0 - 1200 seconds for a 5% signal decrease). For non-binding IgG data analysis, such as seronegative pre-vaccination volunteers, k_{dis} was automatically extrapolated to 1 x 10^{-3} 1/s by the analysis software, preventing misinterpretation. I use all responses and k_{dis} data calculated from the software. Avidity index was calculated as avidity index = response/k_{dis}.

All samples were analyzed in duplicate. Acceptance criteria were set for the assay to ensure each assay run worked properly. Acceptance criteria: DENV-VLP binding at 600 sec: DENV-1: 2.0 - 3.0, DENV-2: 1.7 - 2.7 DENV-3 and -4: 1.1 - 2.1, difference of DENV-VLP binding from average: 70 - 130%, calculation fitting: R^2: more than 0.95, difference of response between two runs: less than 2, difference of avidity index between two runs: less than three. When these data did not meet my acceptance criteria, failed subject assays were repeated. If data did not meet the acceptance criteria three times, these data were not included in the analysis and reported as indeterminant. Total indeterminant assay points were five from 1292 assay data from DEN-203 and one from 288 from DEN-204. Data were calculated to average values of all measured runs. For the purposes of drawing figures, the negative avidity index and negative response were extrapolated to 1.0 and 0.001, respectively. Positive dissociation constant: these data were confirmed calculation errors under LoD samples. Nine data sets from the 1292 assay from DEN-203 were not included in these analyses.

Microneutralization test

Anti-dengue neutralizing antibody titers in response to vaccination with TAK-003 were quantified by MNT, as previously described [71].

Correlation between antibody titers and avidity assay parameters

Post-vaccination avidity assay parameters of response, $k_{dis,}$ and avidity for each serotype in 24 baseline seronegative and 19 seropositive samples from DEN-203 were analyzed for correlation with MNT titers. Each serotype avidity index was also analyzed for correlations. This analysis did not include pre-vaccination sample data. Further correlation analyses were performed using data sets stratified by the strength of binding (k_{dis}) to DENV-VLPs. Correlations between avidity indices and neutralizing antibody titers were analyzed for each stratified data set: low log_{10} k_{dis}, middle log_{10} k_{dis}, and high log_{10} k_{dis}. DENV-1: $Log_{10}[k_{dis}]$: -4.7 - -4.2: N = 75, -4.2 - -3.9: N = 74, -3.9 - -1.9: N = 76, DENV-2: $Log_{10}[k_{dis}]$: -4.7 - -4.6, N = 77, $Log_{10}[k_{dis}]$: -4.6 - -4.0, N = 77, $Log_{10}[k_{dis}]$: -4.0 - -2.8, N = 76, DENV-3: $Log_{10}[k_{dis}]$: -4.7 - -4.6: N = 75, -4.6 - -4.0: N = 75, - -4.0 - -1.9: N = 73, DENV-4: $Log_{10}[k_{dis}]$: -4.7 - -4.6: N = 66, -4.6 - -3.8: N = 65, -3.8 - -2.6: N = 66. Response values under the LoD were removed from correlation analysis. LoD: DENV-1: 0.017, DENV-2: 0.015, DENV-3: 0.018, DENV-4: 0.014 (**Table 7**)

Statistical analysis

All data were analyzed by GraphPad Prism™ software (version 8.0.0, San Diego, CA, USA). Wilcoxon signed-rank test were applied to compare each visiting day with day 0 for avidity parameters, response, $k_{dis,}$ and avidity index. Correlation analysis between avidity parameters and MNT titers was used with linear regression curves for log_{10} converted data set. LoD was

established as three times assay noise in accordance with American Society for Testing and Materials (ASTM) E685-93 (2013) [204].

Results

Reactivity and specificity of anti-dengue antibody panels

As expected, all four DENV-VLPs contained E-prM and M proteins, as determined by SDS-PAGE. (**Figure 8A**). Antigenicity of DENV-VLPs was evaluated using a panel of anti-dengue monoclonal antibodies (**Figure 8B and 8C**). Cross-reactive fusion loop specific monoclonal antibodies 4G2, WNV-E60, and 1M7 bound to VLPs of all serotypes. Serotype-specific neutralizing antibodies DENV1-E106 for DENV-1, 2D22 for DENV-2, 5J7 for DENV-3, and DV4-75 for DENV-4 recognize quaternary epitopes and domain III [198-201, 205]. Each serotype-specific antibody bound the corresponding DENV-VLP and did not bind to VLPs of the other three serotypes. Therefore, I concluded that, unlike soluble E protein, DENV-VLPs retain DENV quaternary epitopes.

Optimization of antibody purification from human serum

First, I compared Protein A and Protein G Sepharose purification using different elution pH. Antibody yield was high with Protein A Sepharose elution at pH 3.0 and Protein G Sepharose elution at pH 2.7 or 2.5 (**Figure 9A**). I selected Protein G Sepharose because Protein A weakly binds IgM [206], which could contribute to non-specific binding in the assay. Next, I determined the minimum volume of serum required. An antibody yield of 10 mg/mL and purity of > 90% was obtained by purifying antibodies from 30 - 200 µL human serum using Protein G Sepharose

(**Figure 9B**). I defined the serum volume requirement as 50 - 200 µL. Next, IgG yield between operators and occasions was confirmed. The range of antibody yield was 81 - 106% when purifying IgG from 100 µL serum using Protein G Sepharose (**Table 8**).

Optimization of Avidity assay

Association was optimized using anti-dengue polyclonal antibody purified from DEN-203 serum. Avidity index, calculated by response/k_{dis}, increased when association time increased from 600 to 1800 sec (**Figure 10A**) and reached a plateau using 3 - 5 µg/mL biotinylated DENV-VLP (**Figure 10A**). For dissociation, some samples showed two-phase curves, a high dissociation constant in the early phase and a lower constant in the late phase (**Figure 10B**). Dissociation fitting of 30 - 600 sec showed good fitting and observed a higher dissociation constant than a fitting of 30 - 1200 sec (**Figure 10B**). Response of polyclonal dengue antibodies was at IgG concentrations up to 250 µg/mL (**Figure 11A**). Thus, avidity assay parameters were optimized as follows: antibody concentration: 125 µg/mL, Biotinylated DENV-VLP: 5 µg/mL, Association: 1800 sec, Dissociation: 1200 sec, Dissociation constant analysis: 30 - 1200 sec. Next, the reproducibility of the avidity assay was confirmed; Reproducibility was determined using five biotinylated DENV-1 VLP lots (**Figure 10C**). For intra-plate reproducibility, the coefficient of variation (CV) of Log_{10}[Avidity index] ranged from 2.46 to 10.08%, and the inter-plate range was 99 - 108%. (**Table 9**). High linearity between response and IgG concentration was observed for all serotypes (DENV-1: $p < 0.0001$ $R^2 = 0.977$). However, k_{dis} rates were not depend on antibody concentrations (DENV-1: $p = 0.0001$, $R^2 = 0.137$). Avidity index, calculated by response/k_{dis}, also showed a positive correlation with IgG concentrations (DENV-1: $p < 0.0001$ $R^2 = 0.495$) (**Figure 10D and 11B**).

Polyclonal serum antibody avidity after vaccination

Sequential serum samples from 56 DEN-203 volunteers (Day 0, 28, 90, 120, and Day 360) were analyzed to assess the kinetics of antibody avidity following the administration of first (Day 0) and second (Day 90) TAK-003 doses. Kinetics of polyclonal antibody affinity maturation differed among individual DEN-203 study volunteers, with two different general patterns observed, each in about half of the vaccinated individuals. In some individuals, polyclonal affinity maturation gradually increased after the first vaccination and increased further following the second vaccination. For example, volunteer #1022005 (**Figure 12A**), after initial vaccination, antibody dissociation constant (k_{dis}) gradually decreased between Day 28 and Day 90. The k_{dis} further decreased on Day 120, following the second vaccination on Day 90, and remained stable through Day 180 (**Figure 12C**). Avidity index, calculated by response/k_{dis}, reflects these changes; the value increased from 0 to 120 days and remained stable through Day 180 (**Figure 12C**). In other individuals, avidity index increased rapidly following the first vaccine dose, and the high avidity antibodies persisted in the serum throughout 360 days. For example, in study volunteer #1044010 (**Figure 12B**), antibody responses were high and k_{dis} low at 28 days, translating to a high avidity index at the first post-vaccination time point, a pattern which persisted throughout the 360 days study period (**Figure 12C**).

Among the 56 DEN-203 volunteers, 37 individuals were seronegative for any dengue antibodies prior to vaccination, as determined by neutralizing antibody assay [71]. In baseline seronegative volunteers, binding antibody responses were negative before vaccination and significantly increased after a single dose for all serotypes (**Figure 13A**). Overall, responses increased slightly

after the second vaccine dose (Day 120) and declined but remained positive at Day 360. Within each individual, kinetics of polyclonal antibody affinity maturation was similar among the four DENV serotypes, though the magnitude of DENV-specific binding antibodies varied among serotypes. Generally, responses were highest to DENV-2 and lowest to DENV-4. Binding k_{dis} (**Figure 14A**) for all four dengue serotypes decreased over time, demonstrating increasing antibody binding strength to DENV-VLPs. The k_{dis} in 0% (DENV-1) to 22% (DENV-3) sera reached less than 2×10^{-5} 1/s, meaning the antibodies bound too tightly to be dissociated within 1200 seconds. Avidity increased significantly after the first vaccine dose and continued to increase or remain stable throughout the one-year period of observation (**Figure 15A**). Avidity of antibodies to DENV-1, -2, and -3 were similar, while DENV-4 antibody avidity overall was lowest. In general, in seronegative study volunteers, after vaccination, the strength of serum polyclonal antibody binding and avidity index to all four DENV serotypes increased over time, and the high avidity antibodies persisted in the serum through 360 days.

Among the 56 DEN-203 volunteers, 19 DEN-203 volunteers were seropositive for antibodies against at least one dengue serotype prior to vaccination. As expected, many seropositive vaccine recipients had positive responses pre-vaccination (**Figure 15B**). Pre-vaccination binding antibodies to all four serotypes were present in most individuals. Responses increased overall post-vaccination and persisted to Day 360 in the majority of individuals (**Figure 13B**). The serum of some seropositive vaccine recipients contained high-avidity antibodies prior to vaccination, as demonstrated by low k_{dis} on Day 0. Post-vaccination, k_{dis} decreased over time for all serotypes (**Figure 14B**), 6% (DENV-1) to 50% (DENV-4) of volunteers for each serotype reached undetectable dissociation at Day 120. Avidity indices for all four dengue serotypes

increased over time (**Figure 15B**). In general, both pre- and post-vaccination avidity indices in seropositive individuals were higher than in seronegative individuals. Overall, vaccination increased polyclonal serum antibody avidity in seropositive individuals, but the increase was less than in seronegative individuals due to the presence of high avidity antibodies prior to vaccination in some samples. In seropositive individuals, high avidity antibodies persisted in serum throughout the one-year period of observation.

To confirm the results of DEN-203, sera from 36 randomly selected DEN-204 volunteers collected on Day 1 and Day 180 were tested to assess the impact of vaccination on avidity (**Figure 13C, 14C, and 15C**). As in DEN-203, responses in DEN-204 seronegative volunteers were negative pre-vaccination and were significantly increased for all four dengue serotypes at Day 180 after a single dose of TAK-003 (**Figure 13C**). Binding antibody responses were lowest for DENV-4 and similar for DENV-1, -2, and -3. Dissociation constant, $k_{dis,}$ decreased for all four serotypes at Day 180 (**Figure 14C**). Avidity increased significantly after vaccination, with the highest avidity antibodies to DENV-1, -2, and -3 and lower DENV-4 avidity (**Figure 15C**).

Most baseline seropositive vaccine recipients were positive for binding antibody responses to all four dengue serotypes and displayed high-avidity antibodies prior to vaccination, as demonstrated by low k_{dis} on Day 1 **(Figure 14C**). Post-vaccination increases in binding antibodies and decrease in k_{dis} was marginal for all serotypes, and consequently, avidity index increased marginally after vaccination (**Figure 15C and 13C**).

Correlation between antibody titers and avidity index

I assessed the degree of correlation between neutralizing antibody titers and avidity index parameters in DEN-203 study sera. When combining data for 43 subjects and study days for each dengue serotype, I found weak to no correlation between MNT titer and response, $k_{dis,}$ or avidity index (**Figure 16, 17 and Table 10**). Likewise, there was a weak to no correlation between MNT titer and avidity index when results on each study day were analyzed separately (**Figure 18 and 19**). However, there was a good to weak correlation among each serotype avidity index (**Figure 20**)

Next, I analyzed the degree of correlation between neutralizing antibody titer and avidity index in samples with high, medium, and low k_{dis} values, representing sera with a low, medium, and high degree of antibody affinity maturation. For all serotypes, the degree of correlation between MNT and avidity index was lowest among samples with high k_{dis} values (less affinity matured: DENV-1: $p < 0.0001$, $R^2 = 0.193$, DENV-2: $p = 0.382$, $R^2 = 0.010$, DENV-3: $p < 0.0001$, $R^2 = 0.341$, DENV-4: $p < 0.0001$, $R^2 = 0.551$) and highest in samples with lower k_{dis} values (more affinity matured: DENV-1: $p < 0.0001$, $R^2 = 0.403$, DENV-2: $p < 0.0001$, $R^2 = 0.623$, DENV-3: $p < 0.0001$, $R^2 = 0.814$, DENV-4: $p < 0.0001$, $R^2 = 0.623$) (**Figure 21, 22 and Table 11**). These trends were also observed between MNT and responses. Thus, this finding suggests a relationship between high-affinity antibodies and neutralizing activity.

Discussion

The process of antibody affinity maturation forms the basis for the evolution of effective antibody responses to specific pathogens from the diverse B cell repertoire. The importance of antibody affinity maturation to effective antiviral responses is well established. Influenza antibody affinity correlates with neutralization potency and breadth [207]. Affinity maturation of

B cells specific for conserved epitopes after sequential exposure to infection is required for protection from re-infection by diverse influenza viruses [208]. A common theme of successful antiviral immunity is the induction of high-affinity functional antibodies to conserved epitopes in the context of abundant ineffective immune responses to variable viral epitopes.

Information on antibody affinity maturation following dengue infection is limited; dengue disease severity was associated with a lower antibody avidity index, as assessed by ELISA [65]. Similarly, antibody avidity to ZIKV E-protein negatively correlated with disease severity [64]. Repeated dengue infections have increased monoclonal and polyclonal antibody avidity and neutralization potency [209].

Collectively, antibodies with increased affinities after antigen exposure contribute to an overall increase in polyclonal antibody avidity. The measurement of avidity index, response divided by dissociation constant, was proposed by Lynch [90] and reflects both antibody concentration and affinity maturation. Methods to measure polyclonal antibody avidity to peptides or soluble proteins have been reported [64, 88-91], yet characterization of polyclonal antibody avidity to viral particles or other particulate antigens has proven challenging. I have developed a novel assay to assess the avidity of serum polyclonal antibodies specific for DENV-1, -2, -3, and -4 particles by BLI. Antigen selection and characterization are critical factors in developing dengue antibody assays. Limitations in the use of DENV-VLPs as an antigen include differences in the arrangement of E-dimers on VLPs versus virions and potential differences in the maturation state of VLPs and virions [176]. Nevertheless, VLPs are non-infections, more stable than live virions, can be purified, and retain many antigenic features of dengue virions [176].

I found that reproducible avidity measurement required purification of IgG from serum. Several methods are available for rapid and simple purification of serum IgG [88, 91]; however, some non-specific binding remains. Protein G Sepharose was selected to further reduce non-specific binding activity. Even after IgG purification, the 384-well plate format of the Octet HTX makes it possible to test avidity to all four dengue serotypes using less than 50 μL serum.

As antibody avidity increased rapidly in serum of some volunteers following TAK-003 vaccination, it was necessary to use a high ionic strength buffer to accelerate antibody dissociation. Two-phase dissociation was observed in some volunteers: a higher dissociation constant in the early phase and a lower constant in the later phase. Similar kinetics of dissociation constant have been reported previously [90]. These changes may be caused by antibody re-binding to DENV-VLP. Therefore, 50% dissociation curves (600 sec) were applied to measure the dissociation constant to prevent overestimation.

BLI was used to study kinetics of polyclonal serum avidity to DENV-1, -2, -3, and -4 following vaccination of dengue seropositive and seronegative volunteers with TAK-003. In seronegative volunteers, antibody affinity maturation was observed at the beginning of the first vaccination, as evidenced by the decline of antibody dissociation constant. Further decline in antibody dissociation constant was also observed in some individuals following the second TAK-003 dose. In general, high avidity antibodies persisted in the serum through the 360-day follow-up period. Prior dengue exposure, determined by seropositivity, increased antibody avidity. In general, if high avidity antibodies were present in a dengue serotype, vaccination did not increase

avidity, but post-vaccination antibody avidity was increased in seropositive volunteers with lower avidity serum antibodies pre-vaccination. The volunteers in DEN-203 and DEN-204 represented a range of ages (1.5 to 45 years) and geographical locations (Puerto Rico, Colombia, Singapore, Thailand, Dominican Republic, Panama, and the Philippines). Avidity results were consistent between the two studies, and avidity testing was conducted on sera that were broadly representative of the studies as a whole in terms of tetravalent seroconversion rate. Overall, the results demonstrate that vaccination with TAK-003 can drive polyclonal antibody affinity maturation in seronegative and seropositive adults and children across dengue-endemic regions.

Surprisingly, a correlation between MNT titer and avidity assay parameters was weak. The correlation between MNT titer and avidity index was highest in samples with higher affinity maturation. I hypothesized that neutralizing antibodies might be selected during the affinity-maturation process; therefore, a higher correlation was observed with low k_{dis} subjects. Correlation between neutralizing antibodies and affinity maturation has been described for HIV and influenza antibodies [210, 211]. Different viruses may elicit high avidity antibodies that vary in functional properties. The functional antiviral activities of other dengue-specific affinity matured antibodies will be assessed in future studies.

In conclusion, I have developed a novel, high-throughput avidity assay using DENV-VLPs and applied it to evaluate the evolution of polyclonal serum antibody avidity following vaccination with a tetravalent dengue vaccine candidate, TAK-003, in two phase 2 trials. Vaccination drove antibody affinity maturation against all four dengue serotypes, with high-affinity antibodies detectable in serum through one-year post-vaccination. The development of this method will

facilitate a deeper understanding of the mechanisms of induction of immunity to dengue infection and vaccination, including the relationship between affinity matured antibodies and protection against dengue infection.

Figures

Figure 7 Dengue avidity assay using bio-layer interferometry technology.

A: SA Biosensor, **B**: Binding of 5 µg/mL biotinylated DENV-VLP in 0.1% BSA-PBST, **C:** Association of purified anti-dengue antibody from vaccinated serum in 0.1% BSA-PBST (1800 sec.), **D**: Dissociation of purified anti-dengue antibody from SA Biosensor in 0.1% BSA-PBST 0.35 M NaCl (1200 sec.).

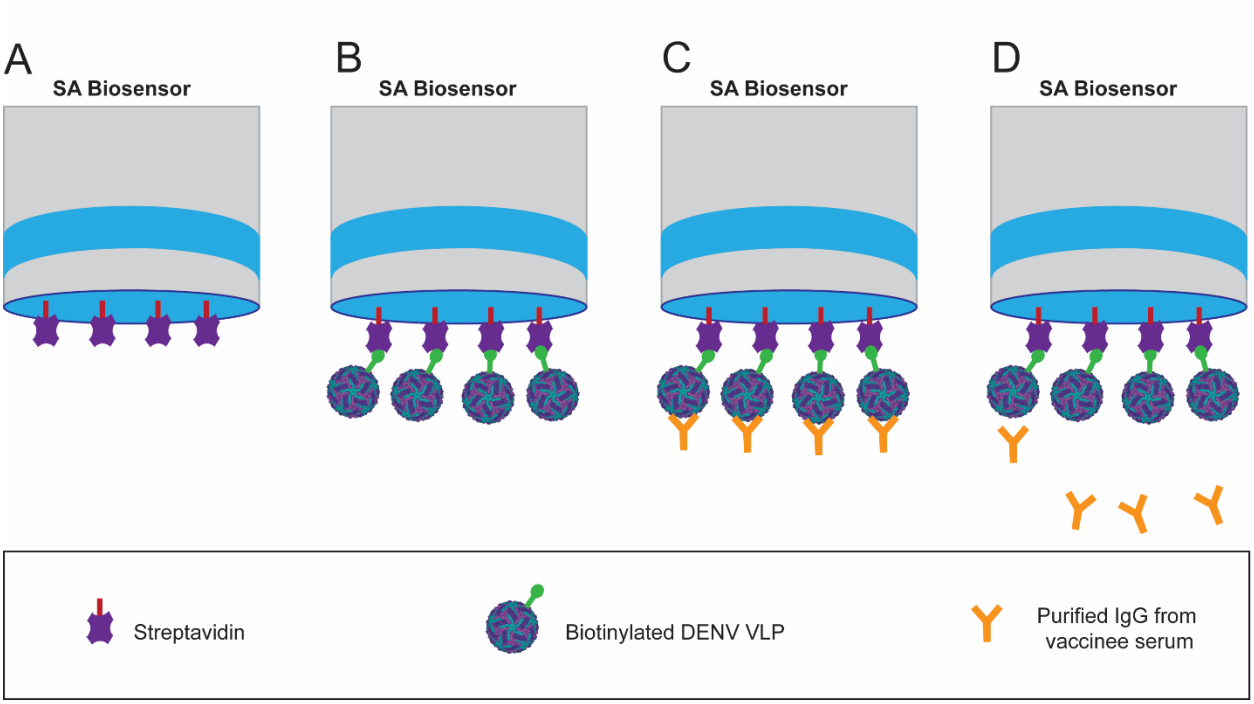

Figure 8 Reactivity of anti-dengue monoclonal antibodies to biotinylated dengue VLPs.

A: SDS-PAGE of DENV-VLPs; VLP were reduced, and 20 μg of VLP were applied to 10 - 20% Tricine SDS-PAGE and stained by Simple Stain Blue (ThermoFisher Scientific). **B:** Reactivity of anti-dengue monoclonal antibodies panel: Response of 10 μg/mL of anti-dengue mAbs at 600sec association were measured by Octet Red or Octet HTX systems using 5 μg/mL biotinylated VLP in SA or SAX biosensor. mAb panels: clone: specificity: epitopes of dengue E-protein: 4G2: CR, fusion loop [139], WNV-E60: CR, fusion loop [196], 1M7: CR, fusion loop [197], DENV1-E106: DENV-1 specific, domain III [198], 2D22: DENV-2 specific, domain III [199], 5J7: DENV-3 specific, QE [200], and DV4-75: DENV-4 specific, domain III [201]: QE, quaternary E-protein; CR, cross-reactive. Data of 4G2, WNV-E60, 2D22, and DV4-75 were measured three times and showed an average. 1M7, DENV-E106, 5J7 were measured once. **C:** Dose dependence of anti-dengue monoclonal antibodies**:** 4G2, WNV-E60, and DV4-75 antibody clones were diluted from 0.01 to 10 μg/mL to measure response at 600 sec of association. All data were measured three times and showed average ± SD.

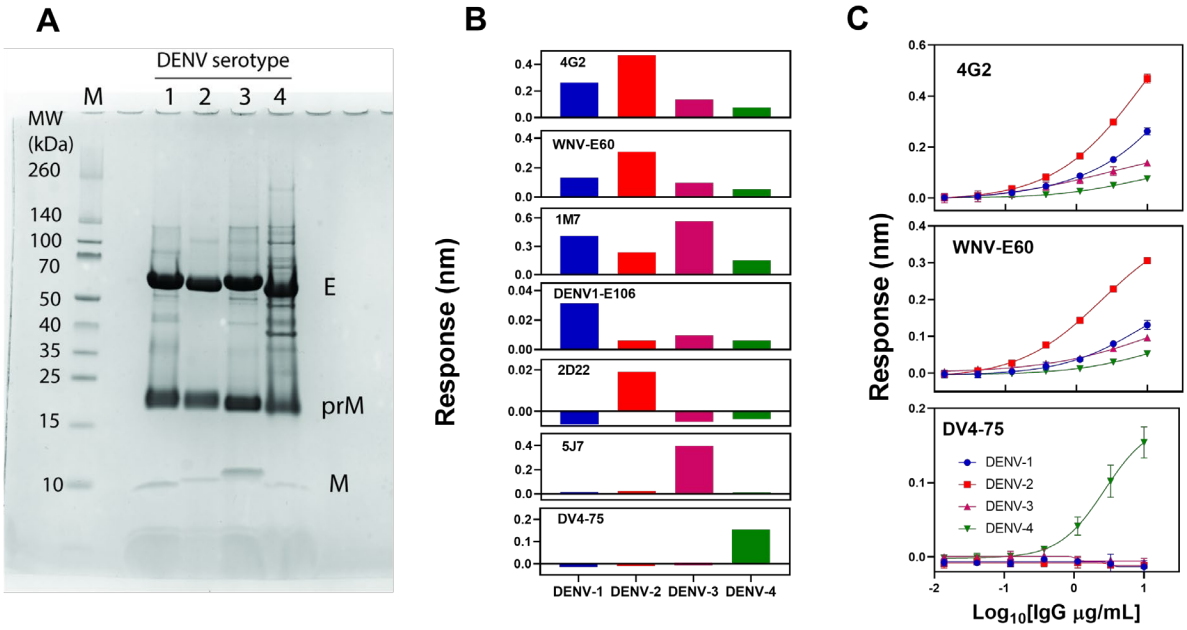
A
DENV serotype
M
1 2 3 4
MW
(kDa)
260
140
100
70
50
40
35
25
15
10
E
prM
M
B
Response (nm)
4G2
WNV-E60
1M7
DENV1-E106
2D22
5J7
DV4-75
DENV-1 DENV-2 DENV-3 DENV-4
C
Response (nm)
4G2
WNV-E60
DV4-75
DENV-1
DENV-2
DENV-3
DENV-4
Log10[IgG µg/mL]

Figure 9 Optimization of anti-dengue polyclonal antibody purification from human serum

A: Optimization of Protein G Sepharose elution conditions: 0.2 mL of dengue standard serum was mixed with 3 mL of Protein A MAPSII binding buffer and 0.6 mL of 50% Protein A Sepharose or 3 mL of D-PBS and 0.6 mL of 50% Protein G Sepharose for 90 min. Washed with Protein A MAPSII Binding buffer or D-PBS and eluted in 0.1M Glycine buffer pH 3.0 - pH 2.5. Eluate was immediately neutralized to pH 7.0 - 7.5 with 1M Tris-HCl pH 8.0 and exchanged buffer to D-PBS using Amicon® Ultra-4. Purity was measured by NuPAGE (ThermoFisher Scientific), and purified antibody avidity assay was measured using biotinylated DENV-1 VLP and Octet RED system (Sartorius). **B**: Optimization of serum volume: 0.03 - 0.2 mL of DEN-203 volunteer (clinical trial NCT01511250: 1044010 Day 90) serum was mixed with 3 mL of D-PBS and 0.6 mL of 50% Protein G Sepharose for 90 min and washed with D-PBS and eluted in 0.1M Glycine buffer pH 2.7. Eluate was immediately neutralized to pH 7.0 - 7.5 with 1M Tris-HCl pH 8.0 and exchanged buffer to D-PBS using Amicon® Ultra-4. Purity was measured by NuPAGE, and purified antibody avidity assay was measured using biotinylated DENV-1 VLP and Octet RED system.

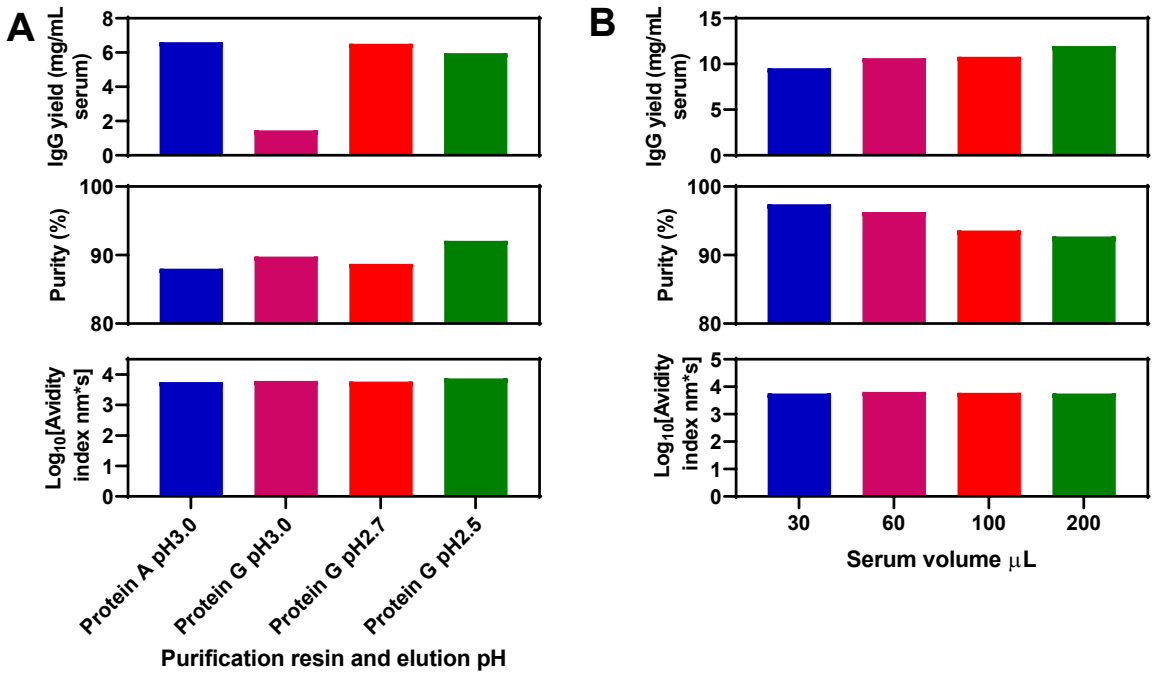
A
IgG yield (mg/mL serum)
Purity (%)
Log10[Avidity index nm*s]
Protein A pH3.0
Protein G pH3.0
Protein G pH2.7
Protein G pH2.5
Purification resin and elution pH
B
IgG yield (mg/mL serum)
Purity (%)
Log10[Avidity index nm*s]
30
60
100
200
Serum volume µL

Figure 10 Optimization of Avidity assay

A: Optimization of association and VLP concentration: Antibody avidity index was measured using Octet HTX (Sartorius) and DENV-1, 2, 3 and 4 VLP. 125 μg/mL anti-dengue polyclonal antibody purified form DEN-203 volunteer serum (NCT01511250: DENV-1: 1071001 Day 90, DENV-2: 1071009 Day 90, DENV-3: 1083005 Day 0, DENV-4: 1093001 Day 90) measured association and dissociation constant. Association time changed from 600, 900 and 1800 sec at biotinylated DENV-VLP 5 μg/mL, and biotinylated VLP concentrations changed from 1, 3, and 5 μg/mL at 1800 sec association time. Data were measured eight times, and the bar graph showed an average ± SD. **B**: Optimization of dissociation constant analysis: Biosensorgram of anti-dengue polyclonal antibody purified form DEN-203 volunteer serum (NCT01511250: 1081001 Day 0: 250 μg/mL) were generated by Otet RED systems and 5 μg/mL DENV-3 VLP. Dissociation constant was analyzed from 30 to 600 sec, red, and from 30 to 1200 sec, blue. Nine different biosensorgrams measured antibody dissociation constants and showed average ± SD. **C**: Difference of biotinylated DENV-1 VLP: Five lots of DENV-1 VLP (Lot no: 15062616, 18011816, 18042710, 19040109 and 20012911) were biotinylated with 50 excess moles of EZ-Link™ Sulfo-NHS-Biotin. Antibody avidity index measured using the Octet HTX system using seven different anti-dengue polyclonal antibodies purified from DEN-203 volunteer serum (NCT01511250: 1044010 Day 90, 1053009 Day 90, 1053011 Day 120, 1071001 Day 90, 1071009 Day 90, 1083005 Day 0 and 1093001 Day 90) at 5 μg/mL of biotinylated DENV-1 VLPs. The graph showed an average ±95% confidence interval. **D**: Linearity of avidity assay: Antibody avidity index was measured using Octet HTX (Sartorius) and biotinylated DENV-1 VLP. Anti-dengue polyclonal antibody from DEN-203 volunteer (NCT01511250:1053005 Day 90) serum was applied to the assay. Antibody concentrations were changed from 10 to 70 μg/mL

and measured 15 times. Data showed average ± SD. Equations: (DENV-1: Response: y = 0.0103 x + 0.087, $Log_{10}[k_{dis}]$; y = 0.0033 x - 3.927, Log_{10}[Avidity index]: y = 0.0076 x + 3.138).

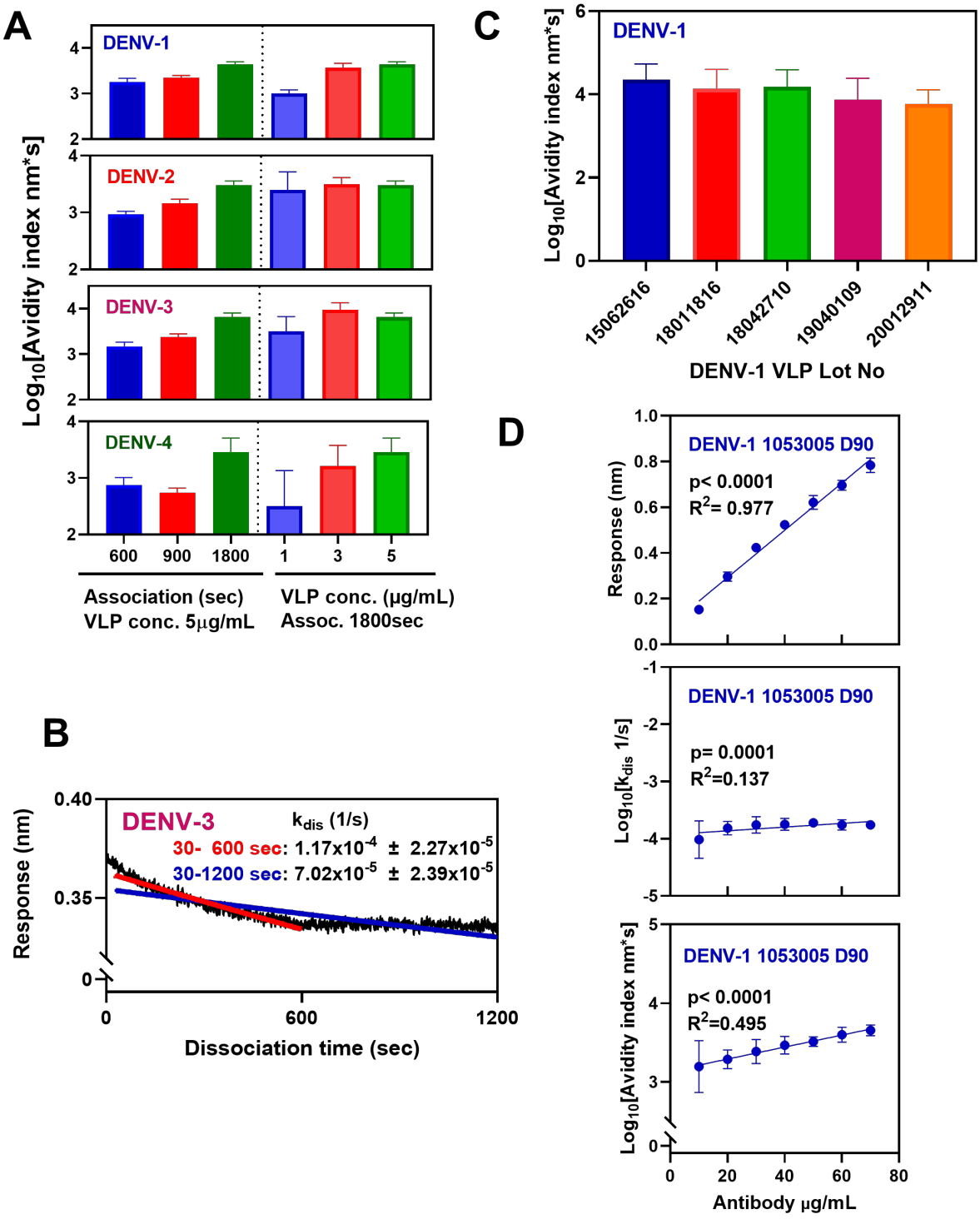

Figure 11 Reactivity of anti-dengue polyclonal antibody to biotinylated VLPs

A: Reactivity of anti-dengue polyclonal antibody: Anti-dengue polyclonal antibody purified form DEN-203 (NCT01511250)volunteer serum (1053005 D90) were diluted from 4 to 250 μg/mL and measured for response using the Octet Red system (Sartorius) and DENV-1, DENV-2, DENV-3, and DENV-4 VLP**. B:** Linearity of Avidity assay**:** Two anti-dengue polyclonal antibodies purified from DEN-203 (NCT01511250) volunteer sera (DENV-2 and DENV-4: 1053011 D120, DENV-3: 1053011 D90) were diluted from 5 - 70 μg/mL and measured avidity using the Octet HTX system and 5 μg/mL DENV-2, DENV-3, and DENV-4 VLP. Assays were run six times with triplicated data points. Data showed average ± SD. Equations (DENV-2 Response: $y = 0.0077 x + 0.081$, $Log_{10}[k_{dis}]$; $y = -0.0040 x - 4.38$, Log_{10}[Avidity index]: $y = 0.0164 x + 3.310$, DENV-3 Response: $y = 0.0087 x + 0.065$, $Log_{10}[k_{dis}]$; $y = -0.0010 x - 4.63$, Log_{10}[Avidity index]: $y = 0.0249 x + 3.544$, DENV-4 Response: $y = 0.0029 x + 0.051$, $Log_{10}[k_{dis}]$; $y = 0.0131 x - 4.37$, Log_{10}[Avidity index]: $y = -0.00085 x + 3.132$)

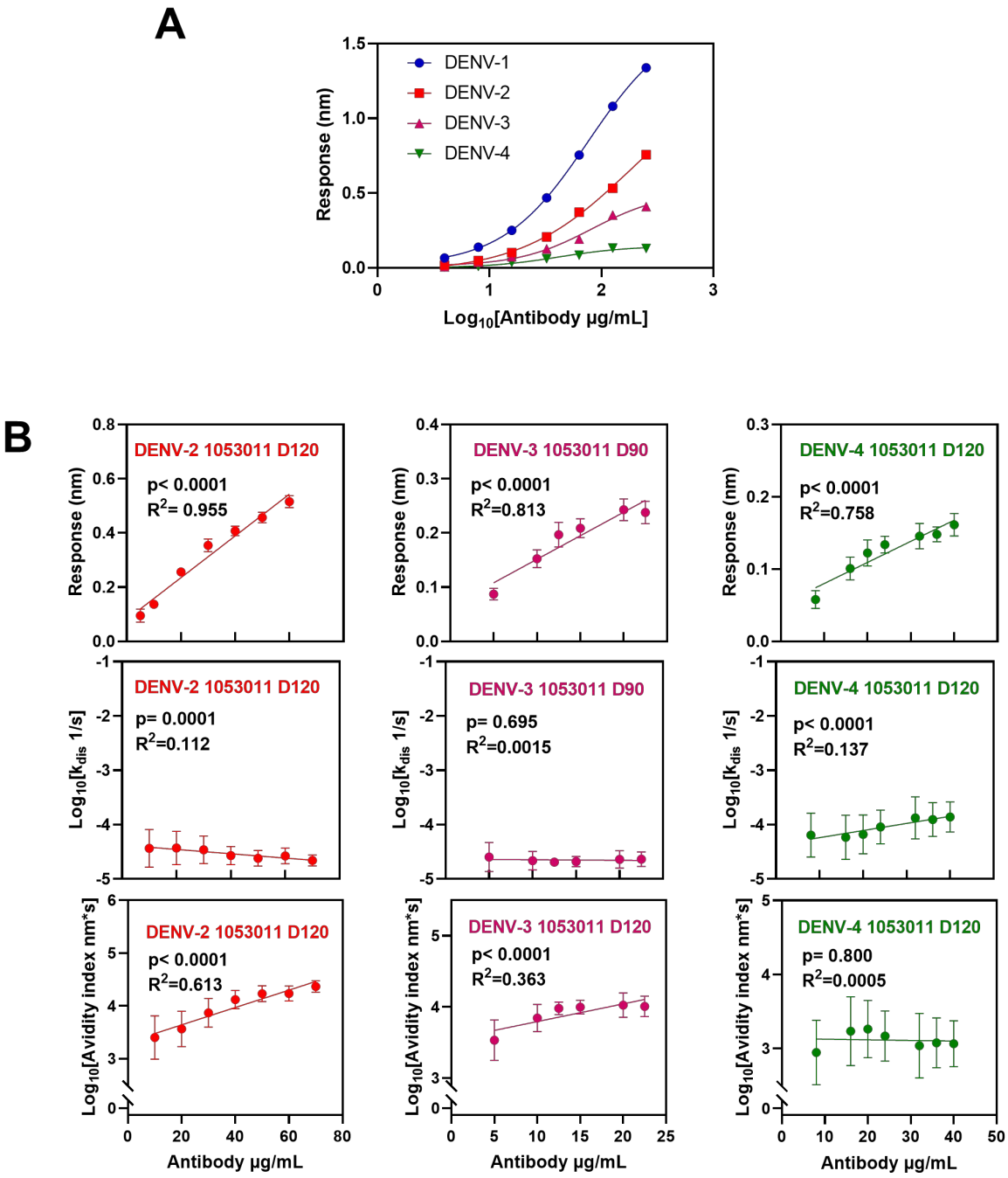
A
DENV-1
DENV-2
DENV-3
DENV-4
Response (nm)
Log10[Antibody µg/mL]
B
DENV-2 1053011 D120
p< 0.0001
R2= 0.955
DENV-3 1053011 D90
p< 0.0001
R2=0.813
DENV-4 1053011 D120
p< 0.0001
R2=0.758
Response (nm)
DENV-2 1053011 D120
p= 0.0001
R2=0.112
DENV-3 1053011 D90
p= 0.695
R2=0.0015
DENV-4 1053011 D120
p< 0.0001
R2=0.137
Log10[Kdis 1/s]
DENV-2 1053011 D120
p< 0.0001
R2=0.613
DENV-3 1053011 D120
p< 0.0001
R2=0.363
DENV-4 1053011 D120
p= 0.800
R2=0.0005
Log10[Avidity index nm*s]
Antibody µg/mL

Figure 12 Biosensorgram of dengue vaccine recipients and avidity assay parameters.

A and B: Biosensorgram (NCT01511250 DEN-203; volunteer **A**: #1022005, **B**: #1044010). Antibody avidity index was measured using the Octet RED system (Sartorius) and DENV-2 virus-like particles. Anti-dengue polyclonal antibody was used at 250 μg/mL to measure response and dissociation constant. Biosensorgram at day 0, 28, 90, 120, 180, and 360 days, black line: dissociation constant calculation curve by Langmuir 1:1 binding model. **C**: Antibody response, $k_{dis,}$ and avidity index of dengue vaccine recipient's serum (● #1022005 and ▲ #1044010) Duplicate and average data did assays were shown.

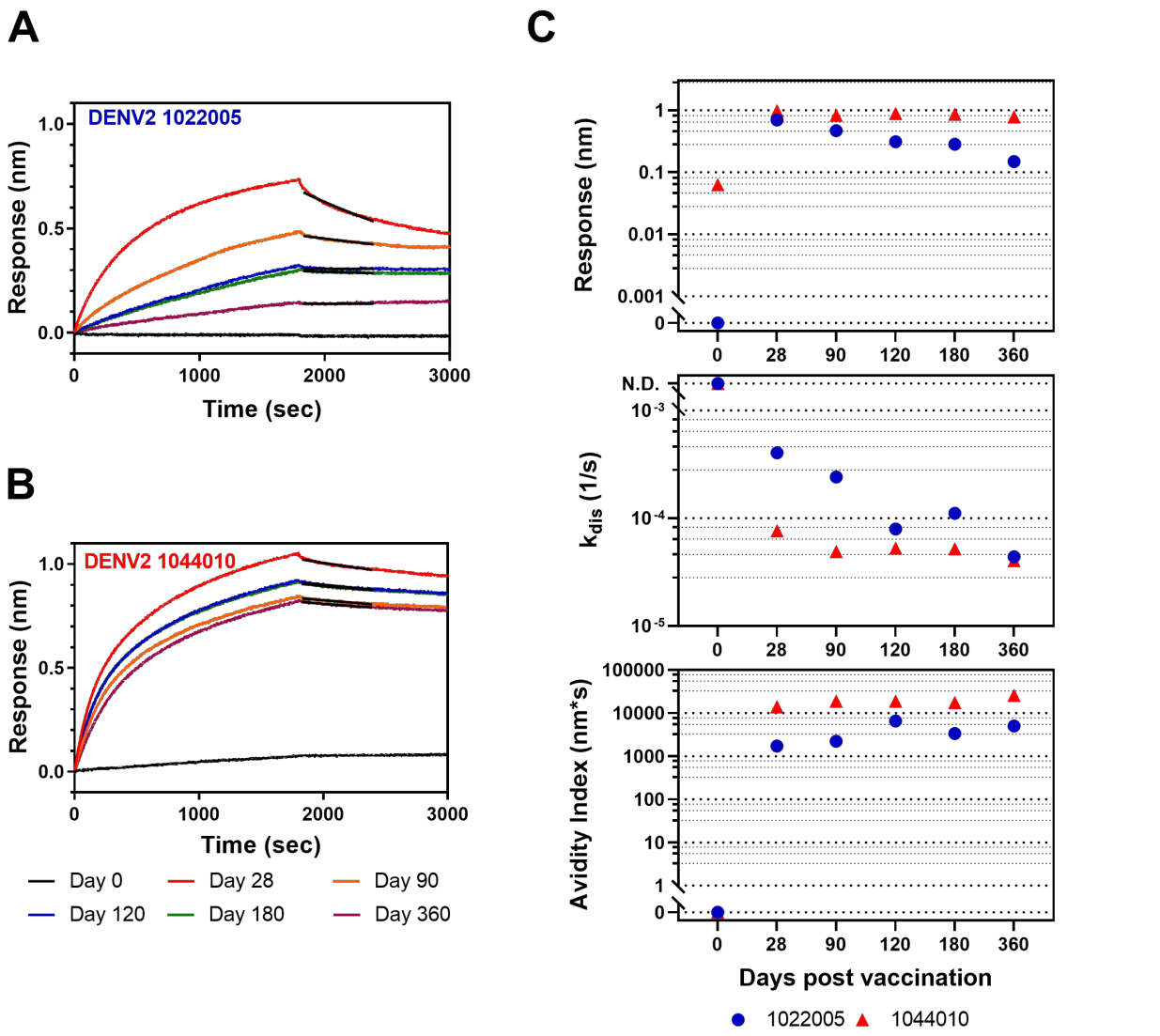
A
DENV2 1022005
Response (nm)
Time (sec)
B
DENV2 1044010
Response (nm)
Time (sec)
Day 0
Day 28
Day 90
Day 120
Day 180
Day 360
C
Response (nm)
N.D.
k_{dis} (1/s)
Avidity Index (nm*s)
Days post vaccination
1022005
1044010

Figure 13 Antibody response of TAK-003 recipients.

A: NCT01511250; DEN-203 baseline seronegative, N = 37, **B**: DEN-203 baseline seropositive, N = 19: **C:** NCT02302066; DEN-204 baseline seronegative, N = 21 and baseline seropositive, N = 15. These data were measured using the Octet HTX system (Sartorius) and DENV-1, DENV-2, DENV-3, and DENV-4 virus-like particles**. A, B:** Box plot: bar min and max, box: 25 and 75 percentile and line: median: DEN-203: Serum samples collected on study Days 0 (baseline / pre-vaccination; first TAK-003 dose administered), 28, 90 (second TAK-003 dose administered), 120, 180, and 360. **C:** Box plot: bar min and max, box: 25 and 75 percentile and line: median: DEN-204: Serum samples collected on study Day 0 (baseline / pre-vaccination; first TAK-003 dose administered) and Day 180 (three months after administration of second dose). ****$p < 0.0001$ (Wilcoxon signed-rank test). ***$p < 0.0002$. **$p < 0.0021$. *$p < 0.0332$. vs. Day 0 n.s., not significant. Negative response values were extrapolated to 0.001 for drawing purposes.

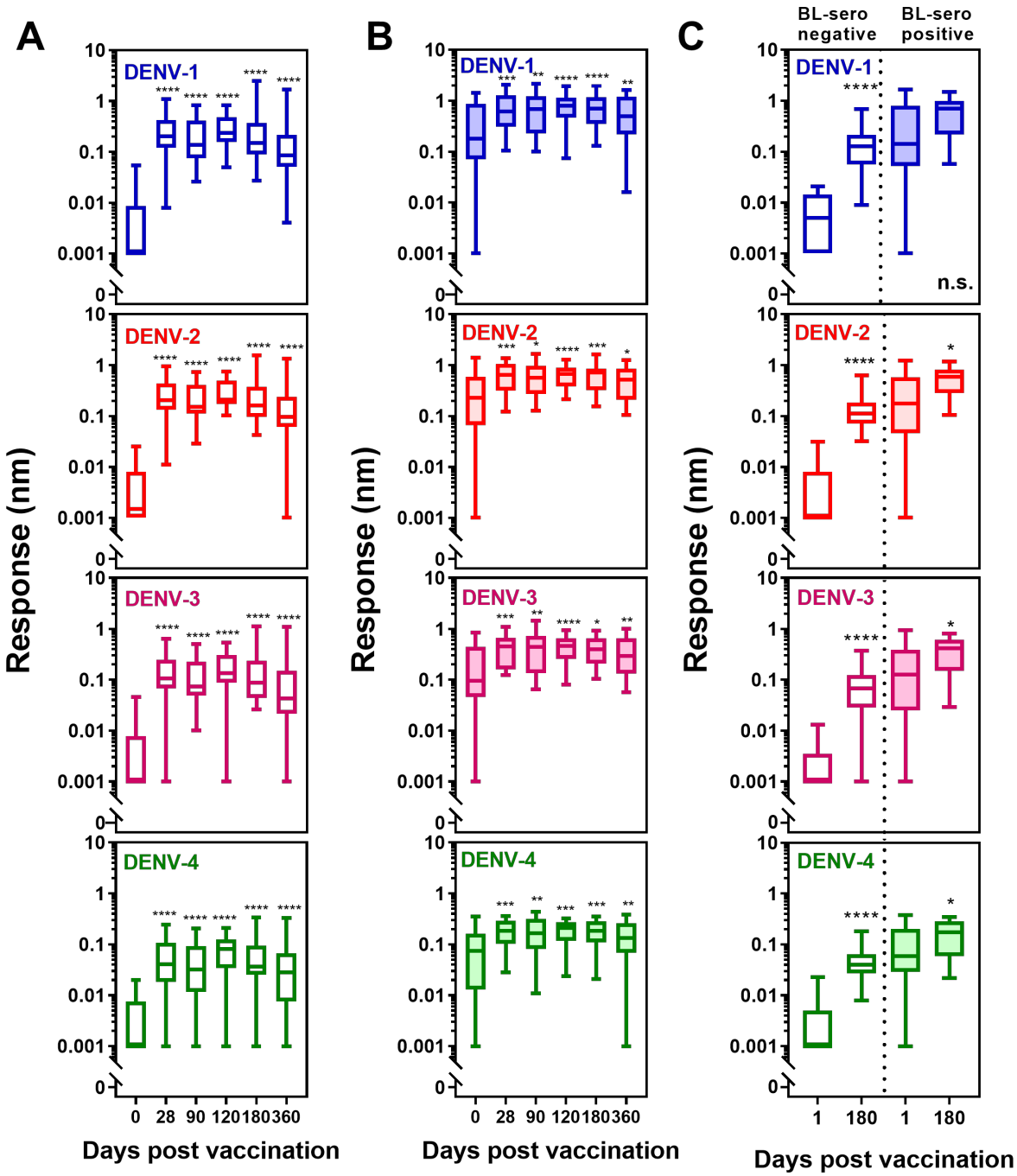
A
B
C
BL-sero negative
BL-sero positive
DENV-1
DENV-2
DENV-3
DENV-4
n.s.
Response (nm)
10
1
0.1
0.01
0.001
0
0 28 90 120 180 360
1 180 1 180
Days post vaccination

Figure 14 Antibody dissociation constant, $k_{dis,}$ of TAK-003 recipients.

A: NCT01511250; DEN-203 baseline seronegative, N = 37, **B**: DEN-203 baseline seropositive, N = 19: **C:** NCT02302066; DEN-204 baseline seronegative, N = 21 and baseline seropositive, N = 15 These data were measured using the Octet HTX system (Sartorius) and DENV-1, DENV-2, DENV-3, and DENV-4 virus-like particles**. A, B:** Box plot: bar min and max, box: 25 and 75 percentile and line: median: DEN-203: Serum samples collected on study Days 0 (baseline/ pre-vaccination; first TAK-003 dose administered), 28, 90 (second TAK-003 dose administered), 120, 180, and 360. **C:** Box plot: bar min and max, box: 25 and 75 percentile and line: median: DEN-204: Serum samples collected on study Day 0 (baseline/ pre-vaccination; first TAK-003 dose administered) and Day 180 (three months after administration of second dose). ****$p < 0.0001$ (Wilcoxon signed-rank test). *** $p < 0.0002$. ** $p < 0.0021$. * $p < 0.0332$. vs. Day 0 n.s., not significant. No binding samples; k_{dis} values were automatically extrapolated to $1x10^{-3}$ 1/s by Octet Data Analysis software HT.

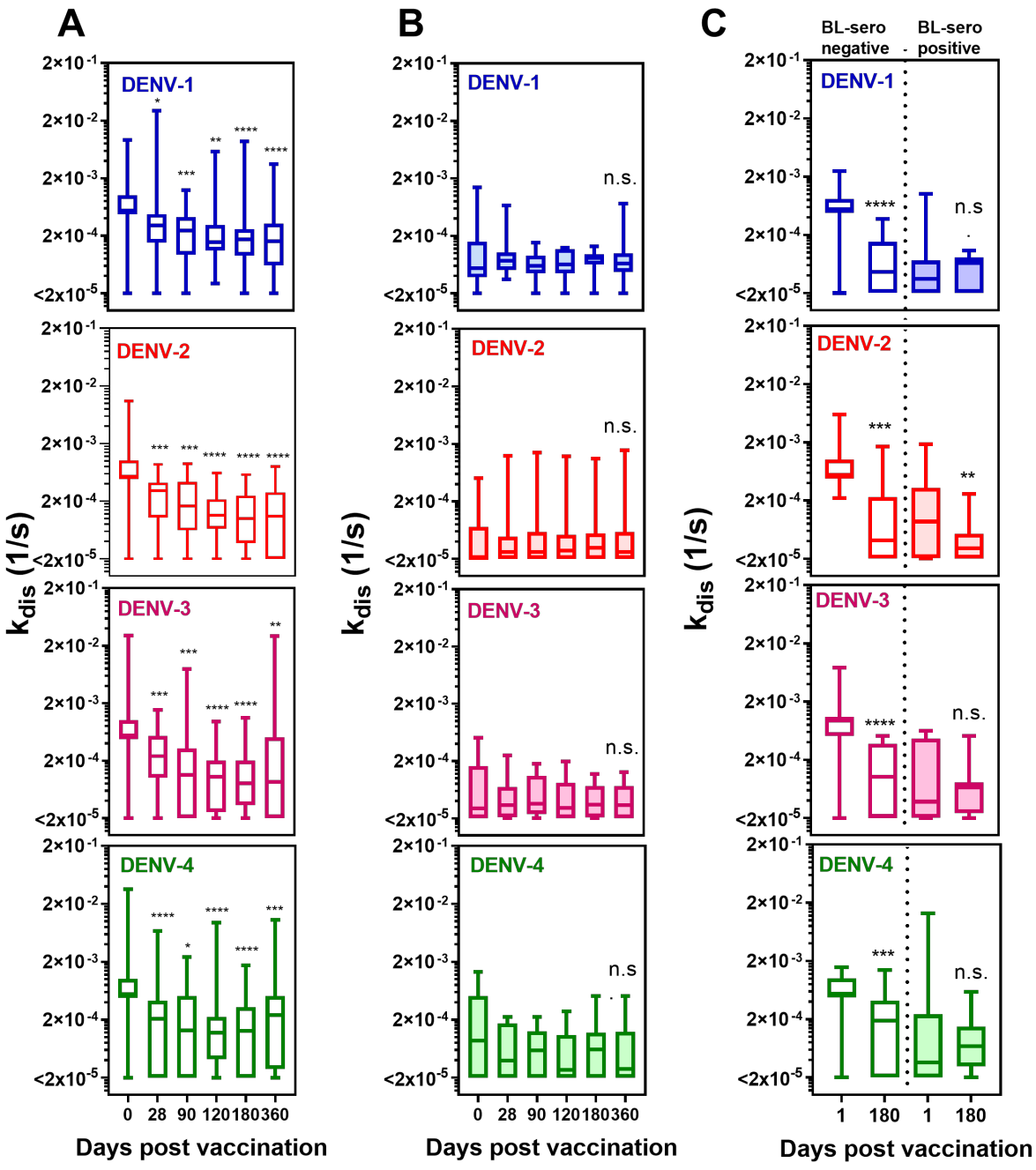
A
B
C
BL-sero negative
BL-sero positive
DENV-1
DENV-2
DENV-3
DENV-4
k_{dis} (1/s)
2×10-1
2×10-2
2×10-3
2×10-4
<2x10-5
n.s.
n.s
0 28 90 120 180 360
1 180 1 180
Days post vaccination

Figure 15 Avidity index of TAK-003 recipients.

A: NCT01511250; DEN-203 baseline seronegative N = 37: **B**: DEN-203 baseline seropositive N = 19: **C**, NCT02302066; DEN-204 baseline seronegative N = 21 and baseline seropositive N = 15. These data were measured using the Octet HTX system (Sartorius) and DENV-1, DENV-2, DENV-3, and DENV-4 virus-like particles**. A, B:** Box plot: bar min and max, box: 25 and 75 percentile and line: median: DEN-203: Serum samples collected on study Days 0 (baseline/ pre-vaccination; first TAK-003 dose administered), 28, 90 (second TAK-003 dose administered), 120, 180, and 360. **C**, Box plot: bar min and max, box: 25 and 75percenttile and line: median: DEN-204: Serum samples collected on study Day 0 (baseline/ pre-vaccination; first TAK-003 dose administered) and Day 180 (three months after administration of second dose). Avidity index = response/ k_{dis}. **** $p < 0.0001$ (Wilcoxon signed-rank test). *** $p < 0.0002$. ** $p < 0.0021$. * $p < 0.0332$. vs. Day 0 n.s., not significant. Negative Avidity index data were extrapolated to 1.0 for drawing purposes.

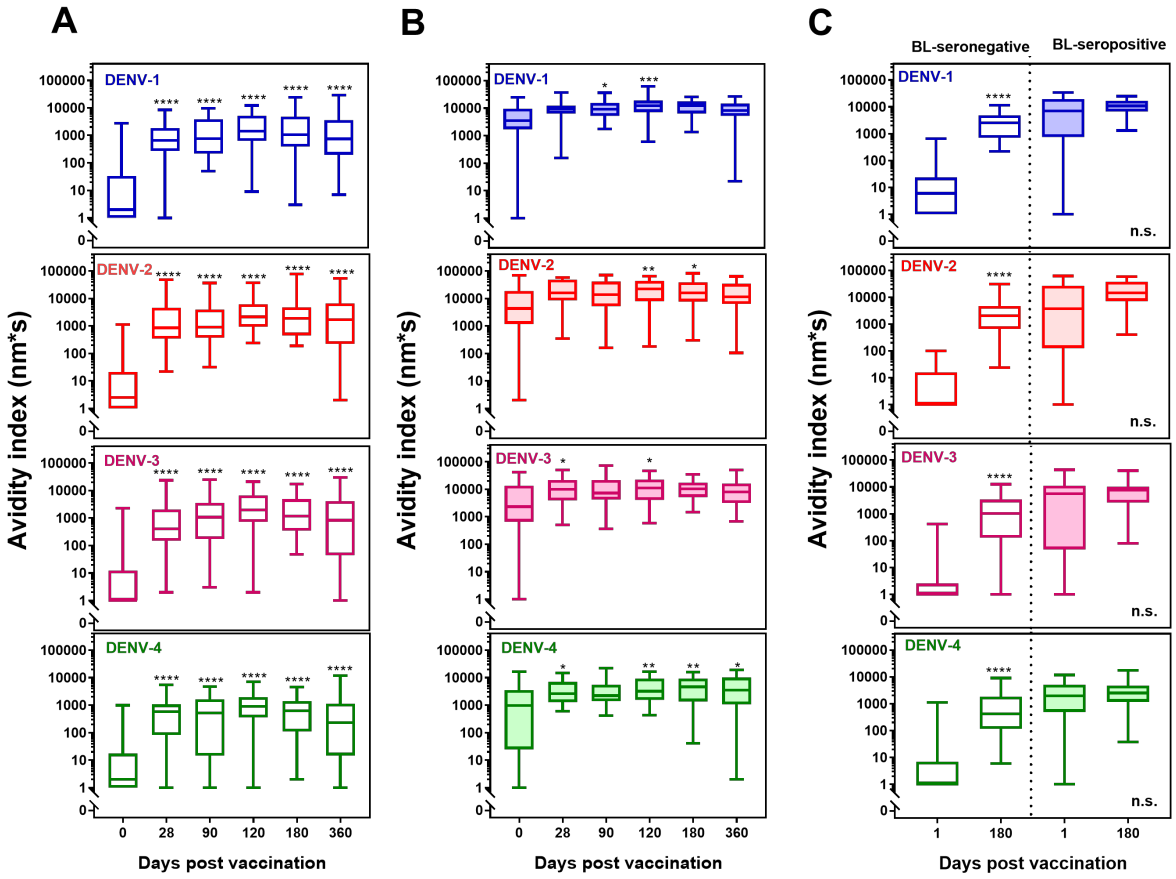
A
B
C
BL-seronegative
BL-seropositive
DENV-1
DENV-2
DENV-3
DENV-4
Avidity index (nm*s)
Days post vaccination
n.s.

Figure 16 Correlation between avidity assay parameters.

Avidity index and MNT titers **A**: DENV-1, **B**: DENV-2, **C**: DENV-3, **D**: DENV-4. 24 baseline seronegative and 19 seropositive volunteer data NCT01511250 (DEN-203) were used except for baseline seronegative Day 0 data. Data points: 226 - 228. open symbols: baseline seropositive, closed symbols: baseline seronegative. Correlations between response, $k_{dis,}$ and MNT titer were shown in **Figure 17,** and correlation analysis data in **Table 10.**

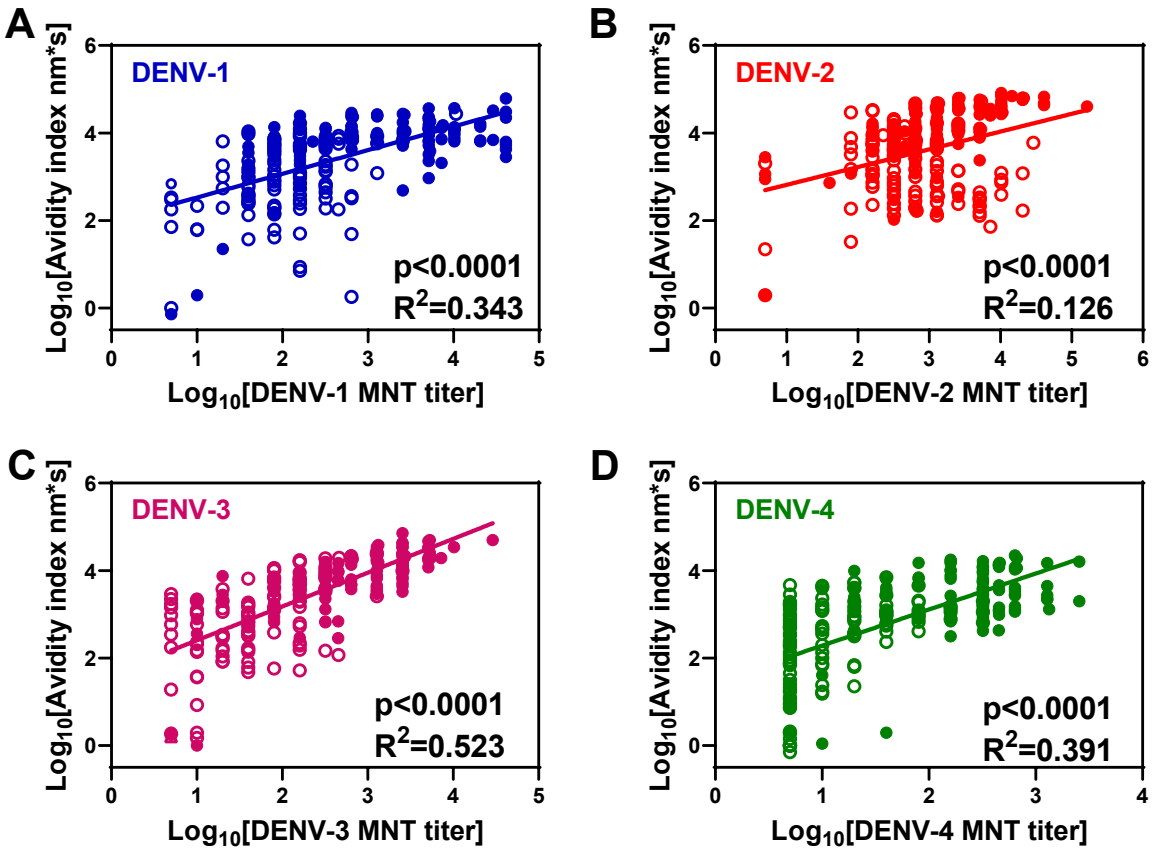

Figure 17 Correlation between avidity assay parameters.

A, response, **B**, k_{dis}, and MNT titers. 24 baseline seronegative and 19 seropositive volunteer data NCT01511250 (DEN-203) were used except for baseline seronegative Day 0 data N = 226 - 228. Open symbols were baseline seropositive and closed symbols were baseline seronegative. Correlation analysis data were shown in Table 10.

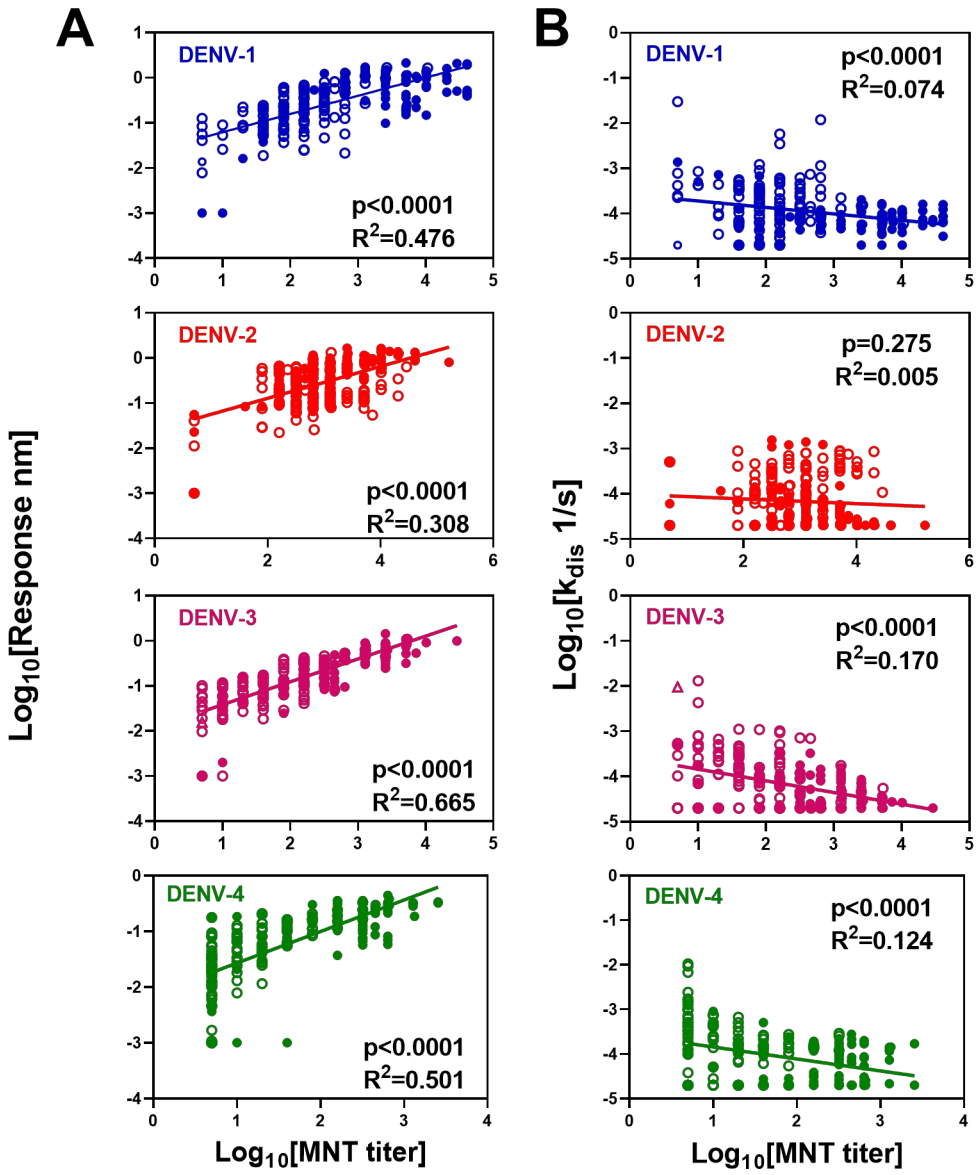

Figure 18 Correlation between avidity index and MNT antibody titer for visiting day (Baseline seronegative).

All baseline seronegative volunteer data were correlated for each visiting day (Day 28, 90, 120, 180, and 360).

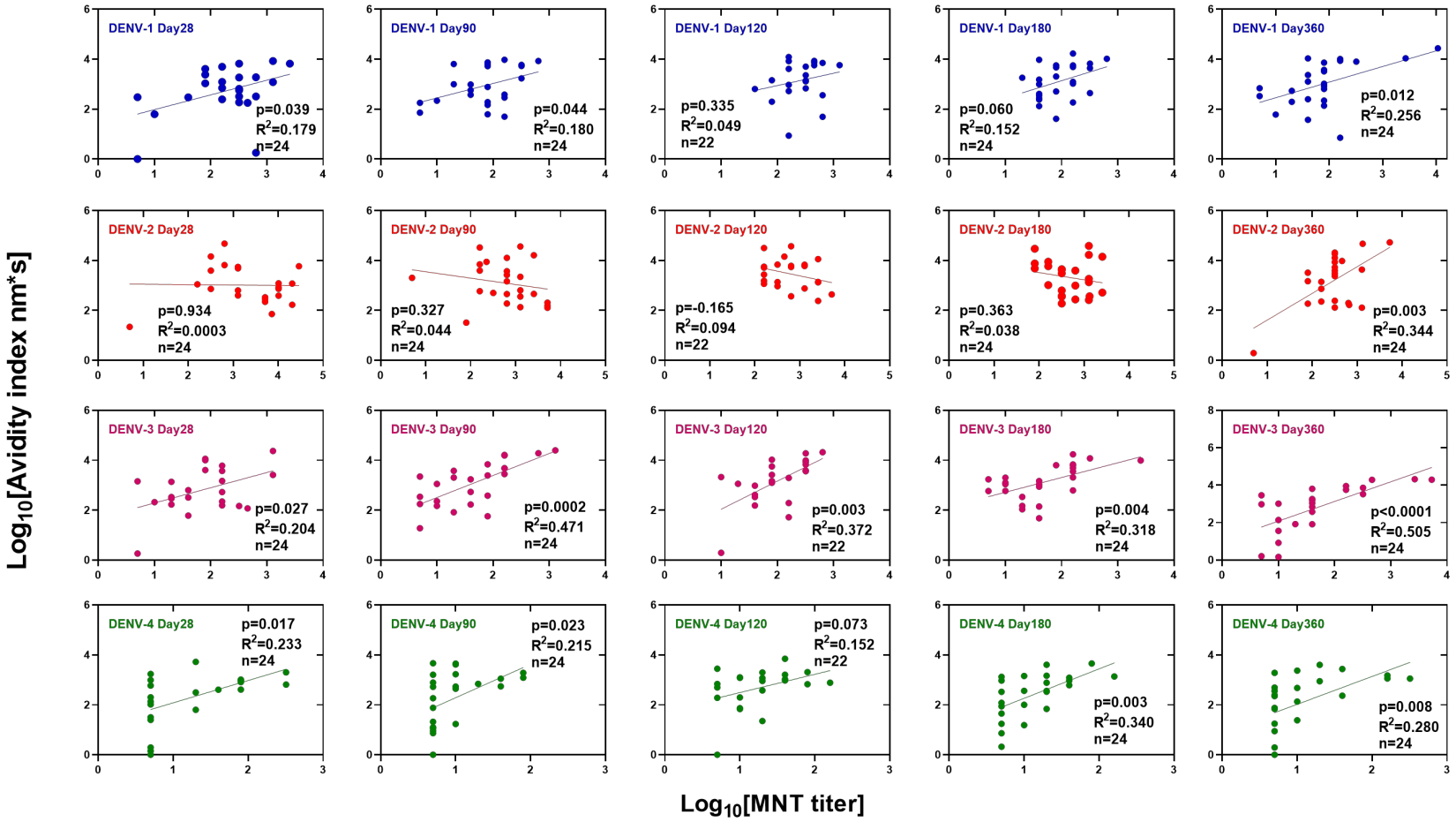

Figure 19 Correlation between avidity index and MNT antibody titer for visiting day (Baseline seropositive).

All baseline seropositive volunteer data were correlated for each visiting day (Day 0, 28, 90, 120, 180, and 360).

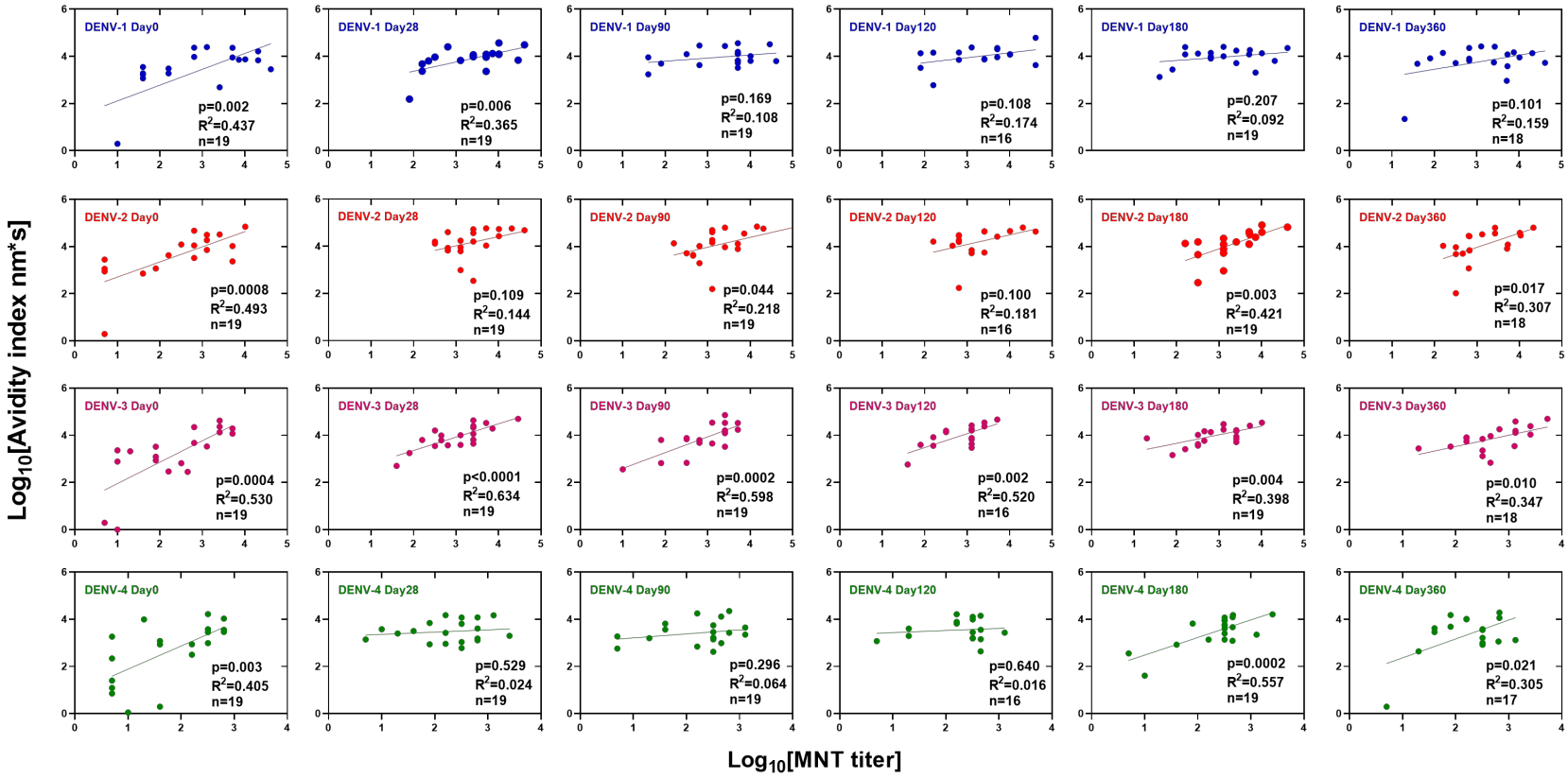

Figure 20 Correlation between avidity index for each serotype.

Avidity index of DEN-203 (NCT01511250: 24 baseline seronegative and 19 seropositive volunteers) was used except for baseline seronegative Day 0. Equations: DENV-2/ DENV-1: y = 0.785 x + 0.552, DENV-3/ DENV-1: y = 0.742 x + 0.887, DENV-3/ DENV-2: y = 0.756 x + 1.06, DENV-4/ DENV-1: y = 0.563 x + 1.824, DENV-4/ DENV-2: y = 0.553 x + 2.060, DENV-4/ DENV-3: y = 0.624 x + 1.620.

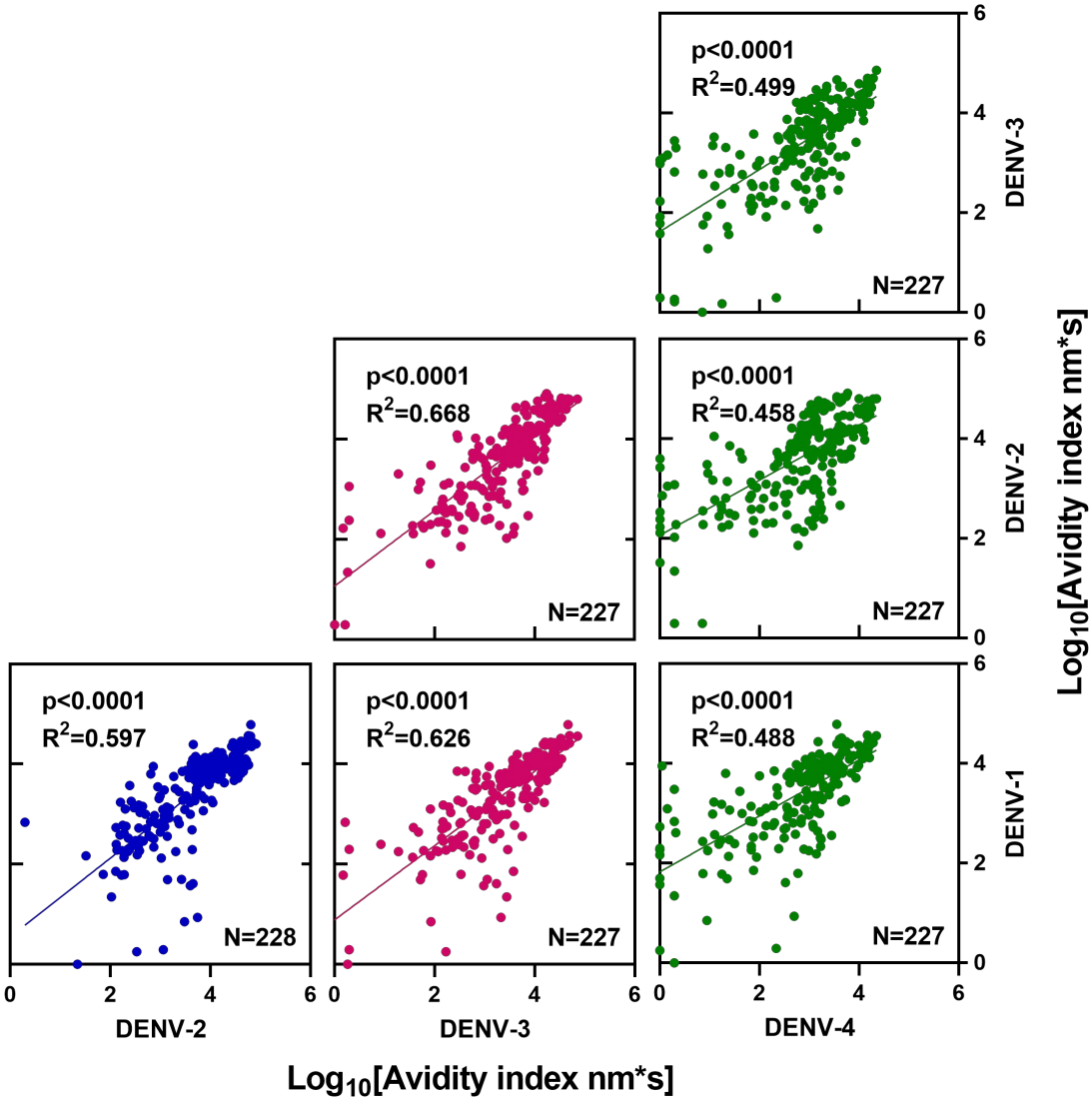

Figure 21 Correlation between avidity index and MNT antibody titer for k_{dis} divided subjects of DENV-2.

A: Correlation analysis using all data sets. N = 230, **B - D:** Correlation analysis data divided into three ranges by Log_{10} k_{dis} values. **B**: $Log_{10}[k_{dis}]$: -4.7 - -4.6, N = 77, **C**: $Log_{10}[k_{dis}]$: -4.6 - -4.0, N = 77, **D**: $Log_{10}[k_{dis}]$: -4.0 - -2.8, N = 76, 24 baseline seronegative and 19 seropositive volunteer data were used and data under response LoD were eliminated from the analysis: DENV-2: 0.015. in **Table 7** LoD: limit of detection. Correlation of DENV-1, DENV-3, and DENV-4 were shown in **Figure 22.** Correlation analysis date parameters were shown in **Table 11**.

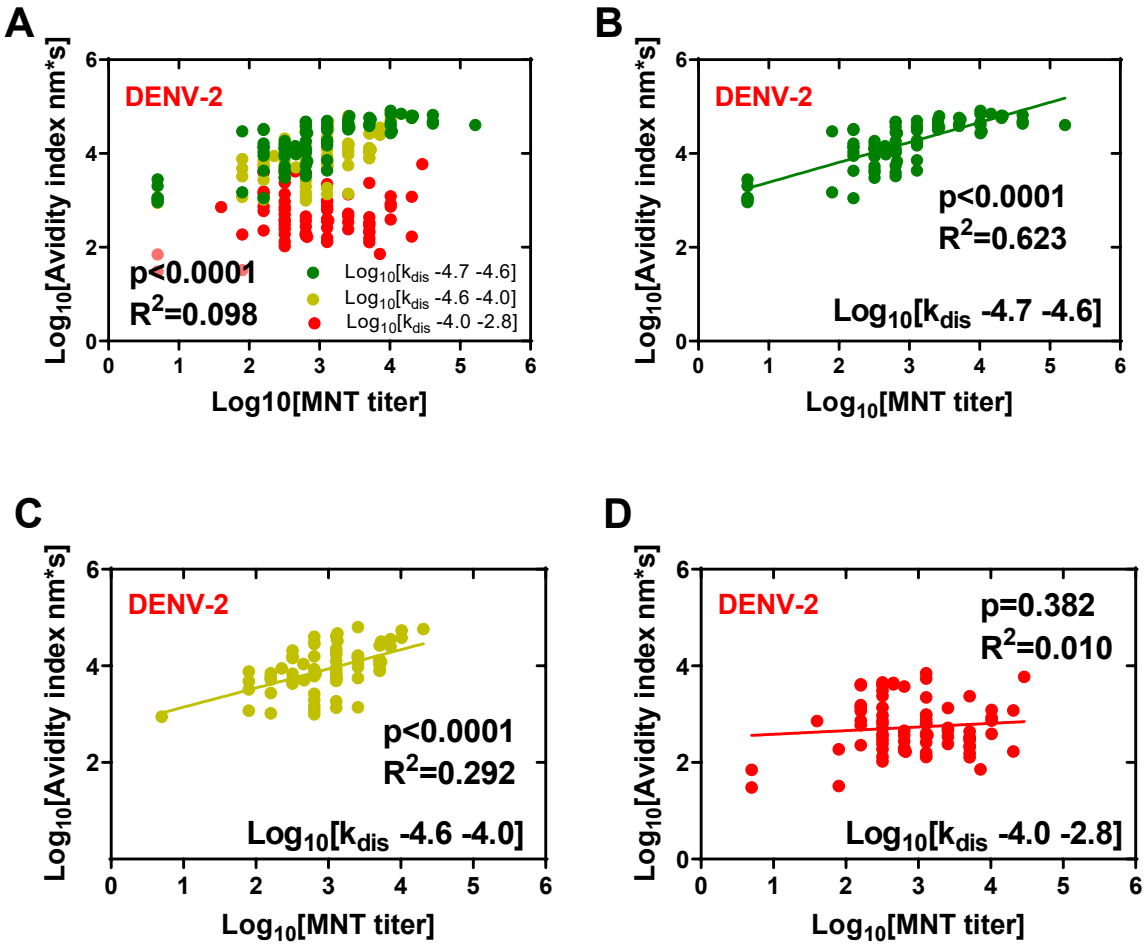
A
DENV-2
p<0.0001
R2=0.098
Log10[kdis -4.7 -4.6]
Log10[kdis -4.6 -4.0]
Log10[kdis -4.0 -2.8]
Log10[Avidity index nm*s]
Log10[MNT titer]
B
DENV-2
p<0.0001
R2=0.623
Log10[kdis -4.7 -4.6]
Log10[Avidity index nm*s]
Log10[MNT titer]
C
DENV-2
p<0.0001
R2=0.292
Log10[kdis -4.6 -4.0]
Log10[Avidity index nm*s]
Log10[MNT titer]
D
DENV-2
p=0.382
R2=0.010
Log10[kdis -4.0 -2.8]
Log10[Avidity index nm*s]
Log10[MNT titer]

Figure 22 Correlation between avidity index and MNT antibody titer for k_{dis} divided subjects.

A correlation analysis using all data sets. **B** correlation analysis data divided into three ranges by Log_{10} k_{dis} values. DENV-1: $Log_{10}[k_{dis}]$: -4.7 - -4.2: N = 75, -4.2 - -3.9: N = 74, -3.9 - -1.9: N = 76, DENV-3: $Log_{10}[k_{dis}]$: -4.7 - -4.6: N = 75, -4.6 - -4.0: N = 75, -4.0 - -1.9: N = 73, DENV-4: $Log_{10}[k_{dis}]$: -4.7 - -4.6: N = 66, -4.6 - -3.8: N = 65, -3.8 - -2.6: N = 66. 24 baseline seronegative and 19 seropositive volunteer data from DEN-203 were used, and data under response LoD were eliminated from the analysis: DENV-1: 0.017, DENV-3: 0.018, DENV-4: 0.014 measured in **Table 7.** LoD: limit of detection. Correlation analysis data were shown in **Table 11**

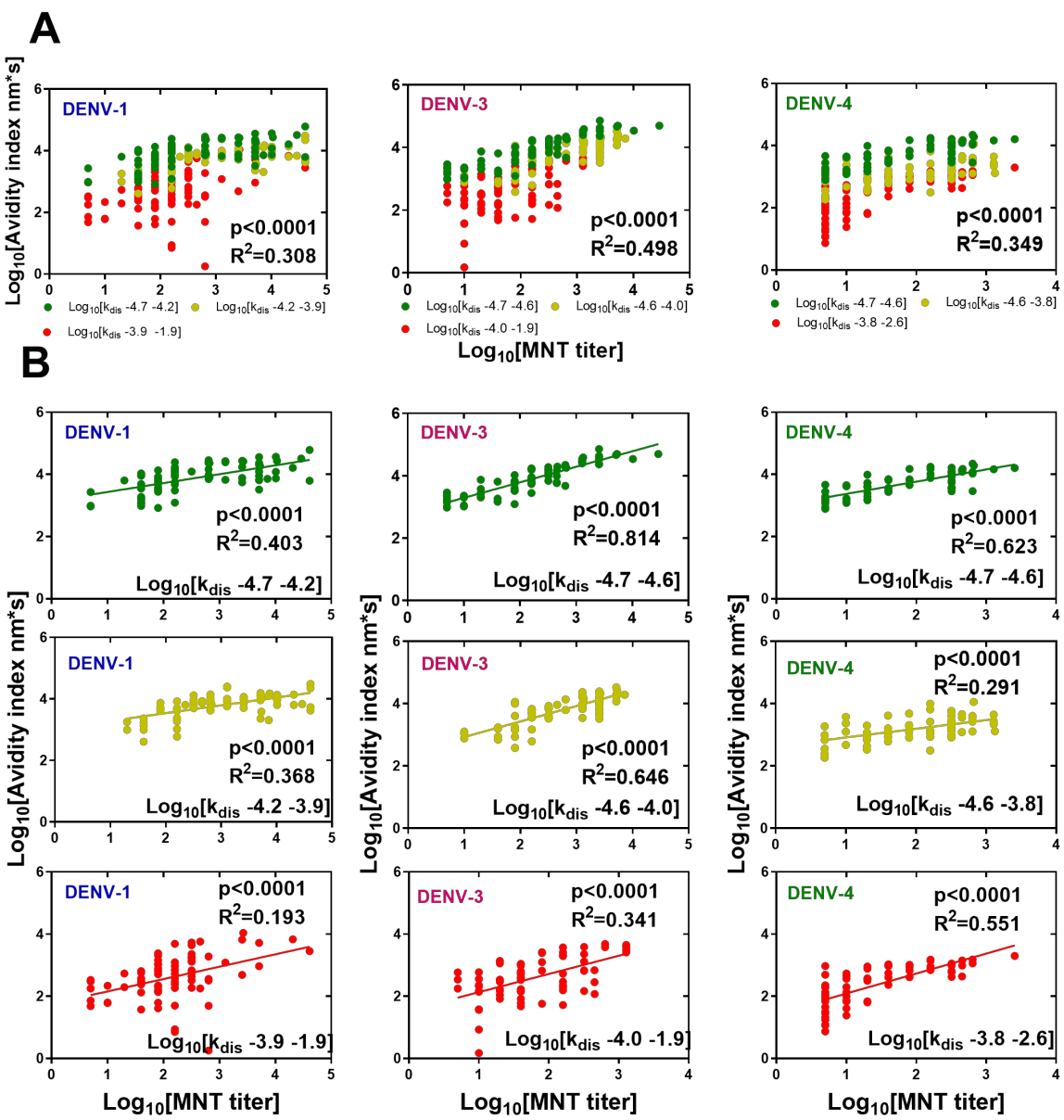
A
DENV-1
p<0.0001
R2=0.308
Log10[kdis -4.7 -4.2]
Log10[kdis -4.2 -3.9]
Log10[kdis -3.9 -1.9]
DENV-3
p<0.0001
R2=0.498
Log10[kdis -4.7 -4.6]
Log10[kdis -4.6 -4.0]
Log10[kdis -4.0 -1.9]
DENV-4
p<0.0001
R2=0.349
Log10[kdis -4.7 -4.6]
Log10[kdis -4.6 -3.8]
Log10[kdis -3.8 -2.6]
Log10[Avidity index nm*s]
Log10[MNT titer]
B
DENV-1
p<0.0001
R2=0.403
Log10[kdis -4.7 -4.2]
DENV-1
p<0.0001
R2=0.368
Log10[kdis -4.2 -3.9]
DENV-1
p<0.0001
R2=0.193
Log10[kdis -3.9 -1.9]
DENV-3
p<0.0001
R2=0.814
Log10[kdis -4.7 -4.6]
DENV-3
p<0.0001
R2=0.646
Log10[kdis -4.6 -4.0]
DENV-3
p<0.0001
R2=0.341
Log10[kdis -4.0 -1.9]
DENV-4
p<0.0001
R2=0.623
Log10[kdis -4.7 -4.6]
DENV-4
p<0.0001
R2=0.291
Log10[kdis -4.6 -3.8]
DENV-4
p<0.0001
R2=0.551
Log10[kdis -3.8 -2.6]
Log10[Avidity index nm*s]
Log10[MNT titer]

Tables

Table 6 Maximum noise measurement of Avidity assay.

Sample ID and serotype		Max Noise nm			Summary	
		Run1	Run2	Run3		
DENV-1	Sample ID: DEN203 1044008_D0	0.0055	0.0049	0.0061	DENV-1	Noise
	Sample ID: DEN203 1044008_D0	0.0050	0.0053	0.0062	Max	0.0075
	Sample ID: DEN203 1044010_D0	0.0062	0.0045	0.0055	Min	0.0044
	Sample ID: DEN203 1044010_D0	0.0062	0.0052	0.0061	Average	0.0056
	Sample ID: DEN203 1053005_D0	0.0051	0.0044	0.0055	SD	0.0007
	Sample ID: DEN203 1053005_D0	0.0056	0.0065	0.0075	CV%	13%
DENV-2	Sample ID: DEN203 1044008_D0	0.0050	0.0052	0.0049	DENV-2	Noise
	Sample ID: DEN203 1044008_D0	0.0052	0.0043	0.0051	Max	0.0057
	Sample ID: DEN203 1044010_D0	0.0050	0.0040	0.0057	Min	0.0040
	Sample ID: DEN203 1044010_D0	0.0049	0.0048	0.0053	Average	0.0049
	Sample ID: DEN203 1053005_D0	0.0041	0.0056	0.0049	SD	0.0004
	Sample ID: DEN203 1053005_D0	0.0051	0.0048	0.0048	CV%	9%
DENV-3	Sample ID: DEN203 1044008_D0	0.0052	0.0064	0.0049	DENV-3	Noise
	Sample ID: DEN203 1044008_D0	0.0059	0.0055	0.0057	Max	0.0066
	Sample ID: DEN203 1044010_D0	0.0057	0.0064	0.0057	Min	0.0049
	Sample ID: DEN203 1044010_D0	0.0061	0.0060	0.0061	Average	0.0059
	Sample ID: DEN203 1053005_D0	0.0062	0.0063	0.0060	SD	0.0004
	Sample ID: DEN203 1053005_D0	0.0060	0.0063	0.0066	CV%	7%
DENV-4	Sample ID: DEN203 1044008_D0	0.0041	0.0042	0.0046	DENV-4	Noise
	Sample ID: DEN203 1044008_D0	0.0053	0.0042	0.0044	Max	0.0056
	Sample ID: DEN203 1044010_D0	0.0037	0.0050	0.0049	Min	0.0037
	Sample ID: DEN203 1044010_D0	0.0056	0.0042	0.0046	Average	0.0045
	Sample ID: DEN203 1053005_D0	0.0046	0.0044	0.0043	SD	0.0005
	Sample ID: DEN203 1053005_D0	0.0051	0.0042	0.0043	CV%	10%

Table 7. Limit of detection of response for Avidity assay

Serotype	N	Noise ± SD (nm) (CV%)	LoD (nm) (Noise X 3)
DENV-1	18	0.0056 ± 0.0007 (CV% 13.1%)	0.017
DENV-2	18	0.0049 ± 0.0004 (CV% 8.9%)	0.015
DENV-3	18	0.0059 ± 0.0004 (CV% 7.3%)	0.018
DENV-4	18	0.0045 ± 0.0005 (CV% 10.3%)	0.014

Table 8 Antibody purification yield for different operators and occasions.

Operator	N	IgG yield mg/mL serum Mean ± SD (CV%)	% of differences	Purity (%) Mean ± SD
A	16	8.36 ± 0.63 (CV% 7.6%)	100%	95.8 ± 1.12
A	16	8.89 ± 0.54 (CV% 6.1%)	106%	95.9 ± 0.97
B	15	6.77 ± 0.58 (CV% 8.5%)	81%	94.1 ± 2.67

Table 9 Intra-plate differences and inter-assay differences of Avidity assay

Serotype	DENV-1		DENV-2		DENV-3		DENV-4	
Sample ID and visit days	1053005_90Day		1053005_90Day		1053005_90Day		1053011_90Day	
	N	Response (nm) Mean ± SD (CV%)	N	Response (nm) Mean ± SD (CV%)	N	Response (nm) Mean ± SD (CV%)	N	Response (nm) Mean ± SD (CV%)
1st run	42	0.558 ± 0.033 (CV% 5.96%)	42	0.328 ± 0.023 (CV% 6.90%)	42	0.188 ± 0.022 (CV% 11.70%)	42	0.195 ± 0.018 (CV% 9.20%)
2nd run	42	0.523 ± 0.033 (CV% 6.24%)	42	0.324 ± 0.029 (CV% 8.99%)	42	0.193 ± 0.019 (CV% 9.60%)	35	0.196 ± 0.015 (CV% 7.61%)
difference 1st and 2nd run		1.06		1.01		0.97		0.99
	N	Log_{10}[Avidity index (nm*s)] Mean ± SD (CV%)	N	Log_{10}[Avidity index (nm*s)] Mean ± SD (CV%)	N	Log_{10}[Avidity index (nm*s)] Mean ± SD (CV%)	N	Log_{10}[Avidity index (nm*s)] Mean ± SD (CV%)
1st run	42	3.544 ± 0.087 (CV% 2.46%)	42	3.787 ± 0.271 (CV% 7.17%)	42	3.691 ± 0.372 (CV% 10.08%)	42	3.172 ± 0.191 (CV% 6.03%)
2nd run	42	3.552 ± 0.103 (CV% 2.91%)	42	3.498 ± 0.290 (CV% 8.29%)	42	3.604 ± 0.295 (CV% 8.20%)	35	3.206 ± 0.252 (CV% 7.87%)
difference 1st and 2nd run		0.99		1.08		1.02		0.99

Table 10 Correlation parameters between avidity assay parameters (response, k_{dis}, and avidity index) and MNT titers

Serotype	N	Log_{10}[MNT titer] vs Log_{10}[Response]			Log_{10}[MNT titer] vs Log_{10}[k_{dis}]			Log_{10}[MNT titer] vs Log_{10}[Avidity index]		
		R^2	p-value	Equation	R^2	p-value	Equation	R^2	p-value	Equation
DENV-1	226	0.476	<0.0001	y = 0.404 x - 1.610	0.074	<0.0001	y = -0.142 x - 3.579	0.343	<0.0001	y = 0.541 x + 1.986
DENV-2	228	0.308	<0.0001	y = 0.353 x - 1.600	0.005	0.275	y = -0.052 x - 4.010	0.126	<0.0001	y = 0.405 x + 2.410
DENV-3	226	0.665	<0.0001	y = 0.507 x - 1.923	0.170	<0.0001	y = -0.258 x - 3.578	0.523	<0.0001	y = 0.773 x + 1.632
DENV-4	227	0.501	<0.0001	y = 0.566 x - 2.135	0.124	<0.0001	y = -0.268 x - 3.574	0.391	<0.0001	y = 0.824 x + 1.461

Table 11 Correlation parameters between avidity index and MNT titer for k_{dis} divided subjects.

Serotype	$Log_{10}[k_{dis}]$ range		N	Log_{10}[Avidity index] vs Log_{10}[MNT titer]		
				R^2	p-value	Equation
DENV-1	-4.7	-1.9	225	0.308	<0.0001	y = 0.459 x + 2.240
	-4.7	-4.2	75	0.403	<0.0001	y = 0.286 x + 3.150
	-4.2	-3.9	74	0.368	<0.0001	y = 0.254 x + 3.033
	-3.9	-1.9	76	0.193	<0.0001	y = 0.398 x + 1.756
DENV-2	-4.7	-2.8	230	0.098	<0.0001	y = 0.325 x + 2.668
	-4.7	-4.6	77	0.623	<0.0001	y = 0.426 x + 2.960
	-4.6	-4.0	77	0.292	<0.0001	y = 0.396 x + 2.749
	-4.0	-2.8	76	0.010	0.382	y = 0.076 x + 2.508
DENV-3	-4.7	-1.9	223	0.498	<0.0001	y = 0.657 x + 1.956
	-4.7	-4.6	75	0.814	<0.0001	y = 0.498 x + 2.795
	-4.6	-4.0	75	0.646	<0.0001	y = 0.497 x + 2.435
	-4.0	-1.9	73	0.341	<0.0001	y = 0.586 x + 1.545
DENV-4	-4.7	-2.6	197	0.349	<0.0001	y = 0.547 x + 2.128
	-4.7	-4.6	66	0.623	<0.0001	y = 0.392 x + 2.983
	-4.6	-3.8	65	0.291	<0.0001	y = 0.279 x + 2.638
	-3.8	-2.6	66	0.551	<0.0001	y = 0.643 x + 1.446

General Discussion

Antibody affinity maturation is a critical process for acquiring the immune response following vaccination and enhances antiviral functions, such as virus neutralization [61], antibody-mediated complement, and effector-dependent cytotoxicity [57, 62]. However, few reports focusing on antibody affinity maturation by flavivirus vaccines have been reported. Therefore, the objective of this thesis was to elucidate the antibody affinity maturation of ZIKV and DENV vaccines.

Anti-ZIKV antibodies were discovered from ZIKV vaccine candidate immunized rabbits. High SHM and CDR mutations were observed in the antibodies and found to be significantly correlated with antibody functions, such as Luminex assay, equilibrium dissociation constants (K_D), dissociation constant (k_{dis}), and neutralizing activities (**Figure 5C**). However, rabbits have unique and robust immune systems and are frequently used to discover highly selective and high-affinity antibodies [135, 212]. Thus, the difference between human and rabbit immune systems has to be considered when extrapolating results from rabbits to humans. In terms of heavy and light chain variable region antibody repertoires, humans and rabbits possess a variety of functional genotype genes (heavy chain: human 51 and rabbit 39, kappa chain human 39 and rabbit: 64, Lambda chain: human 32 and rabbit 20, from IMGT database: **https://www.imgt.org/IMGTrepertoire/Proteins/**) [213]. Both species have similar heavy chain CDR3 lengths (human: mean = 15.3±4.0 AA, mode =15 AA, rabbit: mean =14.8±3.6 AA, mode =13 AA) [138]. Niu et al. also reported that the average SHM ratio of human anti-ZIKV mAbs DNA was 6.91% (1.72 − 14.78%) [214]. I reported that rabbit anti-ZIKV mAb SHM levels were almost identical to human mAb's SHM (**Table 3**). These findings indicate that rabbit and human antibody affinity maturation and functions are comparable.

Premembrane (prM) protein is believed to escape premature fusion in the exit pathway [215]. However, the prM protein functions remain unclear. Recently, anti-prM antibodies revealed a function that prM protein can contribute to pathogenesis [216]. Thus, the need for anti-prM antibodies was plunged to elucidate the prM protein functions. However, the antibody discovery was challenging; only one prM mAb, 278-11, out of 8 anti-ZIKV mAbs was discovered from the study. Interestingly, 278-11 showed high heavy chain SHM (17.9%) and CDR mutations (47.1%). The high SHM value may adjust the prM protein structure. Beltramello et al. discovered 70 anti-DENV mAbs from five human patients; only six prM mAbs and dominance were domain I/II (34 clones) and domain III (13 clones) [217]. Smith et al. reported that 4 - 18 amino acids of heavy chain variable region (approximately 110 amino acids [218]) were mutated from 26 anti-DENV prM mAbs [219]. DENV and ZIKV pr protein are cleaved by furin in the endoplasmic reticulum, and then the virus matures [220]. The antibody generation mechanisms of DENV/ ZIKV prM have not been elucidated. However, these findings are similar to prM antibody clone 278-11.

SHM, CDR mutation, and FWR mutation were not correlated with antibody binding parameters and neutralizing titers for all eight antibodies, including neutralizing and non-neutralizing antibodies (**Figure 5A and B**). However, significant correlations were observed for five neutralizing antibodies for heavy chain analysis (**Figure 5C**). One non-neutralizing antibody, mAb 278-11, recognized prM (**Figure 3**), and the binding activities were weaker than neutralizing mAbs: Luminex assay (EC_{50} 278-11, 23800 ng/mL, neutralizing mAbs 12.3 - 89.9 ng/mL) and kinetic analysis, K_D (278-11, 0.45 nM, neutralizing mAbs, 0.2 -0.4 nM) and k_{dis} (278-11, 8.49 x 10^{-5}, neutralizing mAbs, 2.59 - 6.34 x 10^{-5} 1/s) (**Figure 1A, 2C and Table 1**). However, heavy chain SHM of 278-11 (17.9%) were relatively higher than neutralizing mAbs

(11.1 - 20.6%: **Table 3**), disrupting the correlation analysis. On the other hand, Five neutralizing mAbs were bound to domain III or quaternary epitopes of domain I and III (**Figure 3**). These findings suggested that selecting the same binding domains or mAbs character was necessary for correlation analysis between SHM and antibody functions.

Focus on five neutralizing antibodies; significant negative correlations were observed for VH chain but weak and no correlation for VL chain (**Figure 5C and D**). The importance of antibody heavy chain for antigen binding was widely known [221-223]. For example, Sela-Culang et al. reported higher percentages of antigen contact for heavy-chain amino acids but lower for light-chain from the structural analysis [224]. Light chain affinity matured anti-interleukin-3 mAb decreased K_D value from 1.9 pM to 0.142 pM; however, mutated to three amino acids in heavy chain CDR2 mutations accelerated K_D to 0.032 pM [225]. Interestingly, camel, alpaca, and llama antibodies have only heavy chain, and show solid binding to antigens [226]. Caplacizumab, a nanobody, llama antibody derivative, was approved by the Food and Drug Administration for rare blood clotting disorder in 2019 [227]. Thus, my findings were entirely consistent with these scientific reports.

Heavy chain CDR3 was pivotal for antibody bindings: specificity and affinity [228-231]. Heavy chain CDR3 amino acids were from the diversity (D) region, and amino acid insertion and deletion frequently occurred, followed by AID modification [232]. Thus, heavy chain CDR3 SHM cannot be analyzed by IMGT/V-QUEST [81]. Therefore, the CDR3 lengths were compared with antibody functions. Contrary to expectations, only neutralizing titers correlated with CDR3 lengths, but there was little to no correlation between CDR3 lengths and antibody binding parameters (**Figure 5C**). Neutralization antibodies may be essential to cover more extensive virus surface-to-cell-binding areas for inhibition. Thus, a longer heavy chain CDR3

lengths are needed. However, antibody binding activity needs precision fitting to the virus surfaces, not covering a large area. Thus, there were no correlations with CDR3 length. The data suggested heavy chain CDR3 amino acid mutations would be a more critical factor for antibody bindings [231].

CDR mutations were significantly correlated with the antibody kinetic analysis parameters of anti-ZIKV mAbs, such as K_D and k_{dis}. However, the correlation between CDR mutations and association constant (k_a) was relatively weak (**Figure 5C and 23**). Therapeutic antibody candidates are matured artificially to enhance their affinity and efficacies *in vitro*. Randomly mutated CDR libraries harboring to phage or yeast display were applied to select high-binding clones [233, 234]. Wang et al. reported that affinity-matured antibodies by phage display drastically reduced k_{dis}. However, no increase in k_a was observed [235]. The differences in the correlations of k_a and k_{dis} with CDR mutations in my study were consistent with their results. These data suggest that the avidity assay's antibody dissociation constant (k_{dis}) is a critical parameter that reflects antibody affinity maturation.

A novel DENV avidity assay was developed using BLI and DENV-VLPs to visualize affinity maturation with k_{dis}. This assay was performed for two phase 2 clinical trials of a tetravalent dengue vaccine candidate (TAK-003) for children, adolescents, and adults in dengue-endemic regions. Vaccination of TAK-003 decreased k_{dis} (**Figure 14**) and increased the response and avidity index one month after vaccinations and sustained by one year for baseline seronegative volunteers (**Figure 13 and 15**). These results indicated that a novel avidity assay can be used to evaluate polyclonal antibody affinity maturation from serum. The latest technology can analyze SHM and CDR amino acid mutation from serum polyclonal antibodies [86], but the data only covers dominant antibodies and cannot reflect all polyclonal antibodies. However, considering

the significant correlation between k_{dis} and CDR mutations of anti-ZIKV mAbs (**Figure 23**), DENV vaccination may trigger antibody amino acid mutations in the B cell repertoire,

Overall, the correlation between avidity index and neutralizing titers was either weak or absent (**Figure 16**). A correlation was observed between avidity index and neutralizing titers for lower k_{dis}, the highest degree of antibody affinity maturation; however, no correlation was observed for higher k_{dis}, the lowest degree of antibody affinity maturation (**Figure 21**). Therefore, the following hypothesis was proposed (**Figure 24**). Low-affinity maturated antibodies comprise a wide variety of neutralizing/ non-neutralizing antibodies as antibody-expressing B cells are not selected in the germinal center (GC) and do not induce apoptosis. Furthermore, the process of affinity maturation predominantly selects neutralizing antibody-expressing B cells in GC to protect against virus infection. High affinity matured/ neutralizing antibody-expressing B cells differentiate into plasma cells secreting antibodies or memory B cells preparing for future virus infections. Whereas, non-affinity matured antibody-expressing B cells were induced apoptosis. The selection of affinity-matured antibodies might increase the proportion of high neutralizing antibodies and cause a correlation between avidity index and neutralizing titer for the highest degree of antibody affinity maturation, lower k_{dis} subjects.

The selection mechanism of neutralizing antibodies during affinity maturation has not yet been elucidated. However, there are two possibilities that the neutralizing antibodies are selectively affinity-matured. The first aspect is the high antigenicity of neutralizing epitopes. The most high-neutralizing mAbs were reported to bind to domain III [198, 201, 236-241] and E-protein dimer quaternary epitopes [196, 199, 200, 242, 243]. Indeed, anti-ZIKV neutralizing mAbs also bound to domain III and quaternary epitopes of domain I and III (**Figure 3 and Table 1**). These binding epitopes were exposed to the virus surfaces, showed good antigenicity, and might generate

antibodies to protect against the virus during early immunization stages. These neutralizing antibodies continue to undergo antibody affinity maturation in GC, and B cells expressing non-neutralizing antibodies might induce apoptosis.

Another important aspect is the evolution of antibody. Anti-HIV and COVID-19 antibodies have acquired multiple strain-neutralizing activities with high SHM [131, 244, 245]. Correlations between VH, VL mutations, and serum neutralization breath were observed in the analysis of 22 HIV-infected controllers [246]. The mechanism of acquiring the broadly HIV-neutralizing activity is proposed as follows: HIV mutates frequently to escape immune surveillance systems. B cells expressing neutralizing antibodies are stimulated multiple times by different HIV strains, and antibodies are mutated in GC to acquire broad neutralizing activity (**Figure 25**) [247].

Interestingly, anti-DENV serum of TAK-003 was neutralized with three DENV genotype virus strains [248], but the magnitude of antibody affinity maturation was not analyzed in this study. However, there are no reports of anti-DENV antibody evolutions. These data suggested that neutralizing anti-DENV antibodies might be selected during antibody affinity maturation by multiple DENV stimulation, such as immunization, infection, and exposure to the virus, the same as the evolution of broadly neutralizing HIV antibodies (**Figure 25**).

Antibody affinity maturation was assessed in the thesis using genomic and serological approaches (**Figure 26**). The Genomic approach uses the data from a single B cell to assess antibody DNA and amino acid mutations. The approach is straightforward because SHM is determined, and antibody functions are comparable with antibody mutations. However, this approach cannot apply to evaluating vaccinated volunteers or natural infection patients. For example, Edwards et al. reported an extensive human antibody repertoire using human phage

display: 2875 positive ELISA hits against B-lymphocyte stimulator protein and 1278 unique antibody amino acid sequences [249]. Thus, B cell sorting is challenging to cover all antibody-expressing B cells because of the low throughput for collecting thousands of single cells.

In contrast, the serological approach uses polyclonal antibodies from serum. The data represents the average values of antibodies in serum; however, the serological data reflect the efficacy of virus protection. The conventional avidity assay, ELISA disrupted chaotropic reagents (8 M urea or 1 M NaSCN), can measure the strength of polyclonal antibodies [65, 87], but cannot evaluate antibody affinity maturation. The assay reacts within several hours and evaluates the equilibrium state of antibody binding to antigens. Thus, the assay evaluates the "static state," not the "dynamic state," of antibody binding. Moreover, the newly developed avidity assay monitors the antibody association/ dissociation process of the antigen-binding biosensors over time and measures the antibody affinity in a dynamic state. Thus, k_{dis} can be assessed from the assay, which is one of the critical parameters of antibody affinity maturation. Therefore, the avidity assay in the thesis represents significant progress in evaluating serum polyclonal antibody affinity maturation.

To summarize, the antibody affinity maturation process initiated by flavivirus vaccinations was elucidated from DNA mutations to serum antibody affinity (**Figure 27**). High CDR mutations were observed for anti-ZIKV mAbs and correlated with antibody affinity parameters, such as K_D and k_{dis}. A novel avidity assay to assess k_{dis} from human serum was developed, and a significant decrease in k_{dis} was observed in DENV baseline seronegative volunteers after vaccination. The correlation of avidity index and neutralizing titer was observed in high affinity matured subjects. Finally, I conclude that antibody affinity maturation is essential for the protection against virus infections.

Figures

Figure 23 Correlation analysis of CDRH mutations and antibody association constant (k_a), dissociation constant (k_{dis}) of anti-ZIKV mAbs

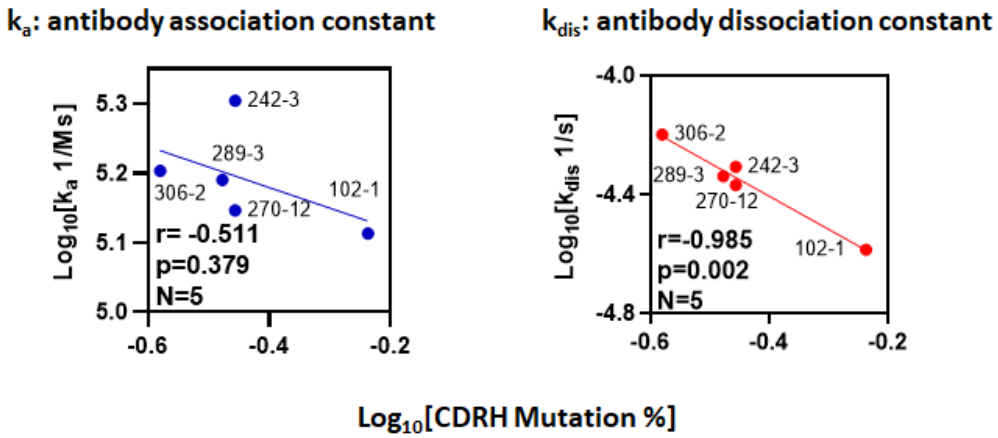

CDR mutations weakly correlated with k_a but strongly correlated with K_{dis}
Antibody dissociation constant was a critical parameter reflecting CDR mutations

Figure 24 Selection of high affinity/ neutralizing anti-DENV antibodies during antibody affinity maturation

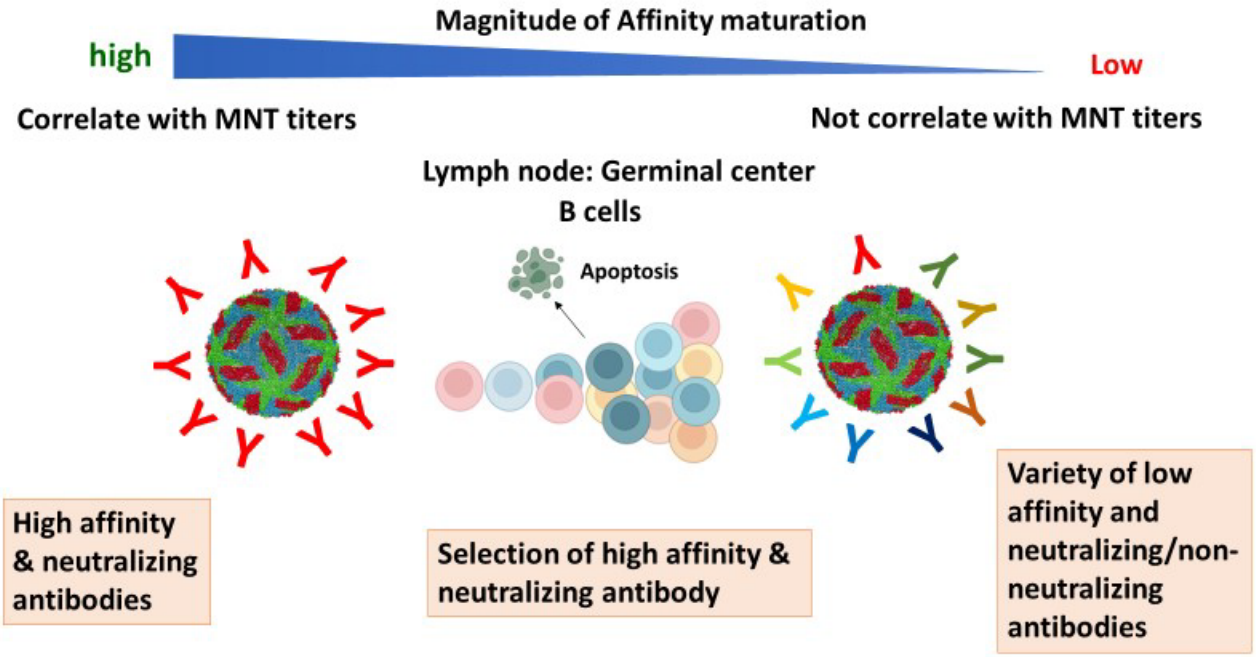

Figure 25 [Hypothesis] Mechanism of selection of high affinity and neutralizing anti-DENV antibody during antibody affinity maturation.

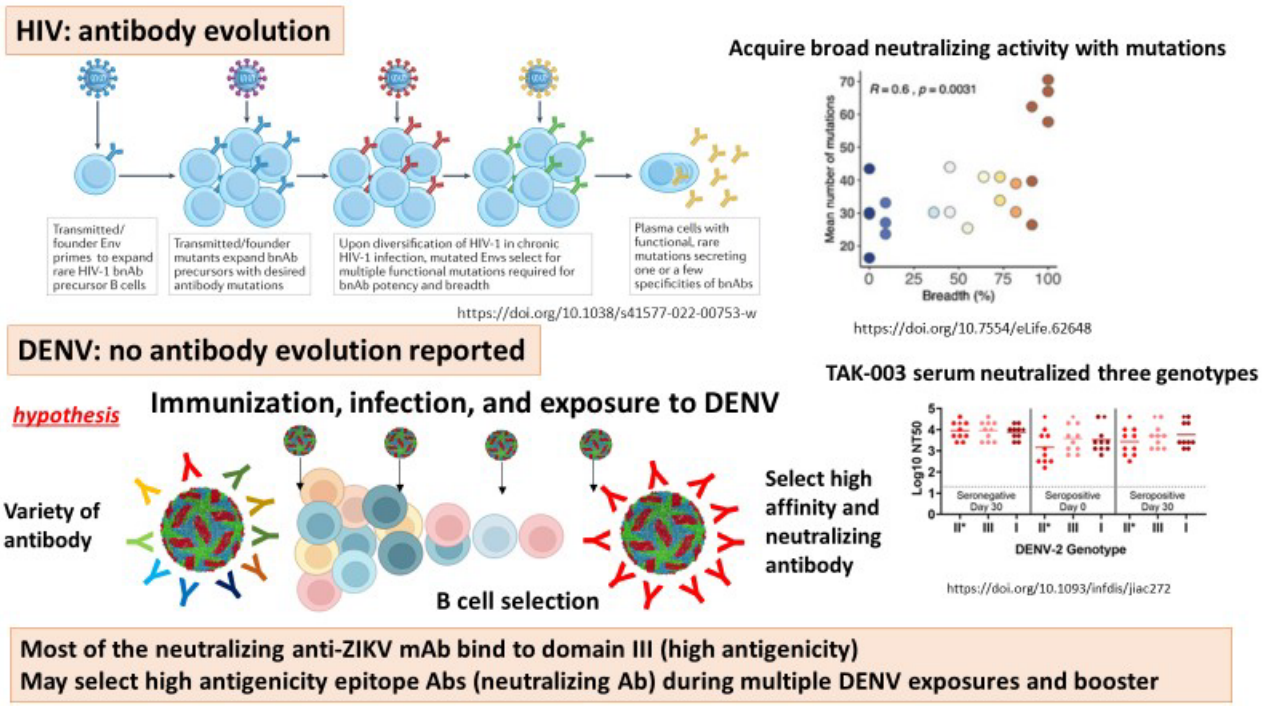

Figure 26 Summary of genomic and serological approaches for antibody affinity maturation evaluation.

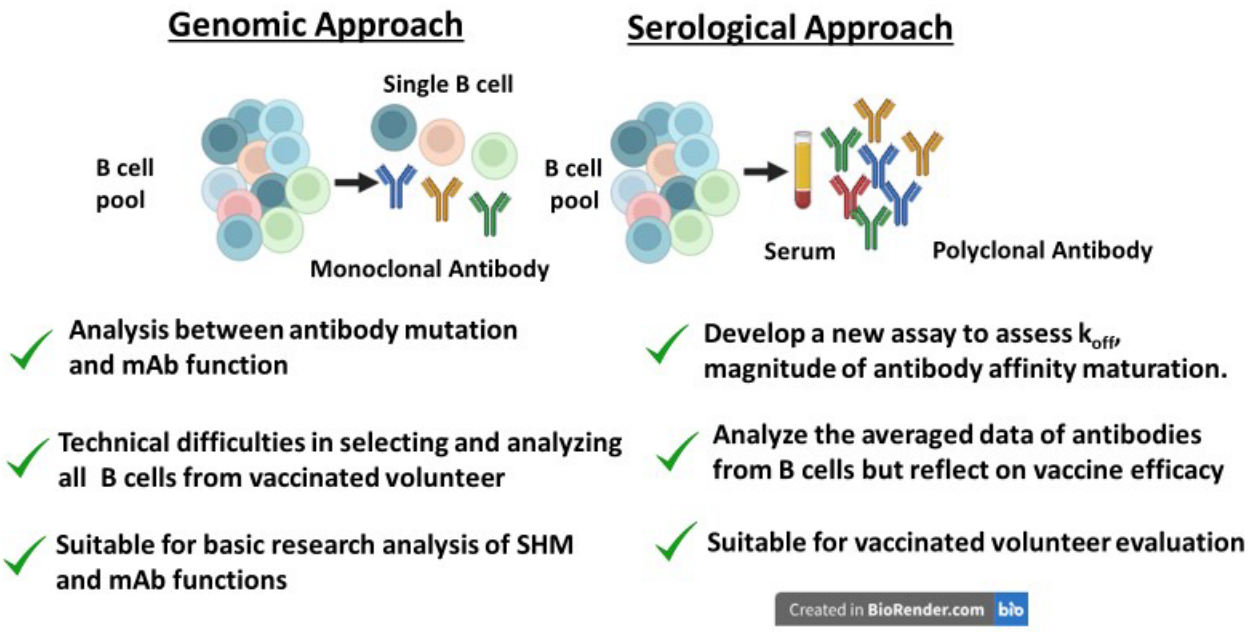

Figure 27 Graphic summary: Studies of Affinity Maturation of Anti-flavivirus Antibody during Vaccination.

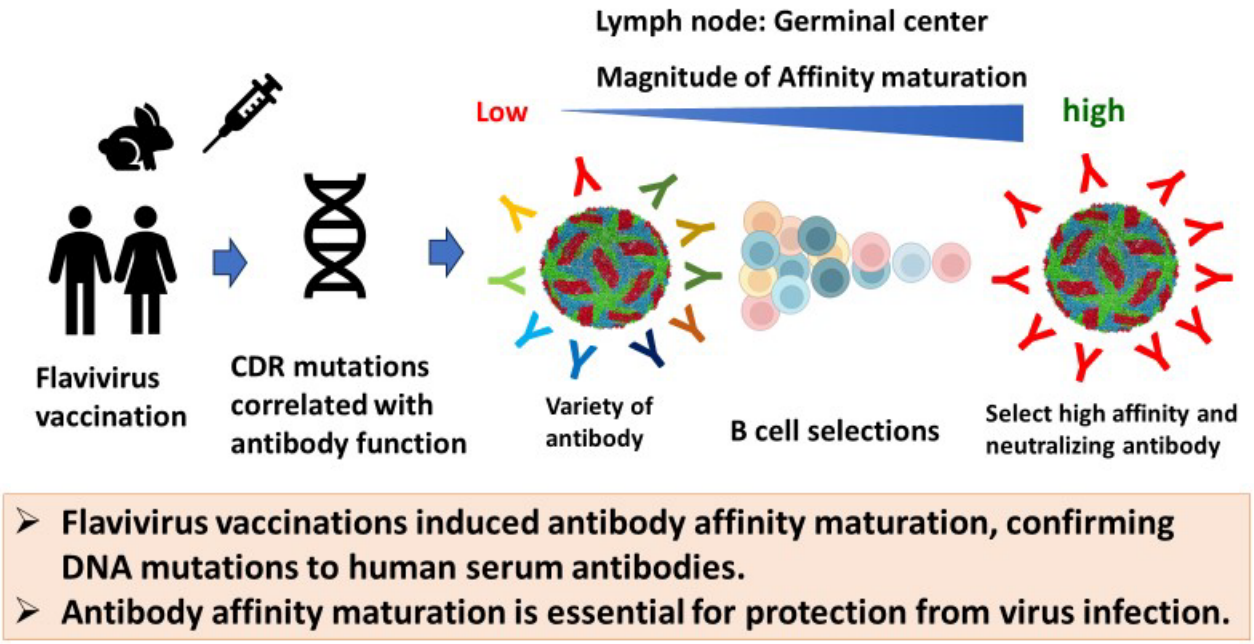

- Flavivirus vaccinations induced antibody affinity maturation, confirming DNA mutations to human serum antibodies.
- Antibody affinity maturation is essential for protection from virus infection.

Acknowledgment

I am deeply grateful to Professors Kenji Miura, Kentaro Nakano, Shuichi Kuwayama, and Kazuto Nakada, University of Tsukuba, for guiding my work and valuable discussions throughout my doctoral program.

I appreciate Drs David Dominguez, Ankita Sanjali, Jonathan Hernandez, Fue Vang, Lovkesh Karwal, Zhang Li Springer, Ivo Wortmann, Maima M Kaiser Tawnya Nead, Xuemei Li, and all members of Vaccine Business Unit Research and Analytics of Takeda Pharmaceutical Inc for technical support, discussion and suggestion.

I appreciate Drs. Edgar Davidson, Mallorie E. Fouch, and Benjamin J. Doranz of Integra Molecular for analyzing anti-ZIKV mAb binding epitopes and suggestions for manuscript editing.

I also express great appreciation for Drs Micheal Egan, Jill A. Livengood, Mark Lyons, Eric Shaw, Ralph Braun, Subash C. Das, and Hansi J. Dean of Takeda Pharmaceutical Vaccine Business Unit Assay Development and Discovery for suggestions and discussion during my doctoral programs.

I greatly appreciate Drs Eric Crampon and Bertolotti-Ciarlet Andrea of Takeda Pharmaceutical Vaccine Business Unit Research and Analytics for supporting my doctoral programs.

Finally, I appreciate my family's continuous support during my doctoral programs.

Reference

1. Littman RJ. The Plague of Athens: Epidemiology and Paleopathology. Mount Sinai Journal of Medicine: A Journal of Translational and Personalized Medicine **2009**; 76:456-67.
2. Zietz BP, Dunkelberg H. The history of the plague and the research on the causative agent Yersinia pestis. Int J Hyg Environ Health **2004**; 207:165-78.
3. Mandal S, Mandal MD, Pal NK. Cholera: a great global concern. Asian Pac J Trop Med **2011**; 4:573-80.
4. Berche P. The enigma of the 1889 Russian flu pandemic: A coronavirus? Presse Med **2022**; 51:104111-.
5. Rosner D. "Spanish flu, or whatever it is...": The paradox of public health in a time of crisis. Public Health Rep **2010**; 125 Suppl 3:38-47.
6. Zhu N, Zhang D, Wang W, et al. A Novel Coronavirus from Patients with Pneumonia in China, 2019. N Engl J Med **2020**; 382:727-33.
7. Curtis V, Schmidt W-P, Luby SP, Florez R, Toure O, Biran A. Hygiene: new hopes, new horizons. The Lancet Infectious Diseases **2011**; 11:312 - 21.
8. Riedel S. Edward Jenner and the history of smallpox and vaccination. Proc (Bayl Univ Med Cent) **2005**; 18:21-5.
9. Boylston A. The origins of vaccination: myths and reality. J R Soc Med **2013**; 106:351-4.
10. Gröschel DH, Hornick RB. Who introduced typhoid vaccination: Almroth Write or Richard Pfeiffer? Rev Infect Dis **1981**; 3:1251-4.
11. Hicks DJ, Fooks AR, Johnson N. Developments in rabies vaccines. Clin Exp Immunol **2012**; 169:199-204.
12. 10, Diphtheria Toxoid–, Tetanus Toxoid–, and Acellular Pertussis–Containing Vaccines. Adverse Effects of Vaccines: Evidence and Causality. Washington (DC): National Academies Press (US), **2011**.
13. Kim YH, Hong KJ, Kim H, Nam JH. Influenza vaccines: Past, present, and future. Rev Med Virol **2022**; 32:e2243.
14. Frierson JG. The yellow fever vaccine: a history. Yale J Biol Med **2010**; 83:77-85.
15. Kuchar E, Karlikowska-Skwarnik M, Han S, Nitsch-Osuch A. Pertussis: History of the Disease and Current Prevention Failure. Adv Exp Med Biol **2016**; 934:77-82.

16. Tan SY, Ponstein N. Jonas Salk (1914-1995): A vaccine against polio. Singapore Med J **2019**; 60:9-10.
17. Pattyn J, Hendrickx G, Vorsters A, Van Damme P. Hepatitis B Vaccines. The Journal of Infectious Diseases **2021**; 224:S343-S51.
18. Conis E. Measles and the Modern History of Vaccination. Public Health Rep **2019**; 134:118-25.
19. Grabenstein JD, Klugman KP. A century of pneumococcal vaccination research in humans. Clinical Microbiology and Infection **2012**; 18:15-24.
20. Peltola H. Worldwide Haemophilus influenzae type b disease at the beginning of the 21st century: global analysis of the disease burden 25 years after the use of the polysaccharide vaccine and a decade after the advent of conjugates. Clin Microbiol Rev **2000**; 13:302-17.
21. Glass RI, Tate JE, Jiang B, Parashar U. The Rotavirus Vaccine Story: From Discovery to the Eventual Control of Rotavirus Disease. The Journal of Infectious Diseases **2021**; 224:S331-S42.
22. Jackson DA, Symons RH, Berg P. Biochemical method for inserting new genetic information into DNA of Simian Virus 40: circular SV40 DNA molecules containing lambda phage genes and the galactose operon of Escherichia coli. Proc Natl Acad Sci U S A **1972**; 69:2904-9.
23. Ljubojević S. The human papillomavirus vaccines. Acta Dermatovenerol Croat **2006**; 14:208.
24. A Brief History of Vaccination. Available at: **https://www.who.int/news-room/spotlight/history-of-vaccination/a-brief-history-of-vaccination**. Accessed 20 April 2023.
25. Vaccine Types. Available at: **https://www.hhs.gov/immunization/basics/types/index.html**. Accessed 16 Nov 2023.
26. Orenstein WA, Ahmed R. Simply put: Vaccination saves lives. Proc Natl Acad Sci U S A **2017**; 114:4031-3.
27. Notifiable Diseases and Mortality Tables. MMWR Morb Mortal Wkly Rep **2016**; 65:Nd-38.
28. Roush SW, Murphy TV. Historical comparisons of morbidity and mortality for vaccine-preventable diseases in the United States. Jama **2007**; 298:2155-63.
29. Saleh A, Qamar S, Tekin A, Singh R, Kashyap R. Vaccine Development Throughout History. Cureus **2021**; 13:e16635.
30. Meyer H, Ehmann R, Smith GL. Smallpox in the Post-Eradication Era. Viruses **2020**; 12.

31. Schroeder HW, Jr., Cavacini L. Structure and function of immunoglobulins. J Allergy Clin Immunol **2010**; 125:S41-S52.
32. Mantis NJ, Rol N, Corthésy B. Secretory IgA's complex roles in immunity and mucosal homeostasis in the gut. Mucosal Immunol **2011**; 4:603-11.
33. Poole JA, Rosenwasser LJ. The role of immunoglobulin E and immune inflammation: implications in allergic rhinitis. Curr Allergy Asthma Rep **2005**; 5:252-8.
34. Gutzeit C, Chen K, Cerutti A. The enigmatic function of IgD: some answers at last. Eur J Immunol **2018**; 48:1101-13.
35. Administer the Vaccine(s). Available at: **https://www.cdc.gov/vaccines/hcp/admin/administer-vaccines.html**. Accessed 16 November 2023.
36. Rahmani A, Montecucco A, Kusznir Vitturi B, Debarbieri N, Dini G, Durando P. Long-Term Effectiveness of Hepatitis B Vaccination in the Protection of Healthcare Students in Highly Developed Countries: A Systematic Review and Meta-Analysis. Vaccines (Basel) **2022**; 10:1841.
37. Palgen JL, Feraoun Y, Dzangué-Tchoupou G, et al. Optimize Prime/Boost Vaccine Strategies: Trained Immunity as a New Player in the Game. Front Immunol **2021**; 12:612747.
38. Mai AS, Lee A, Tay RYK, et al. Booster doses of COVID-19 vaccines for patients with haematological and solid cancer: a systematic review and individual patient data meta-analysis. Eur J Cancer **2022**; 172:65-75.
39. Haniffa M, Gunawan M, Jardine L. Human skin dendritic cells in health and disease. J Dermatol Sci **2015**; 77:85-92.
40. Liu Z, Roche PA. Macropinocytosis in phagocytes: regulation of MHC class-II-restricted antigen presentation in dendritic cells. Frontiers in Physiology **2015**; 6.
41. ten Broeke T, Wubbolts R, Stoorvogel W. MHC class II antigen presentation by dendritic cells regulated through endosomal sorting. Cold Spring Harb Perspect Biol **2013**; 5:a016873-a.
42. Smith KG, Hewitson TD, Nossal GJ, Tarlinton DM. The phenotype and fate of the antibody-forming cells of the splenic foci. Eur J Immunol **1996**; 26:444-8.
43. Ademokun A, Wu Y-C, Martin V, et al. Vaccination-induced changes in human B-cell repertoire and pneumococcal IgM and IgA antibody at different ages. Aging Cell **2011**; 10:922-30.

44. Victora GD, Nussenzweig MC. Germinal Centers. Annual Review of Immunology **2022**; 40:413-42.
45. Henry B, Laidlaw BJ. Functional heterogeneity in the memory B-cell response. Current Opinion in Immunology **2023**; 80:102281.
46. Ellebedy AH, Krammer F, Li G-M, et al. Induction of broadly cross-reactive antibody responses to the influenza HA stem region following H5N1 vaccination in humans. Proceedings of the National Academy of Sciences **2014**; 111:13133-8.
47. Allen CDC, Ansel KM, Low C, et al. Germinal center dark and light zone organization is mediated by CXCR4 and CXCR5. Nature Immunology **2004**; 5:943-52.
48. Klein U, Dalla-Favera R. Germinal centres: role in B-cell physiology and malignancy. Nature Reviews Immunology **2008**; 8:22-33.
49. Doria-Rose NA, Joyce MG. Strategies to guide the antibody affinity maturation process. Curr Opin Virol **2015**; 11:137-47.
50. Stavnezer J, Schrader CE. IgH chain class switch recombination: mechanism and regulation. Journal of immunology (Baltimore, Md : 1950) **2014**; 193:5370-8.
51. Feng Y, Seija N, Di Noia JM, Martin A. AID in Antibody Diversification: There and Back Again. Trends Immunol **2020**; 41:586-600.
52. Chaudhuri J, Tian M, Khuong C, Chua K, Pinaud E, Alt FW. Transcription-targeted DNA deamination by the AID antibody diversification enzyme. Nature **2003**; 422:726-30.
53. Wei L, Chahwan R, Wang S, et al. Overlapping hotspots in CDRs are critical sites for V region diversification. Proc Natl Acad Sci U S A **2015**; 112:E728-37.
54. Tang C, Bagnara D, Chiorazzi N, Scharff MD, MacCarthy T. AID Overlapping and Polη Hotspots Are Key Features of Evolutionary Variation Within the Human Antibody Heavy Chain (IGHV) Genes. Frontiers in Immunology **2020**; 11.
55. Klasse PJ, Sattentau QJ. Occupancy and mechanism in antibody-mediated neutralization of animal viruses. J Gen Virol **2002**; 83:2091-108.
56. Parren PW, Burton DR. The antiviral activity of antibodies in vitro and in vivo. Adv Immunol **2001**; 77:195-262.
57. Nascimento EJM, Norwood B, Parker A, Braun R, Kpamegan E, Dean HJ. Development and Characterization of a Multiplex Assay to Quantify Complement-Fixing Antibodies against Dengue Virus. Int J Mol Sci **2021**; 22.

58. Laoprasopwattana K, Libraty DH, Endy TP, et al. Antibody-Dependent Cellular Cytotoxity Mediated by Plasma Obtained before Secondary Dengue Virus Infections: Potential Involvement in Early Control of Viral Replication. The Journal of Infectious Diseases **2007**; 195:1108-16.
59. Agrawal P, Nawadkar R, Ojha H, Kumar J, Sahu A. Complement Evasion Strategies of Viruses: An Overview. Front Microbiol **2017**; 8:1117.
60. Nascimento EJM, Norwood B, Kpamegan E, et al. Antibodies Produced in Response to a Live-Attenuated Dengue Vaccine are Functional in Activating the Complement System. The Journal of Infectious Diseases **2022**.
61. Nakagama Y, Candray K, Kaku N, et al. Antibody Avidity Maturation Following Recovery From Infection or the Booster Vaccination Grants Breadth of SARS-CoV-2 Neutralizing Capacity. The Journal of Infectious Diseases **2022**; 227:780-7.
62. Hashimoto G, Wright PF, Karzon DT. Antibody-dependent cell-mediated cytotoxicity against influenza virus-infected cells. J Infect Dis **1983**; 148:785-94.
63. Manuylov V, Burgasova O, Borisova O, et al. Avidity of IgG to SARS-CoV-2 RBD as a Prognostic Factor for the Severity of COVID-19 Reinfection. Viruses **2022**; 14.
64. Ravichandran S, Hahn M, Belaunzarán-Zamudio PF, et al. Differential human antibody repertoires following Zika infection and the implications for serodiagnostics and disease outcome. Nat Commun **2019**; 10:1943.
65. Lau L, Green AM, Balmaseda A, Harris E. Antibody avidity following secondary dengue virus type 2 infection across a range of disease severity. J Clin Virol **2015**; 69:63-7.
66. Luo YR, Chakraborty I, Yun C, Wu AHB, Lynch KL. Kinetics of Severe Acute Respiratory Syndrome Coronavirus 2 (SARS-CoV-2) Antibody Avidity Maturation and Association with Disease Severity. Clinical Infectious Diseases **2020**; 73:e3095-e7.
67. Cotton R, Milstein C. Fusion of two immunoglobulin-producing myeloma cells. Nature **1973**; 244:42-3.
68. Parray HA, Shukla S, Samal S, et al. Hybridoma technology a versatile method for isolation of monoclonal antibodies, its applicability across species, limitations, advancement and future perspectives. Int Immunopharmacol **2020**; 85:106639.
69. Mitra S, Tomar PC. Hybridoma technology; advancements, clinical significance, and future aspects. J Genet Eng Biotechnol **2021**; 19:159.

70. Johnson AJ, Martin DA, Karabatsos N, Roehrig JT. Detection of anti-arboviral immunoglobulin G by using a monoclonal antibody-based capture enzyme-linked immunosorbent assay. J Clin Microbiol **2000**; 38:1827-31.
71. Osorio JE, Velez ID, Thomson C, et al. Safety and immunogenicity of a recombinant live attenuated tetravalent dengue vaccine (DENVax) in flavivirus-naive healthy adults in Colombia: a randomised, placebo-controlled, phase 1 study. Lancet Infect Dis **2014**; 14:830-8.
72. Bohning K, Sonnberg S, Chen HL, et al. A high throughput reporter virus particle microneutralization assay for quantitation of Zika virus neutralizing antibodies in multiple species. PLoS One **2021**; 16:e0250516.
73. Spieker-Polet H, Sethupathi P, Yam PC, Knight KL. Rabbit monoclonal antibodies: generating a fusion partner to produce rabbit-rabbit hybridomas. Proc Natl Acad Sci U S A **1995**; 92:9348-52.
74. Smith SA, Crowe JE, Jr. Use of Human Hybridoma Technology To Isolate Human Monoclonal Antibodies. Microbiol Spectr **2015**; 3:Aid-0027-2014.
75. Hofmann D, Lai JR. Exploring Human Antimicrobial Antibody Responses on a Single B Cell Level. Clin Vaccine Immunol **2017**; 24.
76. Winters A, McFadden K, Bergen J, et al. Rapid single B cell antibody discovery using nanopens and structured light. MAbs **2019**; 11:1025-35.
77. Zucha D, Kubista M, Valihrach L. Tutorial: Guidelines for Single-Cell RT-qPCR. Cells **2021**; 10.
78. Sanger F, Nicklen S, Coulson AR. DNA sequencing with chain-terminating inhibitors. Proc Natl Acad Sci U S A **1977**; 74:5463-7.
79. Mishra AK, Mariuzza RA. Insights into the Structural Basis of Antibody Affinity Maturation from Next-Generation Sequencing. Front Immunol **2018**; 9:117.
80. Lefranc MP. IMGT, the international ImMunoGeneTics information system: a standardized approach for immunogenetics and immunoinformatics. Immunome Res **2005**; 1:3.
81. Brochet X, Lefranc MP, Giudicelli V. IMGT/V-QUEST: the highly customized and integrated system for IG and TR standardized V-J and V-D-J sequence analysis. Nucleic Acids Res **2008**; 36:W503-8.
82. Fulton RJ, McDade RL, Smith PL, Kienker LJ, Kettman JR, Jr. Advanced multiplexed analysis with the FlowMetrixTM system. Clinical Chemistry **1997**; 43:1749-56.

83. Dysinger M, King LE. Practical quantitative and kinetic applications of bio-layer interferometry for toxicokinetic analysis of a monoclonal antibody therapeutic. J Immunol Methods **2012**; 379:30-41.
84. O'Shannessy DJ, Brigham-Burke M, Soneson KK, Hensley P, Brooks I. Determination of rate and equilibrium binding constants for macromolecular interactions using surface plasmon resonance: use of nonlinear least squares analysis methods. Anal Biochem **1993**; 212:457-68.
85. Nguyen HH, Park J, Kang S, Kim M. Surface plasmon resonance: a versatile technique for biosensor applications. Sensors (Basel) **2015**; 15:10481-510.
86. Guthals A, Gan Y, Murray L, et al. De Novo MS/MS Sequencing of Native Human Antibodies. J Proteome Res **2017**; 16:45-54.
87. Boxus M, Lockman L, Fochesato M, Lorin C, Thomas F, Giannini SL. Antibody avidity measurements in recipients of Cervarix vaccine following a two-dose schedule or a three-dose schedule. Vaccine **2014**; 32:3232-6.
88. Canelle Q, Dewé W, Innis BL, van der Most R. Evaluation of potential immunogenicity differences between Pandemrix™ and Arepanrix™. Hum Vaccin Immunother **2016**; 12:2289-98.
89. Dennison SM, Reichartz M, Seaton KE, et al. Qualified Biolayer Interferometry Avidity Measurements Distinguish the Heterogeneity of Antibody Interactions with Plasmodium falciparum Circumsporozoite Protein Antigens. J Immunol **2018**; 201:1315-26.
90. Lynch HE, Stewart SM, Kepler TB, Sempowski GD, Alam SM. Surface plasmon resonance measurements of plasma antibody avidity during primary and secondary responses to anthrax protective antigen. J Immunol Methods **2014**; 404:1-12.
91. Persson J, Zhang Y, Olafsdottir TA, et al. Nasal Immunization Confers High Avidity Neutralizing Antibody Response and Immunity to Primary and Recurrent Genital Herpes in Guinea Pigs. Front Immunol **2016**; 7:640.
92. Monath TP, Vasconcelos PF. Yellow fever. J Clin Virol **2015**; 64:160-73.
93. Roy SK, Bhattacharjee S. Dengue virus: epidemiology, biology, and disease aetiology. Canadian Journal of Microbiology **2021**; 67:687-702.
94. Yun SI, Lee YM. Japanese encephalitis: the virus and vaccines. Hum Vaccin Immunother **2014**; 10:263-79.
95. Rossi SL, Ross TM, Evans JD. West Nile virus. Clin Lab Med **2010**; 30:47-65.

96. Lazear HM, Diamond MS. Zika Virus: New Clinical Syndromes and Its Emergence in the Western Hemisphere. J Virol **2016**; 90:4864-75.
97. Flaviviridae. Available at: **https://www.cdc.gov/vhf/virus-families/flaviviridae.html**. Accessed 16 November 2023.
98. Yellow Fever. Available at: **https://www.paho.org/en/topics/yellow-fever**. Accessed 16 November 2023.
99. Quan TM, Thao TTN, Duy NM, Nhat TM, Clapham H. Estimates of the global burden of Japanese encephalitis and the impact of vaccination from 2000-2015. Elife **2020**; 9:e51027.
100. Petersen LR, Jamieson DJ, Powers AM, Honein MA. Zika Virus. N Engl J Med **2016**; 374:1552-63.
101. Bhatt S, Gething PW, Brady OJ, et al. The global distribution and burden of dengue. Nature **2013**; 496:504-7.
102. About Dengue: What You Need to Know. Available at: **https://www.cdc.gov/dengue/about/index.html**. Accessed 16 November 2023.
103. Torres-Flores JM, Reyes-Sandoval A, Salazar MI. Dengue Vaccines: An Update. BioDrugs **2022**; 36:325-36.
104. Gubler DJ KG, Markoff L. Flaviviruses. Philadelphia, PA: Lippincott Williams & Wilkins Publishers, **2007** Fields virology, 5th ed).
105. Foy BD, Kobylinski KC, Chilson Foy JL, et al. Probable non-vector-borne transmission of Zika virus, Colorado, USA. Emerg Infect Dis **2011**; 17:880-2.
106. Mlakar J, Korva M, Tul N, et al. Zika Virus Associated with Microcephaly. N Engl J Med **2016**; 374:951-8.
107. Musso D, Cao-Lormeau VM, Gubler DJ. Zika virus: following the path of dengue and chikungunya? Lancet **2015**; 386:243-4.
108. Duffy MR, Chen TH, Hancock WT, et al. Zika virus outbreak on Yap Island, Federated States of Micronesia. N Engl J Med **2009**; 360:2536-43.
109. Cao-Lormeau VM, Musso D. Emerging arboviruses in the Pacific. Lancet **2014**; 384:1571-2.
110. Musso D, Nilles EJ, Cao-Lormeau VM. Rapid spread of emerging Zika virus in the Pacific area. Clin Microbiol Infect **2014**; 20:O595-6.

111. Schuler-Faccini L, Ribeiro EM, Feitosa IM, et al. Possible Association Between Zika Virus Infection and Microcephaly - Brazil, 2015. MMWR Morb Mortal Wkly Rep **2016**; 65:59-62.
112. Brasil P, Pereira JP, Jr., Moreira ME, et al. Zika Virus Infection in Pregnant Women in Rio de Janeiro. N Engl J Med **2016**; 375:2321-34.
113. Fauci AS, Morens DM. Zika Virus in the Americas--Yet Another Arbovirus Threat. N Engl J Med **2016**; 374:601-4.
114. Heymann DL, Hodgson A, Sall AA, et al. Zika virus and microcephaly: why is this situation a PHEIC? Lancet **2016**; 387:719-21.
115. Musso D, Ko AI, Baud D. Zika Virus Infection - After the Pandemic. N Engl J Med **2019**; 381:1444-57.
116. Hill SC, Vasconcelos J, Neto Z, et al. Emergence of the Asian lineage of Zika virus in Angola: an outbreak investigation. Lancet Infect Dis **2019**; 19:1138-47.
117. Sapkal GN, Yadav PD, Vegad MM, Viswanathan R, Gupta N, Mourya DT. First laboratory confirmation on the existence of Zika virus disease in India. J Infect **2018**; 76:314-7.
118. Phatihattakorn C, Wongsa A, Pongpan K, et al. Seroprevalence of Zika virus in pregnant women from central Thailand. PLoS One **2021**; 16:e0257205.
119. Tun MMN, Mori D, Sabri SB, et al. Serological Evidence of Zika Virus Infection in Febrile Patients and Healthy Blood Donors in Sabah, Malaysian Borneo, 2017-2018. Am J Trop Med Hyg **2021**.
120. Ngwe Tun MM, Kyaw AK, Hmone SW, et al. Detection of Zika Virus Infection in Myanmar. Am J Trop Med Hyg **2018**; 98:868-71.
121. Gobillot TA, Kikawa C, Lehman DA, et al. Zika Virus Circulates at Low Levels in Western and Coastal Kenya. J Infect Dis **2020**; 222:847-52.
122. Diarra I, Nurtop E, Sangaré AK, et al. Zika Virus Circulation in Mali. Emerg Infect Dis **2020**; 26:945-52.
123. Mengesha Tsegaye M, Beyene B, Ayele W, et al. Sero-prevalence of yellow fever and related Flavi viruses in Ethiopia: a public health perspective. BMC Public Health **2018**; 18:1011.
124. Dai L, Song J, Lu X, et al. Structures of the Zika Virus Envelope Protein and Its Complex with a Flavivirus Broadly Protective Antibody. Cell Host Microbe **2016**; 19:696-704.
125. Pierson TC, Diamond MS. Degrees of maturity: the complex structure and biology of flaviviruses. Curr Opin Virol **2012**; 2:168-75.

126. Roth DB. V(D)J Recombination: Mechanism, Errors, and Fidelity. Microbiol Spectr **2014**; 2.
127. Xu JL, Davis MM. Diversity in the CDR3 region of V(H) is sufficient for most antibody specificities. Immunity **2000**; 13:37-45.
128. Morea V, Tramontano A, Rustici M, Chothia C, Lesk AM. Conformations of the third hypervariable region in the VH domain of immunoglobulins. J Mol Biol **1998**; 275:269-94.
129. Chothia C, Novotný J, Bruccoleri R, Karplus M. Domain association in immunoglobulin molecules. The packing of variable domains. J Mol Biol **1985**; 186:651-63.
130. Herold EM, John C, Weber B, et al. Determinants of the assembly and function of antibody variable domains. Sci Rep **2017**; 7:12276.
131. Klein F, Diskin R, Scheid JF, et al. Somatic mutations of the immunoglobulin framework are generally required for broad and potent HIV-1 neutralization. Cell **2013**; 153:126-38.
132. Henderson R, Watts BE, Ergin HN, et al. Selection of immunoglobulin elbow region mutations impacts interdomain conformational flexibility in HIV-1 broadly neutralizing antibodies. Nat Commun **2019**; 10:654.
133. Koenig P, Lee CV, Walters BT, et al. Mutational landscape of antibody variable domains reveals a switch modulating the interdomain conformational dynamics and antigen binding. Proc Natl Acad Sci U S A **2017**; 114:E486-e95.
134. Zhang YF, Ho M. Humanization of rabbit monoclonal antibodies via grafting combined Kabat/IMGT/Paratome complementarity-determining regions: Rationale and examples. MAbs **2017**; 9:419-29.
135. Justus Weber HPaCR. From rabbit antibody repertoires to rabbit monoclonal antibodies. Experimental & Molecular Medicine **2017**; (2017) 49, e305.
136. Hoang LL, Tang P, Hicks DG, et al. A new rabbit monoclonal E-cadherin antibody [EP700Y] shows higher sensitivity than mouse monoclonal E-cadherin [HECD-1] antibody in breast ductal carcinomas and does not stain breast lobular carcinomas. Appl Immunohistochem Mol Morphol **2014**; 22:606-12.
137. Pope ME, Soste MV, Eyford BA, Anderson NL, Pearson TW. Anti-peptide antibody screening: selection of high affinity monoclonal reagents by a refined surface plasmon resonance technique. J Immunol Methods **2009**; 341:86-96.

138. Lavinder JJ, Hoi KH, Reddy ST, Wine Y, Georgiou G. Systematic characterization and comparative analysis of the rabbit immunoglobulin repertoire. PLoS One **2014**; 9:e101322.
139. Halstead SB, Venkateshan CN, Gentry MK, Larsen LK. Heterogeneity of infection enhancement of dengue 2 strains by monoclonal antibodies. J Immunol **1984**; 132:1529-32.
140. Huang Y, Gu B, Wu R, Zhang J, Li Y, Zhang M. Development of a rabbit monoclonal antibody group against Smads and immunocytochemical study of human and mouse embryonic stem cells. Hybridoma (Larchmt) **2007**; 26:387-91.
141. Jäger V, Groenewold J, Krüger D, Schwarz D, Vollmer V. High-titer expression of recombinant antibodies by transiently transfected HEK 293-6E cell cultures. BMC Proceedings **2015**; 9:P40.
142. Taki S, Kamada H, Inoue M, et al. A Novel Bispecific Antibody against Human CD3 and Ephrin Receptor A10 for Breast Cancer Therapy. PLoS One **2015**; 10:e0144712.
143. Stettler K, Beltramello M, Espinosa DA, et al. Specificity, cross-reactivity, and function of antibodies elicited by Zika virus infection. Science **2016**; 353:823-6.
144. Harris VM. Protein detection by Simple Western™ analysis. Methods Mol Biol **2015**; 1312:465-8.
145. Davidson E, Doranz BJ. A high-throughput shotgun mutagenesis approach to mapping B-cell antibody epitopes. Immunology **2014**; 143:13-20.
146. Sapparapu G, Fernandez E, Kose N, et al. Neutralizing human antibodies prevent Zika virus replication and fetal disease in mice. Nature **2016**; 540:443-7.
147. Paes C, Ingalls J, Kampani K, et al. Atomic-level mapping of antibody epitopes on a GPCR. J Am Chem Soc **2009**; 131:6952-4.
148. Barba-Spaeth G, Dejnirattisai W, Rouvinski A, et al. Structural basis of potent Zika-dengue virus antibody cross-neutralization. Nature **2016**; 536:48-53.
149. Dejnirattisai W, Wongwiwat W, Supasa S, et al. A new class of highly potent, broadly neutralizing antibodies isolated from viremic patients infected with dengue virus. Nat Immunol **2015**; 16:170-7.
150. Dussupt V, Modjarrad K, Krebs SJ. Landscape of Monoclonal Antibodies Targeting Zika and Dengue: Therapeutic Solutions and Critical Insights for Vaccine Development. Front Immunol **2020**; 11:621043.

151. Wang J, Bardelli M, Espinosa DA, et al. A Human Bi-specific Antibody against Zika Virus with High Therapeutic Potential. Cell **2017**; 171:229-41.e15.
152. Dussupt V, Sankhala RS, Gromowski GD, et al. Potent Zika and dengue cross-neutralizing antibodies induced by Zika vaccination in a dengue-experienced donor. Nat Med **2020**; 26:228-35.
153. Zhao H, Fernandez E, Dowd KA, et al. Structural Basis of Zika Virus-Specific Antibody Protection. Cell **2016**; 166:1016-27.
154. Niu X, Zhao L, Qu L, et al. Convalescent patient-derived monoclonal antibodies targeting different epitopes of E protein confer protection against Zika virus in a neonatal mouse model. Emerg Microbes Infect **2019**; 8:749-59.
155. Tharakaraman K, Watanabe S, Chan KR, et al. Rational Engineering and Characterization of an mAb that Neutralizes Zika Virus by Targeting a Mutationally Constrained Quaternary Epitope. Cell Host Microbe **2018**; 23:618-27.e6.
156. Graham SD, Tu HA, McElvany BD, et al. A Novel Antigenic Site Spanning Domains I and III of the Zika Virus Envelope Glycoprotein Is the Target of Strongly Neutralizing Human Monoclonal Antibodies. J Virol **2021**; 95.
157. Wang L, Wang R, Wang L, et al. Structural Basis for Neutralization and Protection by a Zika Virus-Specific Human Antibody. Cell Rep **2019**; 26:3360-8.e5.
158. Bailey MJ, Broecker F, Freyn AW, et al. Human Monoclonal Antibodies Potently Neutralize Zika Virus and Select for Escape Mutations on the Lateral Ridge of the Envelope Protein. J Virol **2019**; 93.
159. Gao F, Lin X, He L, et al. Development of a Potent and Protective Germline-Like Antibody Lineage Against Zika Virus in a Convalescent Human. Front Immunol **2019**; 10:2424.
160. Wahala WM, Silva AM. The human antibody response to dengue virus infection. Viruses **2011**; 3:2374-95.
161. Burton DR, Hangartner L. Broadly Neutralizing Antibodies to HIV and Their Role in Vaccine Design. Annu Rev Immunol **2016**; 34:635-59.
162. Collins MH, Tu HA, Gimblet-Ochieng C, et al. Human antibody response to Zika targets type-specific quaternary structure epitopes. JCI Insight **2019**; 4.
163. Mascola JR, Haynes BF. HIV-1 neutralizing antibodies: understanding nature's pathways. Immunol Rev **2013**; 254:225-44.

164. Swanstrom JA, Plante JA, Plante KS, et al. Dengue Virus Envelope Dimer Epitope Monoclonal Antibodies Isolated from Dengue Patients Are Protective against Zika Virus. mBio **2016**; 7.
165. Sok D, Laserson U, Laserson J, et al. The effects of somatic hypermutation on neutralization and binding in the PGT121 family of broadly neutralizing HIV antibodies. PLoS Pathog **2013**; 9:e1003754.
166. Georgiev IS, Rudicell RS, Saunders KO, et al. Antibodies VRC01 and 10E8 neutralize HIV-1 with high breadth and potency even with Ig-framework regions substantially reverted to germline. J Immunol **2014**; 192:1100-6.
167. Safdari Y, Farajnia S, Asgharzadeh M, Khalili M. Antibody humanization methods - a review and update. Biotechnol Genet Eng Rev **2013**; 29:175-86.
168. Lefranc MP, Pommié C, Ruiz M, et al. IMGT unique numbering for immunoglobulin and T cell receptor variable domains and Ig superfamily V-like domains. Dev Comp Immunol **2003**; 27:55-77.
169. Chen Z, Ren X, Yang J, et al. An elaborate landscape of the human antibody repertoire against enterovirus 71 infection is revealed by phage display screening and deep sequencing. MAbs **2017**; 9:342-9.
170. Sundling C, Zhang Z, Phad GE, et al. Single-cell and deep sequencing of IgG-switched macaque B cells reveal a diverse Ig repertoire following immunization. J Immunol **2014**; 192:3637-44.
171. Petersen RL. Strategies Using Bio-Layer Interferometry Biosensor Technology for Vaccine Research and Development. Biosensors (Basel) **2017**; 7:49.
172. Müller-Esparza H, Osorio-Valeriano M, Steube N, Thanbichler M, Randau L. Bio-Layer Interferometry Analysis of the Target Binding Activity of CRISPR-Cas Effector Complexes. Frontiers in Molecular Biosciences **2020**; 7.
173. Murali S, Rustandi RR, Zheng X, Payne A, Shang L. Applications of Surface Plasmon Resonance and Biolayer Interferometry for Virus-Ligand Binding. Viruses **2022**; 14:717.
174. Kamat V, Rafique A. Designing binding kinetic assay on the bio-layer interferometry (BLI) biosensor to characterize antibody-antigen interactions. Analytical Biochemistry **2017**; 536:16-31.

175. Kamat V, Rafique A. Extending the throughput of Biacore 4000 biosensor to accelerate kinetic analysis of antibody-antigen interaction. Analytical Biochemistry **2017**; 530:75-86.
176. Metz SW, Thomas A, White L, et al. Dengue virus-like particles mimic the antigenic properties of the infectious dengue virus envelope. Virol J **2018**; 15:60.
177. Teoh EP, Kukkaro P, Teo EW, et al. The structural basis for serotype-specific neutralization of dengue virus by a human antibody. Sci Transl Med **2012**; 4:139ra83.
178. Wu W, Bai Z, Zhou H, et al. Molecular epidemiology of dengue viruses in southern China from 1978 to 2006. Virology journal **2011**; 8:322-.
179. Rush B. An account of the bilious remitting fever: as it appeared in philadelphia, in the summer and autumn of the year 1780. The American Journal of Medicine **1951**; 11:546-50.
180. Kimura R. Inoculation of degue virus into mice. Nippon Igaku **1944**; 3379:629-33.
181. WHO. Dengue and dengue haemorrhagic fever. South-East Asia Region. 1986 ed. Vol. 61, **1986**:4.
182. Working to overcome the global impact of neglected tropical diseases: first WHO report on neglected tropical diseases. World Health Organization, **2010**.
183. Teixeira MG, Costa MC, Coelho G, Barreto ML. Recent shift in age pattern of dengue hemorrhagic fever, Brazil. Emerg Infect Dis **2008**; 14:1663.
184. Organization WH. Dengue haemorrhagic fever: diagnosis, treatment, prevention and control. World Health Organization, **1997**.
185. Report of the Scientific Working Group meeting on Dengue, Geneva, 1−5 October 2006: WHO, **2006**.
186. Buczak AL, Baugher B, Babin SM, et al. Prediction of high incidence of dengue in the Philippines. PLoS neglected tropical diseases **2014**; 8:e2771.
187. Ooi EE, Gubler DJ. Dengue in Southeast Asia: epidemiological characteristics and strategic challenges in disease prevention. Cad Saude Publica **2009**; 25 Suppl 1:S115-24.
188. Salim NAM, Wah YB, Reeves C, et al. Prediction of dengue outbreak in Selangor Malaysia using machine learning techniques. Scientific Reports **2021**; 11:939.
189. Nguyen-Tien T, Do DC, Le XL, et al. Risk factors of dengue fever in an urban area in Vietnam: a case-control study. BMC public health **2021**; 21:664-.
190. Tissera HA, Jayamanne BDW, Raut R, et al. Severe Dengue Epidemic, Sri Lanka, 2017. Emerging infectious diseases **2020**; 26:682-91.

191. Mutheneni SR, Morse AP, Caminade C, Upadhyayula SM. Dengue burden in India: recent trends and importance of climatic parameters. Emerg Microbes Infect **2017**; 6:e70.
192. Khetarpal N, Khanna I. Dengue Fever: Causes, Complications, and Vaccine Strategies. J Immunol Res **2016**; 2016:6803098.
193. Gubler DJ. Dengue and dengue hemorrhagic fever. Clin Microbiol Rev **1998**; 11:480-96.
194. Changal KH, Raina AH, Raina A, et al. Differentiating secondary from primary dengue using IgG to IgM ratio in early dengue: an observational hospital based clinico-serological study from North India. BMC Infect Dis **2016**; 16:715.
195. Bournazos S, Gupta A, Ravetch JV. The role of IgG Fc receptors in antibody-dependent enhancement. Nat Rev Immunol **2020**; 20:633-43.
196. Oliphant T, Engle M, Nybakken GE, et al. Development of a humanized monoclonal antibody with therapeutic potential against West Nile virus. Nat Med **2005**; 11:522-30.
197. Smith SA, de Alwis AR, Kose N, et al. The potent and broadly neutralizing human dengue virus-specific monoclonal antibody 1C19 reveals a unique cross-reactive epitope on the bc loop of domain II of the envelope protein. mBio **2013**; 4:e00873-13.
198. Shrestha B, Brien JD, Sukupolvi-Petty S, et al. The development of therapeutic antibodies that neutralize homologous and heterologous genotypes of dengue virus type 1. PLoS Pathog **2010**; 6:e1000823.
199. de Alwis R, Smith SA, Olivarez NP, et al. Identification of human neutralizing antibodies that bind to complex epitopes on dengue virions. Proc Natl Acad Sci U S A **2012**; 109:7439-44.
200. Fibriansah G, Tan JL, Smith SA, et al. A highly potent human antibody neutralizes dengue virus serotype 3 by binding across three surface proteins. Nature Communications **2015**; 6:6341.
201. Sukupolvi-Petty S, Brien JD, Austin SK, et al. Functional analysis of antibodies against dengue virus type 4 reveals strain-dependent epitope exposure that impacts neutralization and protection. J Virol **2013**; 87:8826-42.
202. Sirivichayakul C, Barranco-Santana EA, Esquilin-Rivera I, et al. Safety and Immunogenicity of a Tetravalent Dengue Vaccine Candidate in Healthy Children and Adults in Dengue-Endemic Regions: A Randomized, Placebo-Controlled Phase 2 Study. J Infect Dis **2016**; 213:1562-72.

203. Sáez-Llorens X, Tricou V, Yu D, et al. Safety and immunogenicity of one versus two doses of Takeda's tetravalent dengue vaccine in children in Asia and Latin America: interim results from a phase 2, randomised, placebo-controlled study. Lancet Infect Dis **2017**; 17:615-25.
204. Standard Practice for Testing Fixed-Wavelength Photometric Detectors Used in Liquid Chromatography. Vol. E685-93. West Conshohocken, PA: ASTM International, **2013**.
205. Fibriansah G, Lok SM. The development of therapeutic antibodies against dengue virus. Antiviral Res **2016**; 128:7-19.
206. Arora S, Saxena V, Ayyar BV. Affinity chromatography: A versatile technique for antibody purification. Methods **2017**; 116:84-94.
207. Pappas L, Foglierini M, Piccoli L, et al. Rapid development of broadly influenza neutralizing antibodies through redundant mutations. Nature **2014**; 516:418-22.
208. Leach S, Shinnakasu R, Adachi Y, et al. Requirement for memory B-cell activation in protection from heterologous influenza virus reinfection. Int Immunol **2019**; 31:771-9.
209. Tsai WY, Lai CY, Wu YC, et al. High-avidity and potently neutralizing cross-reactive human monoclonal antibodies derived from secondary dengue virus infection. J Virol **2013**; 87:12562-75.
210. Zhang R, Verkoczy L, Wiehe K, et al. Initiation of immune tolerance-controlled HIV gp41 neutralizing B cell lineages. Sci Transl Med **2016**; 8:336ra62.
211. Khurana S, Hahn M, Coyle EM, et al. Repeat vaccination reduces antibody affinity maturation across different influenza vaccine platforms in humans. Nat Commun **2019**; 10:3338.
212. Feng L, Wang X, Jin H. Rabbit monoclonal antibody: potential application in cancer therapy. Am J Transl Res **2011**; 3:269-74.
213. Lefranc M-P, Giudicelli V, Duroux P, et al. IMGT®, the international ImMunoGeneTics information system® 25 years on. Nucleic Acids Research **2014**; 43:D413-D22.
214. Niu X, Yan Q, Yao Z, et al. Longitudinal analysis of the antibody repertoire of a Zika virus-infected patient revealed dynamic changes in antibody response. Emerg Microbes Infect **2020**; 9:111-23.
215. Zheng A, Umashankar M, Kielian M. In Vitro and In Vivo Studies Identify Important Features of Dengue Virus pr-E Protein Interactions. PLOS Pathogens **2010**; 6:e1001157.

216. A. Dowd K, Sirohi D, D. Speer S, et al. prM-reactive antibodies reveal a role for partially mature virions in dengue virus pathogenesis. Proceedings of the National Academy of Sciences **2023**; 120:e2218899120.
217. Beltramello M, Williams KL, Simmons CP, et al. The human immune response to Dengue virus is dominated by highly cross-reactive antibodies endowed with neutralizing and enhancing activity. Cell Host Microbe **2010**; 8:271-83.
218. The structure of a typical antibody molecule. New York: Garland Science, **2001** Immunobiology: The Immune System in Health and Disease 5th edition).
219. Smith SA, Nivarthi UK, Alwis Rd, et al. Dengue Virus prM-Specific Human Monoclonal Antibodies with Virus Replication-Enhancing Properties Recognize a Single Immunodominant Antigenic Site. Journal of Virology **2016**; 90:780-9.
220. Zybert IA, van der Ende-Metselaar H, Wilschut J, Smit JM. Functional importance of dengue virus maturation: infectious properties of immature virions. J Gen Virol **2008**; 89:3047-51.
221. Morea V, Tramontano A, Rustici M, Chothia C, Lesk AM. Conformations of the third hypervariable region in the VH domain of immunoglobulins11Edited by I. A. Wilson. Journal of Molecular Biology **1998**; 275:269-94.
222. Xu JL, Davis MM. Diversity in the CDR3 region of VH is sufficient for most antibody specificities. Immunity **2000**; 13:37-45.
223. López-Requena A, Rodríguez M, de Acosta CM, et al. Gangliosides, Ab1 and Ab2 antibodies: II. Light versus heavy chain: An idiotype-anti-idiotype case study. Molecular Immunology **2007**; 44:1015-28.
224. Sela-Culang I, Kunik V, Ofran Y. The Structural Basis of Antibody-Antigen Recognition. Frontiers in Immunology **2013**; 4.
225. Kielczewska A, D'Angelo I, Amador MS, et al. Development of a potent high-affinity human therapeutic antibody via novel application of recombination signal sequence-based affinity maturation. J Biol Chem **2022**; 298:101533.
226. Arbabi-Ghahroudi M. Camelid Single-Domain Antibodies: Historical Perspective and Future Outlook. Front Immunol **2017**; 8:1589.
227. Sheridan C. Llama-inspired antibody fragment approved for rare blood disorder. Nature Biotechnology **2019**; 37:333-4.

228. Rock EP, Sibbald PR, Davis MM, Chien YH. CDR3 length in antigen-specific immune receptors. Journal of Experimental Medicine **1994**; 179:323-8.
229. XIANG J, CHEN Z, DELBAERE LTJ, LIU E. Differences in antigen-binding affinity caused by single amino acid substitution in the variable region of the heavy chain. Immunology & Cell Biology **1993**; 71:239-47.
230. Barrios Y, Jirholt P, Ohlin M. Length of the antibody heavy chain complementarity determining region 3 as a specificity-determining factor. Journal of Molecular Recognition **2004**; 17:332-8.
231. Davis MM. The evolutionary and structural 'logic' of antigen receptor diversity. Seminars in Immunology **2004**; 16:239-43.
232. Hao Q, Zhan C, Lian C, et al. DNA repair mechanisms that promote insertion-deletion events during immunoglobulin gene diversification. Sci Immunol **2023**; 8:eade1167.
233. Thie H, Voedisch B, Dübel S, Hust M, Schirrmann T. Affinity maturation by phage display. Methods Mol Biol **2009**; 525:309-22, xv.
234. Tillotson BJ, Lajoie JM, Shusta EV. Yeast Display-Based Antibody Affinity Maturation Using Detergent-Solubilized Cell Lysates. Methods Mol Biol **2015**; 1319:65-78.
235. Wang Y, Keck ZY, Saha A, et al. Affinity maturation to improve human monoclonal antibody neutralization potency and breadth against hepatitis C virus. J Biol Chem **2011**; 286:44218-33.
236. Chen WH, Chou FP, Wang YK, Huang SC, Cheng CH, Wu TK. Characterization and epitope mapping of Dengue virus type 1 specific monoclonal antibodies. Virol J **2017**; 14:189.
237. Austin SK, Dowd KA, Shrestha B, et al. Structural basis of differential neutralization of DENV-1 genotypes by an antibody that recognizes a cryptic epitope. PLoS Pathog **2012**; 8:e1002930.
238. Sukupolvi-Petty S, Austin SK, Purtha WE, et al. Type- and subcomplex-specific neutralizing antibodies against domain III of dengue virus type 2 envelope protein recognize adjacent epitopes. J Virol **2007**; 81:12816-26.
239. Ji GH, Deng YQ, Yu XJ, et al. Characterization of a Novel Dengue Serotype 4 Virus-Specific Neutralizing Epitope on the Envelope Protein Domain III. PLoS One **2015**; 10:e0139741.

240. Renner M, Flanagan A, Dejnirattisai W, et al. Characterization of a potent and highly unusual minimally enhancing antibody directed against dengue virus. Nat Immunol **2018**; 19:1248-56.
241. Midgley CM, Flanagan A, Tran HB, et al. Structural analysis of a dengue cross-reactive antibody complexed with envelope domain III reveals the molecular basis of cross-reactivity. J Immunol **2012**; 188:4971-9.
242. Rouvinski A, Guardado-Calvo P, Barba-Spaeth G, et al. Recognition determinants of broadly neutralizing human antibodies against dengue viruses. Nature **2015**; 520:109-13.
243. Fibriansah G, Tan JL, Smith SA, et al. A potent anti-dengue human antibody preferentially recognizes the conformation of E protein monomers assembled on the virus surface. EMBO Mol Med **2014**; 6:358-71.
244. Muecksch F, Weisblum Y, Barnes CO, et al. Affinity maturation of SARS-CoV-2 neutralizing antibodies confers potency, breadth, and resilience to viral escape mutations. Immunity **2021**; 54:1853-68.e7.
245. Eshleman SH, Laeyendecker O, Kammers K, et al. Comprehensive Profiling of HIV Antibody Evolution. Cell Rep **2019**; 27:1422-33.e4.
246. Cizmeci D, Lofano G, Rossignol E, et al. Distinct clonal evolution of B-cells in HIV controllers with neutralizing antibody breadth. Elife **2021**; 10:e62648.
247. Haynes BF, Wiehe K, Borrow P, et al. Strategies for HIV-1 vaccines that induce broadly neutralizing antibodies. Nature Reviews Immunology **2023**; 23:142-58.
248. DeMaso CR, Karwal L, Zahralban-Steele M, et al. Specificity and Breadth of the Neutralizing Antibody Response to a Live-Attenuated Tetravalent Dengue Vaccine. The Journal of Infectious Diseases **2022**; 226:1959-63.
249. Edwards BM, Barash SC, Main SH, et al. The remarkable flexibility of the human antibody repertoire; isolation of over one thousand different antibodies to a single protein, BLyS. J Mol Biol **2003**; 334:103-18.